Characterisation of the FitAB Toxin-Antitoxin System in *Neisseria gonorrhoeae*

A thesis

submitted in partial fulfilment

of the requirements for the degree

of

Master of Science (Research) in Biological Sciences

at

The University of Waikato

by

Annmaree Keely Warrender

THE UNIVERSITY OF
WAIKATO
Te Whare Wānanga o Waikato

2019

Abstract

Neisseria gonorrhoeae is the causative agent of the sexually transmitted infection, gonorrhoea. In a standard infection, *N. gonorrhoeae* invade epithelial cells lining the urogenital tract and exit into the sub-epithelial layer. This triggers an immune response that causes the noticeable symptoms of gonorrhoea. Asymptomatic infection occurs when the bacteria persist inside epithelial cells, avoiding detection by the human immune system. Bacterial persistence has been linked to the development of antibiotic resistance, and as such, is a major contributing factor to the success of the pathogen. Mechanisms of adherence and invasion by *N. gonorrhoeae* have been well researched, but little is known about the intracellular lifecycle of the bacteria during infection and persistence.

Toxin-antitoxin (TA) systems have been linked to the formation of persistent populations in bacteria however the role of TA systems in *N. gonorrhoeae* is yet to be investigated. In this thesis, the role of a VapBC TA system in intracellular replication of *N. gonorrhoeae* is investigated and activity of the toxic VapC protein is characterised. The TA system, FitAB, is a protein-protein complex comprised of an antitoxin, FitA, and a toxin, FitB. Activity of FitB is inhibited when in complex with FitA, and the complex is auto-regulatory. Biochemical activity screens using RNA pentaprobe substrates to characterise the activity of FitB show FitB cleaves single-stranded RNA pentaprobes. However, FitB does not cleave short RNA oligonucleotides of the same sequence(s). These results indicate FitB is a magnesium-dependent sequence-specific ribonuclease that cleaves RNA based on sequence and secondary structure.

The potential role of FitAB in persistence of *N. gonorrhoeae* was investigated using intracellular replication experiments. Intracellular replication of a *N. gonorrhoeae fitAB* gene deletion strain showed the most pronounced phenotype seen for a single TA deletion. Intracellular replication of the *fitAB* gene deletion strain is considerably faster than the wild-type within epithelial cells. However, a sudden cell death event occurs in the gene deletion strain suggesting the TA system is essential for sustainable, long-term growth during infection. An understanding of how FitAB regulates intracellular growth will provide insight into the intracellular lifecycle of *N. gonorrhoeae* and the formation of persistent populations.

Acknowledgements

First and foremost I would like to thank my supervisor, Dr. Joanna Hicks. Thank you for all your guidance and support during my masters, you never fail to go above and beyond to help and to answer my never ending questions. I am so grateful to have had you as a mentor since I began in the lab as a summer student, I know I am a better researcher for it.

A special thank you to Professor Vic Arcus. Your knowledge and passion for science continues to inspire me. Thank you for inviting me into your lab and for all the opportunities you have given me.

Thank you to the past and present members of the Proteins and Microbes lab group; Judith, Emma S., Erica, Emma A., Claire, Vikas, Heng, Kirsty, Mitchell, Liz, Emily, Andrew, Keely, Carlin, Daniel and Dr. Ray Cursons. My years as an MSc student would not have been the same without you all. Thank you Judith for your support and positivity, and of course your amazing morning teas. A special thank you in particular to Emma S., Claire, Liz, Erica, Emma A and Dr. Ray Cursons for your invaluable input and support during my masters. I would also like to thank Shaun and Olivia for keeping me sane with our lunchtime catch ups and for sharing in the joys and frustrations that come with MSc research.

Thank you to the University of Waikato for my MSc scholarship, Waikato Graduate Women Educational Trust for my study award, and to the Waikato Medical Research Foundation and the University of Waikato Strategic Investment Fund for funding my project.

Last, but not least, thank you to my family for your unwavering love and support. Especially to mum and dad, thank you for your interest in my research (despite not always understanding it) and for always encouraging me to dream big.

Table of Contents

List of Figures

List of Tables

List of Equations

Abbreviations

A	Adenosine
Arg	Arginine
Asp	Aspartic acid/Aspartate
bp	base pair(s)
BCP	bromo chloropropane
C	Cytosine
cDNA	complementary DNA
CFU	colony forming unit
C-terminal	carboxy terminus
DEPC	diethyl pyruvate carbonate
DMSO	dimethyl sulfoxide
DNase	deoxyribonuclease
ds	double-stranded
EDTA	ethylene diamine tetra-acetic acid (disodium salt)
ESI	electrospray ionisation
FCS	fetal calf serum
fit	fast intracellular trafficking
g	times the force of gravity
G	Guanine
GC	*Neisseria gonorrhoeae* gonococcus
GITC	guanidium isothiocyanate
Gln	Glutamine
Glu	Glutamic acid/Glutamate

HPLC	high performance liquid chromatography
His-tag	poly-histidine tag
IMAC	immobilised metal affinity chromatography
IPTG	isopropylthio-β-D-galactosidase
kb	kilobase
kDa	kilo dalton
LB	luria bertani
MALDI	matrix associated laser desorption ionisation
mAU	milli-absorbance units
Mg^{2+}	Magnesium cation
MGE	mobile genetic element
Mn^{2+}	Manganese cation
mRNA	messenger RNA
MS	mass spectrometry
Native-PAGE	non-denaturing PAGE
NEB	New England Biolabs
nt	Nucleotide(s)
N-terminal	amino terminus
OD	optical density
Oligo	oligonucleotide
PAGE	polyacrylamide gel electrophoresis
PBS	phosphate buffered saline
PCR	polymerase chain reaction
PDB	protein data bank

pI	isoelectric point
PIN	PilT N-terminal domain
pmol	picomole
Pol	polymerase
RHH	ribbon helix helix
RIN	RNA integrity number
RNase	ribonuclease
RNAseq	RNA sequencing
rpm	revolutions per minute
rRNA	ribosomal RNA
RT	reverse-transcription
SDS	sodium dodecyl sulphate
ss	single stranded
T	Thymine
TA	toxin-antitoxin
TAE	tris-acetate-EDTA
TBE	tris-borate-EDTA
TE	trypsin-EDTA
TEMED	N, N, N, N, -tetramethylethylenediamine
TOF	time of flight
Tris	tris(hydroxymethyl)aminomethane
tRNA	transfer RNA
U	uracil
UV	ultra violet

v/v	volume per volume
Vap	virulence associated protein
WT	wild-type

Chapter One

Introduction

Gonorrhoea is a prevalent sexually transmitted infection caused by the pathogenic gonococcus (GC), *Neisseria gonorrhoeae*. Gonorrhoea has become a global health crisis with its high prevalence in the global population and the rapid development of resistance to antibiotics (Edwards & Butler, 2011). There is a pressing need to understand the mechanisms behind GC infection so alternative antimicrobial treatments can be designed. Much research has been carried out regarding the pathobiology of the infection (Edwards & Butler, 2011), as well as gonococcal invasion mechanisms (Hill *et al.*, 2016) and interaction with the host immune system. Little is understood, however, about the intracellular lifecycle of the pathogen. It is apparent that *N. gonorrhoeae* can persist inside the host like other pathogenic microorganisms, which contributes to survival of the pathogen and may be linked to the development of antibiotic resistance. My research aims to characterise a toxin-antitoxin system in *N. gonorrhoeae* and its potential role in persistence.

1.1 Gonorrhoea: the disease and the threat of antibiotic resistance

N. gonorrhoeae is estimated to cause over 78 million infections worldwide, annually (Newman *et al.*, 2015). Initially, when GC infect the lower urogenital tract it causes uncomplicated cervicitis in women and urethritis in men, which are local, self-limiting infections that present observable symptoms (Unemo & Shafer, 2014). In some cases infection can be asymptomatic and these typically go untreated (Edwards & Butler, 2011; Holmes *et al.*, 1971). If left for a long period of time GC can ascend into the upper urogenital tract, causing more complicated infection such as endometritis, pelvic inflammatory disease and epididymitis, which can lead to infertility and ectopic pregnancy (Holmes *et al.*, 1971; Hopper *et al.*, 2000; World Health Organization, 2011). Subclinical infection disproportionately affects men and women, occurring in 10% and 50% of cases respectively (Workowski & Berman, 2007). Asymptomatic, subclinical infection is still transmissible and as such is a major contributing factor to the spread and success of the pathogen, and the emerging resistance to antibiotics (Edwards & Butler, 2011; Workowski &

Berman, 2007). *N. gonorrhoeae* is rapidly developing resistance to frontline antibiotics used worldwide, with most strains displaying reduced susceptibility to all currently available treatment options (Unemo, 2015; Wi *et al.*, 2017). Infection was initially treated with sulphonamides, penicillins, tetracyclines, macrolides, fluoroquinolones and cephalosporins until resistance emerged and spread globally (Unemo, 2015; Wi *et al.*, 2017). An extended-spectrum cephalosporin, ceftriaxone, is still used in some countries as a monotherapy treatment option, however reduced susceptibility has been identified in strains from the USA and more locally in Canterbury, Auckland and Waikato District Health Boards within New Zealand (Alirol *et al.*, 2017; ESR., 2014; Wi *et al.*, 2017). In recent years, a dual-therapy approach, in which two or more antibiotics are used together, most commonly ceftriaxone and azithromycin, has been implemented in an attempt to combat resistance (Wi *et al.*, 2017; Workowski *et al.*, 2015). In February 2018, a strain was isolated from an infected individual in the UK which showed dual-resistance to ceftriaxone and azithromycin combined therapy (Eyre *et al.*, 2018). Other strains identified in the USA also show total resistance and have been classified by the World Health Organisation as 'Superbugs' (Wi *et al.*, 2017).

It is evident that antibiotic resistance of *N. gonorrhoeae* is a global crisis that requires the development of new antibiotics and new treatment regimens to overcome. Understanding gonococcal infection and how the bacteria are capable of developing resistance so rapidly is fundamental to this development.

1.2 Gonococcal mode of infection

GC predominantly infect epithelial cells that line the urogenital tract. Although not completely defined, the mode of adherence by GC is specific to cell type, site of infection, and gender (Edwards & Apicella, 2004). To invade epithelial cells, GC use Type IV pili and various outer membrane proteins to form a tight association with the cell (Edwards & Butler, 2011; Swanson *et al.*, 1987). The bacteria are engulfed into the cell inside a vacuole like structure (Edwards & Butler, 2011). Once inside the host cell, GC either remain on the periphery of the cell and can be recycled back out the apical side of the epithelium, or they traffic to the basolateral side of the cells and are exocytosed into the sub-epithelial layer (Figure 1-1) (Billker

et al., 2002; Evans, 1977; Wang *et al.*, 1998). In some infections, *N. gonorrhoeae* remains inside the mucosal cells in a dormant state (Hopper *et al.*, 2000).

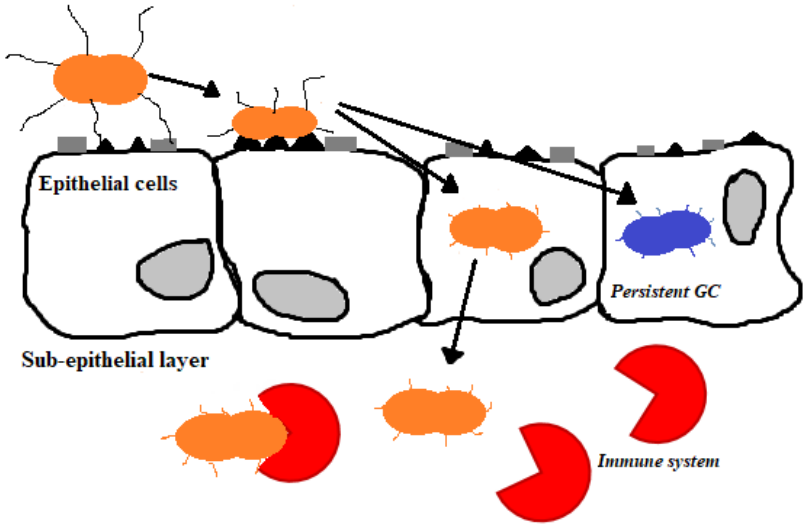

Figure 1-1.Schematic diagram of GC infection. Diploid GC makes contact with receptors on the mucosal cell surface via Type IV pili. The pili retract to strengthen attachment between the bacteria and the cell surface. GC are then internalised into the cell where they either remain inside in a persistent state or transcytose through the basolateral side into the subepithelial layer. Human immune cells detect GC in the subepithelial layer, trigger and immune response and generate symptoms. Figure adapted from (Hill et al., 2016).

Due to the nature of GC infection, observable symptoms such as pustular discharge and inflammation are only generated when the bacteria are attacked by the human immune system (Hill *et al.*, 2016). Immune response is triggered when the bacteria attach to the mucosal cells or when they enter the sub-epithelial layer (Hill *et al.*, 2016). Recruitment of pro-inflammatory cytokines and neutrophils to the site of infection cause the observable symptoms (Fisette *et al.*, 2003; Ramsey *et al.*, 1995). If *N. gonorrhoeae* is in a persistent state, no immune response is triggered and thus infection is asymptomatic (Workowski & Berman, 2007).

Persistent bacteria are a subpopulation of bacteria that differentiate into a dormant state where they do not actively divide (Balaban, 2011; Bigger, 1944). This increases survival of the population during adverse and stressful conditions such as nutrient starvation and antibiotic exposure (Balaban, 2011; Bigger, 1944). Bacteria displaying the persistent phenotype avoid exposure to antibiotics and have a higher tolerance because the cellular processes involved in replication and division that are targeted by antibiotics are downregulated so antibiotics have no effect (Balaban, 2011; Lewis, 2010; Maisonneuve & Gerdes, 2014; Tuomanen, 1986). This is in

contrast to antibiotic resistant phenotypes which act by preventing the antibiotic from binding to its target (Lewis, 2010). Once the antibiotic threat is gone, the dormant subpopulation can actively divide again to repopulate the environment (Balaban, 2011). As *N. gonorrhoeae* is naturally transformable, it readily accepts antibiotic resistant plasmids which may be present during periods of persistence, leading to a resistant phenotype of the new population (Ochman *et al.*, 2000).

Toxin-antitoxin (TA) systems have been linked to bacterial persistence in other pathogenic bacteria (Amitai *et al.*, 2009; Keren *et al.*, 2011) and associated with cellular trafficking of *N. gonorrhoeae* (Hopper *et al.*, 2000). As such, the role of TA systems in persistence of *N. gonorrhoeae* warrants investigation.

1.3 Toxin-Antitoxin Systems

TA systems are complexes found in many prokaryotes and archaea to mediate chromosomal stabilisation, plasmid maintenance, and enhance survival during infection (Gerdes *et al.*, 1986; Lobato-Márquez *et al.*, 2016). The complexes comprise a stable toxin which is inhibited by a less stable antitoxin (Arcus *et al.*, 2011). The toxin and antitoxin are translationally coupled on an auto-regulated, bicistronic operon (Anantharaman & Aravind, 2003). Due to the antitoxin being relatively unstable, eventually it degrades, leaving the toxin uninhibited (Ahidjo *et al.*, 2011; Gerdes *et al.*, 1986; Hayes, 2003). On its own, the toxin is responsible for targeting key physiological processes to inhibit cell growth or induce cell death (Yamaguchi & Inouye, 2011).

The repertoire of biological functions of TA systems is continually expanding as more systems are discovered and characterised. The first TA systems described were labelled plasmid maintenance modules as they mediated the survival of cells that contained the plasmid on which they were encoded (Gerdes *et al.*, 1986; Lobato-Márquez *et al.*, 2016). Upon bacterial replication, if daughter cells did not contain the plasmid, the antitoxin and toxin could not be synthesised. As the toxin is more stable than the antitoxin, the antitoxin would degrade leaving active toxin to arrest cell growth and cause cell death, thus eliminating the cells lacking the plasmid in a process termed ‘post-segregational killing’ (Gerdes *et al.*, 1986). With the era of genome sequencing, came the discovery of TA systems encoded on chromosomes (Gerdes *et al.*, 2005; Pandey & Gerdes, 2005). Some of these systems

were found within or linked to mobile genetic elements (MGE) (Cambray *et al.*, 2010). The function of these systems was proposed to be for maintenance of the MGEs much like the plasmid maintenance TA modules (Hernández-Arriaga *et al.*, 2014). There was, however, a greater abundance of chromosomal TA systems not associated with MGEs. These were proposed to function as stress-response elements, regulating cell growth in response to environmental stressors (Gerdes, 2000). Over recent years, with the use of genome sequencing and bioinformatics, a vast array of TA systems have been discovered throughout the prokaryotic kingdom. The function of which, has been characterised for a number of systems (Gerdes *et al.*, 2005; Harms *et al.*, 2018; Lee & Lee, 2016) while inferred for others based on classification criteria.

TA systems are classified into six 'types' based on the nature and role of the antitoxin (Lobato-Márquez *et al.*, 2016; Page & Peti, 2016). Type I systems have small antisense RNA antitoxins that prevent translation of the corresponding toxin. Type II have protein antitoxins that neutralise the protein toxin and bind upstream of the operon to repress transcription (Lobato-Márquez *et al.*, 2016; McKenzie, 2011). Type III TA systems have small RNA antitoxins that neutralise the toxin by inhibiting its RNase activity (Fineran *et al.*, 2009). Type IV, V and VI systems all have proteinaceous antitoxins. The antitoxins of type IV and V systems act on the target of the toxin to inhibit activity while those of type VI systems bind directly to the toxin, promoting protease degradation (Lobato-Márquez *et al.*, 2016).

Type II TA systems are of particular interest to this project because they have been associated with bacterial persistence by controlling intracellular growth (Amitai *et al.*, 2009; Hopper *et al.*, 2000). Within this group of TA systems, there are 12 super-families which are identified based on the nature of the toxin. These superfamilies are CcdB, Doc, HicAB, HigBA, MazEF, ParDE, VapBC, VapXD, RelBE, YafNO, and ωεζ (Leplae *et al.*, 2011). Multiple TA operons can be found in a single organism, differing in number of copies, the family they belong to and whether they are of chromosomal or plasmid origin (Pandey & Gerdes, 2005). The human pathogen, *Mycobacterium tuberculosis*, for example, has approximately 80 putative TA systems, most of which are Type II systems belonging to several well characterised super-families; 50 VapBC, ten MazEF, two RelBE, two HigBA, two ParDE (Sala *et al.*, 2014). In contrast, *N. gonorrhoeae* has six Type II TA systems:

one VapBC, three RelBE, one MazEF, one HicAB (Shao *et al.*, 2011). The assortment of TA systems present in a genome can also differ between strains within a species, for example, *N. gonorrhoeae* strain FA1090 lacks two of the three RelBE systems found in all other known strains of *N. gonorrhoeae* (Shao *et al.*, 2011).

1.4 Type II TA Systems in *N. gonorrhoeae*

The Type II TA systems in the *N. gonorrhoeae* chromosome include MazEF, RelBE, HicAB and VapBC (Shao *et al.*, 2011). To date, there is very little known about the role of these TA loci in *N. gonorrhoeae*, however, in other prokaryotes, particularly *E. coli*, these TA systems have been relatively well characterised. The structural and functional role of TA loci in other prokaryotes provides an understanding of the potential function of the homologous loci in *N. gonorrhoeae*. This section provides a general description of these TA systems in other prokaryotes.

1.4.1 MazEF

The MazEF TA system has been well studied in many bacteria including *E. coli* (Kamada *et al.*, 2003; Zhang *et al.*, 2003), *Pseudomonas putida* (Miyamoto *et al.*, 2016) and *M. tuberculosis* (Mittenhuber, 1999; Zhu *et al.*, 2006). The *mazEF* operon encodes the antitoxin MazE and the toxin MazF (Aizenman *et al.*, 1996). Two MazE proteins interact with four MazF proteins to form a stable heterohexamer which autoregulates transcription by binding to palindromic repeats in the promoter region of the *mazEF* operon (Aizenman *et al.*, 1996; Kamada *et al.*, 2003). During periods of stress, such as nutrient deprivation, heat shock and antibiotic exposure (Hazan *et al.*, 2004), MazE is degraded by the ClpPA protease, releasing active MazF which leads to programmed cell death or inhibition of cell growth (Aizenman *et al.*, 1996; Kamada *et al.*, 2003). MazF proteins are ribosomal-independent ribonucleases which inhibit cell growth by cleaving mRNA transcripts in a sequence-specific manner (Miyamoto *et al.*, 2016; Zhang *et al.*, 2003). *E. coli* MazF targets the RNA triplet sequence ACA (Zhang *et al.*, 2003) while the MazF homologue from *P. putida* targets the RNA sequence UAC (Miyamoto *et al.*, 2016). Despite different target sequences, cleavage of mRNA transcripts by both MazF proteins interrupts protein synthesis (Miyamoto *et al.*, 2016; Zhang *et al.*, 2003).

The synthesis of large survival proteins is inhibited while the synthesis of death proteins is increased leading to death of a large portion of the population. Uninterrupted expression of small survival proteins, however, allows a small sub-population to survive in a persistent state (Amitai *et al.*, 2009; Miyamoto *et al.*, 2016; Zhang *et al.*, 2003). This bacteriostatic effect of MazF is important for the ultimate survival of the population during periods of stress (Amitai *et al.*, 2009).

1.4.2 RelBE

The *relBE* operon encodes an antitoxin, RelB, and a toxin, RelE which assemble into a heterotetramer (Mattison *et al.*, 2006; Pedersen *et al.*, 2002). The *relBE* promoter is repressed during steady-state growth by the RelBE complex (Christensen *et al.*, 2001). Under amino-acid starvation, RelB is degraded by the Lon protease and transcription is upregulated causing an abundance of RelE (Christensen *et al.*, 2001). In *E. coli*, RelE inhibits protein synthesis by cleaving mRNA at the ribosomal A-site during translation (Christensen & Gerdes, 2003). Global inhibition of translation prevents cell proliferation and colony formation, making the cells bacteriostatic during periods of starvation so they can return to an active state when the nutrients are replenished (Christensen *et al.*, 2001; Pedersen *et al.*, 2002).

1.4.3 HicAB

HicAB was first discovered in *Haemophilus influenza* as two conserved open reading frames in a major pilus gene cluster (Mhlanga-Mutangadura *et al.*, 1998), but was later identified as a TA system using a computational comparative-genome approach (Makarova *et al.*, 2006). The function and structure of HicAB has since been studied in *E. coli* (Jørgensen *et al.*, 2009), *Burkholderia pseudomallei* (Butt *et al.*, 2014; Winter *et al.*, 2018), *Streptococcus pneumonia* (Kim *et al.*, 2018), and *Yersinia pestis* (Bibi-Triki *et al.*, 2014).

Unlike the other Type II TA systems, the gene encoding the toxin (*hicA*) precedes the gene encoding the antitoxin (*hicB*) in the *hicAB* operon (Jørgensen *et al.*, 2009; Makarova *et al.*, 2006). Despite this difference, the mechanisms of the toxin and antitoxin proteins when expressed are similar to that of MazEF and RelBE TA systems (Jørgensen *et al.*, 2009). The HicAB complex is assembled by a HicB homo-dimer binding to two or more HicA monomers (Bibi-Triki *et al.*, 2014; Kim

et al., 2018). The N-terminal region of HicB binds to HicA to neutralise activity while the C-terminal region of HicB contains a ribbon-helix-helix (RHH) DNA-binding domain which binds to DNA in the promoter region of the *hicAB* operon to regulate transcription (Jørgensen *et al.*, 2009; Kim *et al.*, 2018; Makarova *et al.*, 2006). During periods of nutritional stress, HicB is degraded by Lon proteases, inducing transcription of the *hicAB* operon and releasing active HicA (Jørgensen *et al.*, 2009). On its own, HicA has ribonuclease activity against specific mRNA substrates which inhibits protein translation and consequently impedes cell growth and proliferation (Jørgensen *et al.*, 2009).

1.4.4 VapBC

The VapBC (virulence-associated protein) TA family is the most abundant Type II TA system (Arcus *et al.*, 2005; Gerdes *et al.*, 2005). Toxins are classified as VapC if they contain a C-terminal PilT-N (PIN)-domain (Arcus *et al.*, 2011).

The *vapBC* operon encodes the antitoxin, VapB, and the toxin, VapC, with overlapping open reading frames (Figure 1-2) (Arcus *et al.*, 2011). VapB and VapC form a tightly associated dimer where the C-terminus of VapB blocks the active site of one or more VapC molecules to form an inert VapBC complex (Maté *et al.*, 2012; Mattison *et al.*, 2006; Miallau *et al.*, 2009). VapBC in *Rickettsia felis* and *Mycobacterium tuberculosis*, assemble as a heterohexamer (Maté *et al.*, 2012; Min *et al.*, 2012). One VapB binds to a VapC dimer, blocking both VapC active sites by positioning the C-terminal loop in between the dimer interface (Maté *et al.*, 2012; Min *et al.*, 2012). In VapBC TA systems from *Shigella flexneri* and *N. gonorrhoeae* a single VapB molecule blocks the active site of a single VapC molecule and the heterodimers form a stable hetero-octamer (Dienemann *et al.*, 2011; Mattison *et al.*, 2006). To regulate transcription of the *vapBC* operon, the VapBC complex binds to DNA in the promoter region via the RHH DNA binding domain at the N-terminus of VapB (Arcus *et al.*, 2011; Dienemann *et al.*, 2011; Gerdes *et al.*, 2005; Maté *et al.*, 2012; Mattison *et al.*, 2006; Miallau *et al.*, 2009; Min *et al.*, 2012). As VapB is relatively unstable, it is degraded by cellular stress or proteases, enabling magnesium-dependent ribonuclease activity of VapC (Figure 1-2) (Clissold & Ponting, 2000; Winther & Gerdes, 2012)

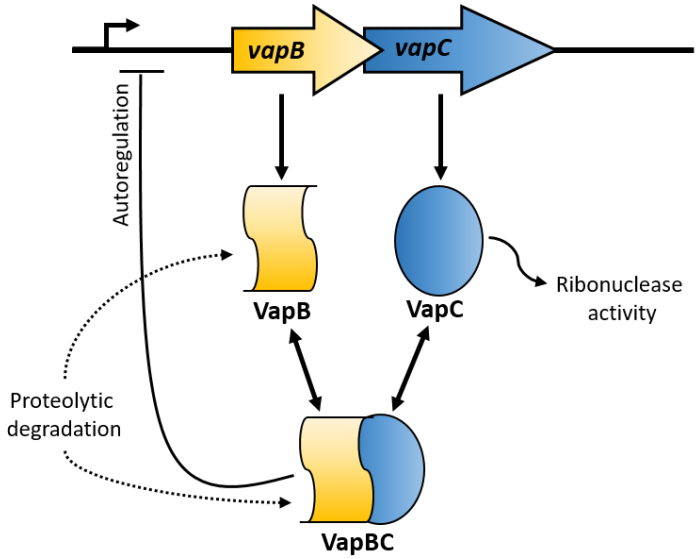

Figure 1-2. Schematic diagram of the VapBC TA system. VapB (yellow) and VapC (blue) are transcribed from a single operon. The VapBC complex binds to *DNA in* the promoter region of the operon to autoregulate transcription. When VapB degrades, VapC becomes an active ribonuclease which is toxic to cell growth by way of its sequence-specific ribonuclease activity.

The C-terminal PIN-domain in VapC proteins is important for metal-cation dependent ribonuclease activity (Arcus *et al.*, 2004; Clissold & Ponting, 2000; Winther & Gerdes, 2011). The structurally conserved PIN-domain fold has a central β-sheet made up of five parallel β-strands with α-helices on both sides (Figure 1-3) (Matelska *et al.*, 2017; Mattison *et al.*, 2006; Min *et al.*, 2012). The active site is a positively charged pocket formed by four highly conserved acidic amino acid residues (three aspartate residues and one glutamate residue) (Figure 1-3) at the C-terminus of the β-strands (Arcus *et al.*, 2005; Min *et al.*, 2012). The conserved residues coordinate either Mg^{2+} or Mn^{2+} (Arcus *et al.*, 2004; Bunker *et al.*, 2008; Matelska *et al.*, 2017; Mattison *et al.*, 2006; Wall & Kaiser, 1999).

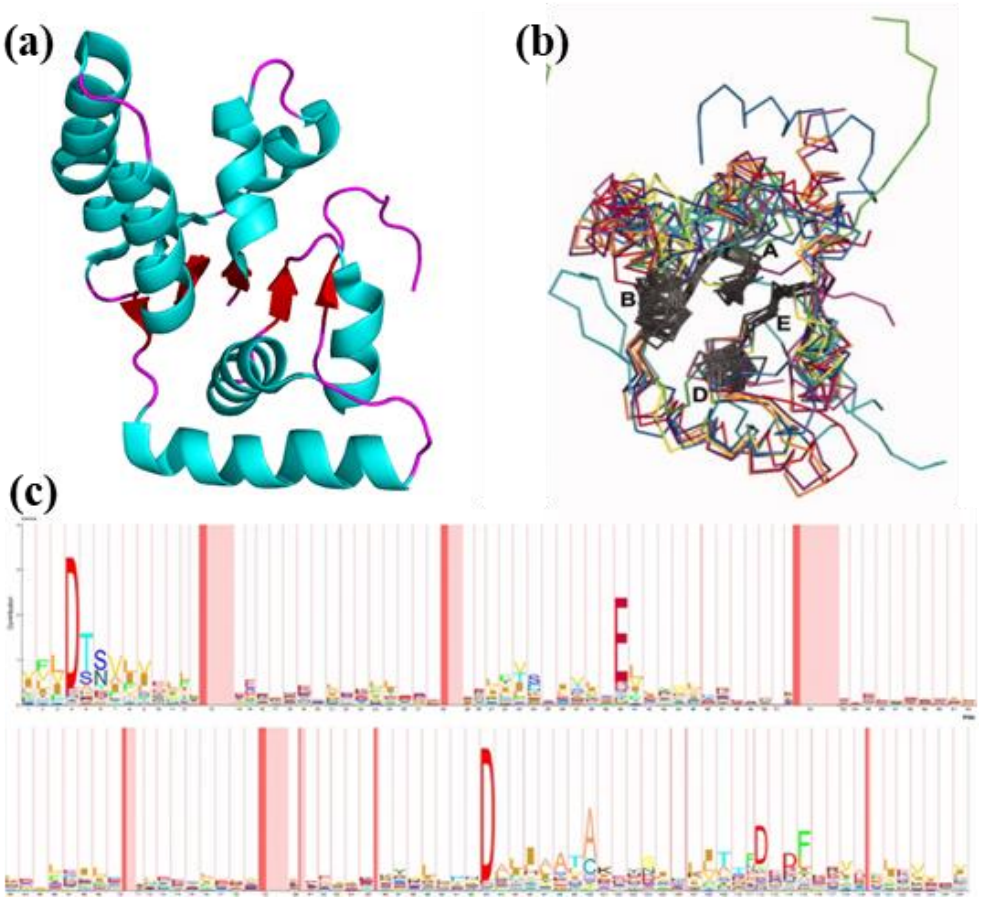

Figure 1-3. VapC C-terminal PIN-domain structure and sequence homology. (a) Ribbon diagram showing the PIN-domain fold. The five β-strands that make up the β-sheet are coloured red, α-helices are coloured teal. Image created in PyMOL using PDB file 2BSQ. (b) A structural alignment of PIN-domain structures shows structural homology within the core of the PIN-domain. The structurally conserved residues are shown in grey labelled in sequence order: A, Asp, B, Glu, D, Asp, E, Asp. Image retrieved from (Bunker et al., 2008). (c) Hidden Markov model showing the conserved residues in the PIN domain. The size of the letter corresponds to the conservation of that amino acid. Retrieved from (Arcus et al., 2011).

The RNA molecules targeted by VapC differ between VapBC systems within a single genome and across prokaryotic domains (Sala *et al.*, 2014; Sharrock *et al.*, 2018). Research has shown VapC proteins have sequence-specific ribonuclease activity (McKenzie *et al.*, 2012b; Sharrock *et al.*, 2018; Winther *et al.*, 2016; Winther & Gerdes, 2011).

The sequence-specificity of VapC proteins from *M. tuberculosis*, *M. smegmatis* and *Pyrobaculum aerophilum* has been characterised using the pentaprobe system (McKenzie *et al.*, 2012a; McKenzie *et al.*, 2012b; Sharrock *et al.*, 2018). Pentaprobes were used as they cover every combination of five bases and can be used to construct single-stranded RNA fragments. (Kwan *et al.*, 2003; McKenzie *et al.*, 2012a; Sharrock *et al.*, 2018). Pentaprobes that are cleaved by VapC were used

to design short oligonucleotides, approximately 30 nucleotides (nt) long, which were used for further ribonuclease activity testing (McKenzie *et al.*, 2012a). The sequence of the VapC cut site was then identified by matrix associated laser desorption ionisation mass spectrometry (MALDI-TOF MS) of the shorter RNA oligonucleotides (McKenzie *et al.*, 2012a).

Using the pentaprobe system and MALDI-TOF MS, $VapC_{MSMEG\_1284}$ from *M. smegmatis* was discovered to have sequence and structural specificity, targeting mRNA transcripts with a AUA(U/A) head, a short 3' RNA hairpin and a G-tail (McKenzie *et al.*, 2012b). These results, in conjunction with *in vivo* analyses, revealed VapC in *M. smegmatis* targets mRNA transcripts involved in metabolism to down-regulate carbon transport and glucose metabolism as a way of regulating sugar utilisation (McKenzie *et al.*, 2012b). VapCs from *M. tuberculosis* share the same optimal cut site of UA*GG (McKenzie *et al.*, 2012a; Sharrock *et al.*, 2018). Due to the abundance of *vapBC* operons in the *M. tuberculosis* genome and the presence of at least five of these VapC toxins with the same target sequence it is suggested that each operon may be activated by different stress conditions (Gupta *et al.*, 2017; Sharrock *et al.*, 2018). The target sequence differed for $VapC_{PAE0151}$ and $VapC_{PAE2754}$ from *P. aerophilum* which were found to cleave G-rich sequences where there is a guanine residue directly before the cut site, with a preference for the sequence GG*UG (McKenzie *et al.*, 2012a). All the VapC proteins analysed using MALDI-TOF MS showed the same mechanism of RNA cleavage, cleaving at the phosphodiester bond resulting in a 3'-OH and a 5'-PO_4 (Sharrock *et al.*, 2018).

Using different approaches, many other VapCs from *M. tuberculosis* have been characterised as sequence-specific ribonucleases, targeting tRNAs (Winther *et al.*, 2016) or 23S rRNA (Winther *et al.*, 2013). A combination of *in vivo* and *in vitro* analyses, including northern blot and primer extension analysis, revealed *M. tuberculosis* VapC20 targets the Sarcin-Ricin loop of 23S rRNA by recognising the SRL stem and cleaving between two essential nucleotides (G2661 and A2662) in the loop region (Winther *et al.*, 2013). This loop is essential for processes involved in translation so by cleaving it VapC20 inhibits global translation and prevents cell growth (Winther *et al.*, 2013). By similar means, other VapCs in *M. tuberculosis* were found to cleave the anticodon-loop of a specific tRNA,

preventing amino acids from being introduced to the A site during translation and ultimately inhibiting protein synthesis (Winther *et al.*, 2016).

VapC proteins from *Salmonella enterica* and from the *Shigella flexneri* virulence plasmid also inhibit global translation by cleaving initiator tRNAs (Winther & Gerdes, 2009, 2011). Upon amino acid starvation or the introduction of chloramphenicol the VapB antitoxin is subject to degradation and transcription of *vapBC* operon is induced resulting in accumulation of free VapC. Active VapC cleaves initiator $tRNA^{fMet}$, inhibiting protein synthesis and cell growth leading to a bacteriostatic state (Winther & Gerdes, 2009, 2011). When environmental conditions return to normal, VapB inhibits activity of VapC and the VapBC complex inhibits further transcription of the *vapBC* operon (Winther & Gerdes, 2009, 2011).

VapC proteins characterised to date have sequence-specific ribonuclease activity that inhibits protein synthesis under conditions of stress (McKenzie *et al.*, 2012b; Sharrock *et al.*, 2018; Winther & Gerdes, 2011). Many VapC proteins characterised from pathogenic bacteria show ribonuclease activity leads to formation of persistent populations (Keren *et al.*, 2011; Sharrock *et al.*, 2018; Winther & Gerdes, 2011). The VapBC TA system in *N. gonorrhoeae* may be playing a similar role during gonococcal infection.

1.5 FitAB: a VapBC TA System in *N. gonorrhoeae*

The VapBC TA system in *N. gonorrhoeae* FitAB is named after a fast intracellular trafficking phenotype observed upon discovery. The *fitAB* operon was identified in a transposon mutagenesis study, screening for molecular mechanisms that affect growth and transcytosis of GC in epithelial cells (Hopper *et al.*, 2000). Transposons were randomly inserted into the genome of *N. gonorrhoeae* and the rate of transepithelial trafficking (transcytosis) across polarised T84 monolayers was measured. Two transposon insertions knocked out expression of the *fitAB* operon and resulted in increased rates of transcytosis compared to *N. gonorrhoeae* wild-type (WT) (Hopper *et al.*, 2000). One transposon insertion, labelled A9, was inserted upstream of the ribosomal binding site of *fitA*, knocking out gene expression of both *fitA* and *fitB* (Figure 1-4). The other insertion, labelled A1, was inserted within the *fitB* gene, knocking out expression of *fitB* (Figure 1-4).

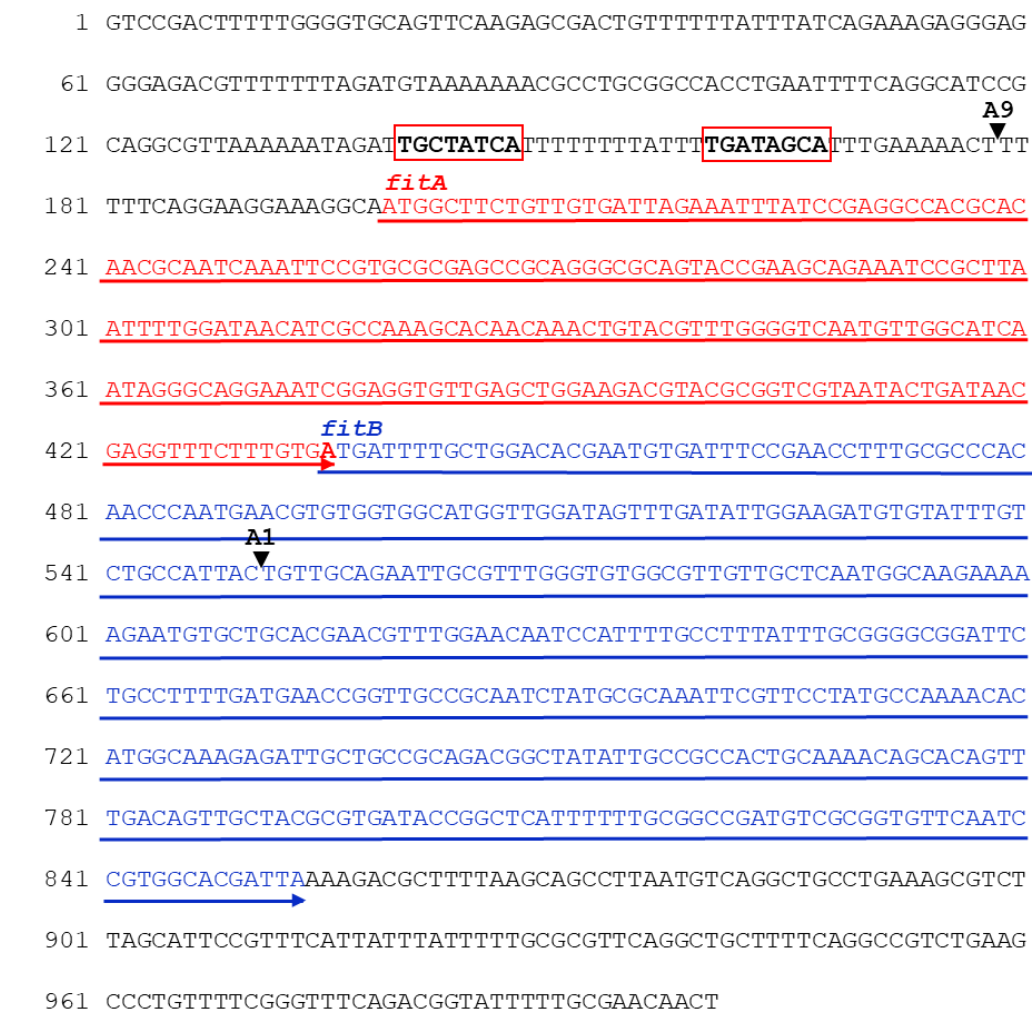

Figure 1-4. Labelled nucleotide sequence of the *fit* operon showing locations of the transposon mutations. The DNA sequence is numbered on the left. Genes are labelled and underlined: *fitA* (red), *fitB* (blue). The single-nucleotide where the stop codon of *fitA* and the start codon of *fitB* overlaps is in bold. The inverted-repeat sequences where the FitA dimer binds to are in bold and boxed. Arrows labelled A9 and A1 mark where transposons were inserted in the mutagenesis screen. Figure adapted from (Hopper et al., 2000). Nucleotide sequence accession number is AF200716 (Hopper et al., 2000).

The rates of intracellular replication of the A9 mutant (*N. gonorrhoeae* Δ*fitAB*) and of *N. gonorrhoeae* WT were measured. *N. gonorrhoeae ΔfitAB* replicated faster than *N. gonorrhoeae* WT (Hopper *et al.*, 2000). When expression of *fitAB* was knocked out, the rate of both transcytosis and intracellular replication were increased suggesting a link between replication inside epithelial cells and transport across the epithelial monolayer (Hopper *et al.*, 2000). Extracellular growth remained the same between *N. gonorrhoeae* WT and Δ*fitAB* strains indicating FitAB is important for replication within epithelial cells but does not affect growth in media (Hopper *et al.*, 2000). No further analysis was carried out to determine the mechanism(s) of growth regulation by FitAB (Hopper *et al.*, 2000). Following this

discovery, FitAB was identified as a Type II VapBC TA system based on genetic and structural analysis (Arcus *et al.*, 2011; Mattison *et al.*, 2006).

The *fitAB* operon is made up of the *fitA* and *fitB* loci with a one-base pair overlap in the stop codon of *fitA* and the start codon of *fitB* (Figure 1-4) (Hopper *et al.*, 2000). This overlap is typical of TA operons which are translationally coupled (Mattison *et al.*, 2006; Wilbur *et al.*, 2005). The unstable antitoxin, FitA, binds to the stable toxin, FitB, to form an inert FitAB complex (Figure 1-5). FitB has a C-terminal PIN-domain, typical of VapBC toxins (Arcus *et al.*, 2011; Mattison *et al.*, 2006). Conserved residues, Asp^{5}, Glu^{42}, Asp^{104}, and Asp^{122}, form a positively charged active site which binds a Mg^{2+} ion (Figure 1-5) (Mattison *et al.*, 2006). When in the FitAB complex, FitA binds into the substrate binding pocket of FitB with a C-terminal α-helix, positioning a positively charged arginine residue (Arg^{68}) into the active site of FitB to neutralise the pocket and inhibit Mg^{2+}-dependent activity of FitB (Figure 1-5)(Mattison *et al.*, 2006).

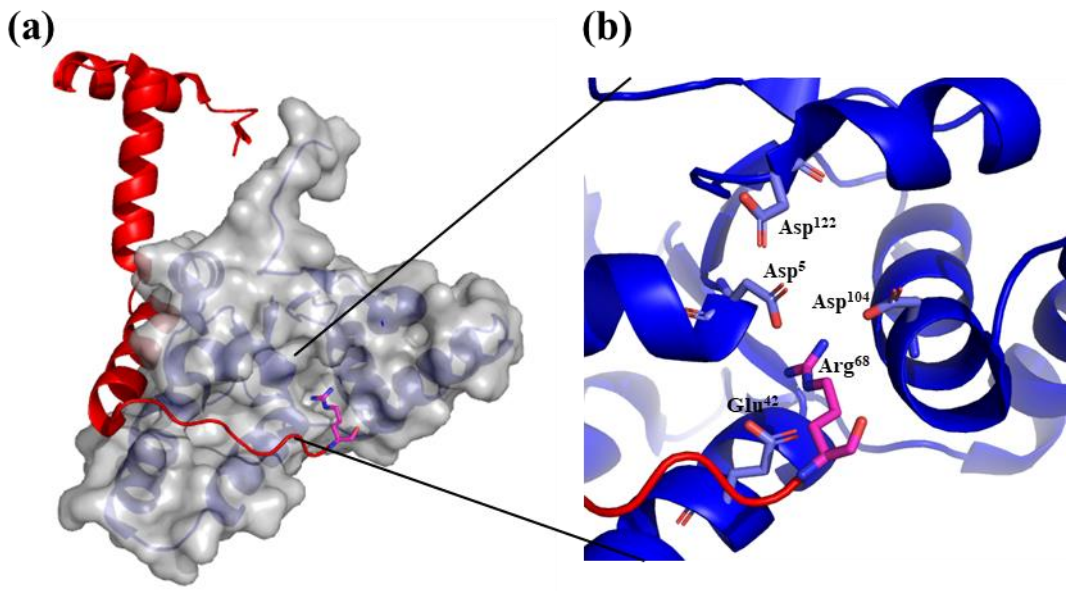

Figure 1-5. Ribbon and surface diagram of FitA binding to FitB with close up of FitB active site. (a) Ribbon diagram of FitA (red) binding to FitB (blue & grey surface). (b) View of the four highly conserved residues in the active site of FitB showing placement of Arg^{68} (pink) from FitA. Residues are labelled with the three letter code and position in the amino acid sequence. When FitA is absent, the four conserved amino acids coordinate an Mg^{2+} ion. Image created in PyMOL using PDB file 2BSQ.

FitAB auto-regulates transcription by binding to promoter DNA of the *fitAB* operon. FitA has an N-terminal DNA binding RHH domain made up of a β-strand and two

α-helices (Mattison *et al.*, 2006). The β-strand is involved in recognising the inverted repeat sequence TGCTATCA-N_{12}-TGATAGCA, while the two α-helices contribute to FitA homodimer formation, important for binding into the major groove of DNA (Figure 1-6) with high affinity to ensure tight regulation of transcription (Mattison *et al.*, 2006; Wilbur *et al.*, 2005). It is hypothesised that FitAB is bound to DNA in the extracellular environment but when the bacteria invade epithelial cells the complex is released, resulting in dissociation of the complex and transcription of the operon (Mattison *et al.*, 2006).

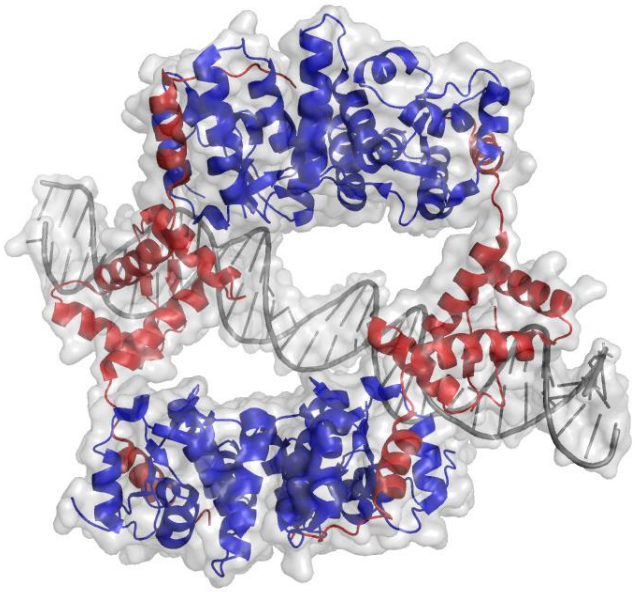

Figure 1-6. Ribbon and surface diagram of FitAB bound to DNA. FitA dimers (red) bind to major grooves in the 36-base pair double-stranded DNA molecule. FitB (blue) bound to FitA form two dimers either side of the DNA. Structure solved by x-ray crystallography (Mattison et al., 2006). PDB file 2BSQ.

The mechanism of growth regulation by FitAB and its role in *N. gonorrhoeae* infection are currently unknown. We hypothesise a general mode of action based on the current structural knowledge and understanding of other VapBC TA systems (Arcus *et al.*, 2011; Mattison *et al.*, 2006; Wilbur *et al.*, 2005; Winther & Gerdes, 2012). When *N. gonorrhoeae* invade epithelial cells, FitAB dissociates from the operon which promotes overexpression of *fitAB*. Conditions of cellular stress or proteases degrade FitA, releasing active FitB which likely cleaves mRNA transcripts to disrupt protein synthesis, causing growth to slow down or cease, and subsequently slowing transepithelial trafficking.

1.6 Research Objectives

The aim of my master's research was to characterise the FitAB TA system in *N. gonorrhoeae* and investigate its role in intracellular replication. The following objectives were set to fulfil this aim:

1) Determine if FitB has ribonuclease activity and characterise the specificity of this activity using biochemical assays.

2) Expand on the intracellular replication experiment performed by Hopper *et al.* (2000) to characterise growth of *N. gonorrhoeae* wild-type and *fitAB* gene deletion strains, within human epithelial cells.

3) Extract RNA from *N. gonorrhoeae* wild-type and *fitAB* gene deletion strains at various time-points during an intracellular replication assay (as in (2)) for RNA-seq. By analysing the transcriptomes of bacteria grown intracellularly, rather than in media alone, we can determine cellular targets of FitB during infection.

Chapter Two

Ribonuclease Activity of FitB

2.1 Introduction

FitAB is a VapBC toxin-antitoxin (TA) system (Arcus *et al.*, 2011; Mattison *et al.*, 2006) that has been implicated in the cellular trafficking of *N. gonorrhoeae* (Hopper *et al.*, 2000). The TA system is comprised of two proteins; an antitoxin, FitA, and a toxin, FitB (Mattison *et al.*, 2006). As with all VapC toxins, FitB has a PIN-domain like fold and possesses an acidic pocket with four residues, Asp^{5}, Glu^{42}, Asp^{104}, and Asp^{122}, which are highly conserved throughout PIN-domain proteins (Arcus *et al.*, 2011; Mattison *et al.*, 2006). PIN-domains generally show metal-dependent ribonuclease activity in prokaryotes (Arcus *et al.*, 2004; Clissold & Ponting, 2000) and many VapC proteins have been characterised as having sequence-specific ribonuclease activity (McKenzie *et al.*, 2012b; Sharrock *et al.*, 2018; Winther & Gerdes, 2011). We, therefore, predict FitB has ribonuclease activity.

Biochemical characterisation of VapC proteins have shown VapC cleaves RNA molecules at specific cut sites, unique to each VapC (McKenzie *et al.*, 2012b; Sharrock *et al.*, 2018; Winther & Gerdes, 2011). The target sequence of VapC proteins from *M. tuberculosis, M. smegamtis* and *P. aerophilum* has been characterised using a method developed in our lab (McKenzie *et al.*, 2012a). This method incorporates the pentaprobe system and MALDI-TOF MS (Figure 2-1) (McKenzie *et al.*, 2012a; McKenzie *et al.*, 2012b; Sharrock *et al.*, 2018). Generally, the ribonuclease activity of each VapC protein was screened against seven RNA pentaprobes that encompass all possible combinations of five bases. Shorter RNA oligonucleotides (oligos) were designed from cut pentaprobes and used for further ribonuclease testing. The target sequence was identified by MALDI-TOF MS analysis of the cut RNA oligos (McKenzie *et al.*, 2012a).

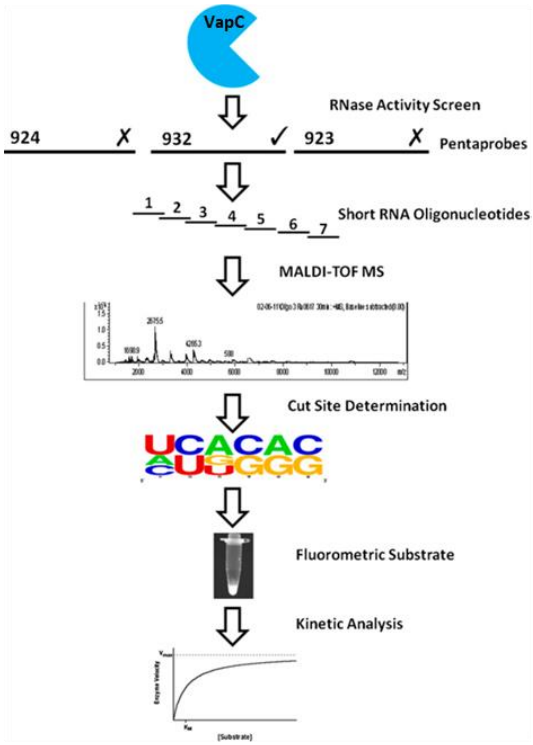

Figure 2-1. Schematic diagram of pentaprobe activity screens, sequence specificity and kinetic analysis. Ribonuclease activity of VapC is tested using pentaprobes and shorter oligonucleotides are designed based on the cut (ticked) pentaprobe. The cut sites are determined by MALDI-TOF MS. Kinetic parameters of VapC are determined by fluorometric analysis. Diagram retrieved from (McKenzie *et al.*, 2012a).

Early attempts to characterise activity of FitB failed to demonstrate any nuclease activity (Mattison *et al.*, 2006). Initially, activity assays were performed using the FitAB complex with single and double stranded RNA and DNA substrates (Mattison *et al.*, 2006). This, unsurprisingly, resulted in no nuclease activity as FitB would have been inhibited by FitA. Assays performed using FitB on its own were limited to a short, 36 base-pair, double-stranded DNA substrate, also resulting in no nucleic acid cleavage (Mattison *et al.*, 2006). Given the current understanding of VapC proteins, we assume no nuclease activity was identified in these experiments as VapC proteins act on RNA substrates rather than DNA (Arcus *et al.*, 2011; McKenzie *et al.*, 2012a; Ramage *et al.*, 2009).

This chapter characterises FitB ribonuclease activity by way of biochemical activity assays, using methods previously established in our lab (McKenzie *et al.*, 2012a).

2.1 Materials & Methods

2.1.1 Methods for cloning *fitAB* and *fitB*

FitAB and *FitB* genes were cloned into expression vectors based on past publications (Mattison *et al.*, 2006; Wilbur *et al.*, 2005). The *fitAB* gene construct was codon optimised for *E. coli* and synthesised by GeneArt (ThermoFisher) for cloning into plasmid pET28b-PstI with PstI and XhoI restriction cut sites for expression with a C-terminal His-tag.

FitAB was PCR amplified using the *fitA*-PstI forward primer (CTAGCTGCAGATGGCTAGCGTTGT) and *fitB*-XhoI reverse primer (CAGTACTCGAGATCATGCCACGGATTA), and *fitB* PCR amplified using the *fitB*-PstI forward primer (TTTACTGCAGATGATTCTGCTGGATAC) and the *fitB*-XhoI reverse primer above. PCR products and pET28b-pstI were digested with PstI-HF and XhoI restriction enzymes (NEB) according to manufacturer's instructions. Restriction enzyme digests were purified using the MoBio Ultraclean DNA Purification kit according to manufacturer's instructions. Purified DNA from each reaction was quantified by NanoDrop^{TM}. Ligation reactions were set up in a 3:1 insert:plasmid molar ratio using T4 DNA ligase (NEB) according to manufacturer's instructions. Ligation reactions were incubate at 20 °C for 2 hours then placed at 4 °C overnight.

Each ligation reaction (*fitAB* and *fitB*) was transformed into chemically competent *E. coli* DH5α and positive transformants selected by growth on LB agar plates supplemented with 50 µg ml^{-1} kanamycin incubated at 37 °C overnight. Plasmids were extracted from transformed colonies using a Qiagen Miniprep kit. Correct insertion of *fitAB* and *fitB* genes was confirmed by sequencing using T7 forward and reverse primers. Sequenced plasmids were then transformed into chemically competent *E. coli* BL21 (DE3) cells. Glycerol stocks of *E. coli* BL21 pET28b-pstI *fitAB* and *E. coli* BL21 pET28b-pstI *fitB* were stored at -80 °C.

2.1.2 FitB large scale expression cultures

The *E. coli* BL21 (DE3) pET28b-pstI *fitB* glycerol stock was thawed on ice and was streaked onto LB agar supplemented with 50 µg ml^{-1} kanamycin and incubated at 37 °C overnight. A single colony was taken from the plate and added to 10 ml LB broth supplemented with 50 µg ml^{-1} kanamycin. Cultures were incubated at 37 °C,

180 rpm overnight. These cultures were then transferred to 1 L LB broth with 50 µg ml^{-1} kanamycin in a 2 L baffled flask. These were incubated at 37 °C, 200 rpm for approximately 3 hours until the cultures reached an OD_{600} of approximately 0.5 to 0.6. Protein expression was induced by addition of 1 ml 0.75 M IPTG (final concentration 0.75 mM). The expression culture was then incubated at 22 °C, 200 rpm for 14 hours.

Cells were harvested by centrifugation at 4,600 *g* for 20 min at 4 °C and the supernatant removed. The cell pellet was resuspended in 15 ml Lysis buffer (50 mM $NaHPO_4$ pH 7.4, 200 mM NaCl, 20 mM Imidazole) and pooled in a 50 ml falcon tube. Resuspended cells were centrifuged at 4,600 *g* for 20 min at 4 °C and the supernatant was removed. The cell pellet was stored at -80 °C until purification.

2.1.3 FitAB large scale expression cultures

FitAB expression cultures were set up as per the protocol for FitB (section 2.1.2) except 2 L expression cultures were incubated at 37 °C, 200 rpm for 3 hours following IPTG induction.

2.1.4 Methods for protein analysis

2.1.4.1 SDS-PAGE

SDS-PAGE gels consisted of a resolving gel (15% acrylamide) and a stacking gel (5% acrylamide). Gels were poured in a Hoeffer five gel multi-gel caster. The resolving gel solution (Table 2-1) was poured into the gel plates, approximately 2 cm from the top. Two millilitres of isopropanol was gently pipetted on top of the resolving gel and the gel was left to set at room temperature (RT) for approximately 40 min. Once set, the isopropanol was decanted and the stacking gel (Table 2-1) poured on top of the resolving gel. Gel combs were added to each gel and the stacker gel was left to set as above.

Table 2-1. Recipe for 15% SDS-PAGE gels (to make five mini-gels).

	Resolving gel (15%)	Stacking gel (5%)
Water	7.05 ml	8.5 ml
30% Acrylamide	15 ml	2.125 ml
Resolving Buffer (1.5 M Tris, pH 8.8)	7.5 ml	-
Stacking Buffer (1.0 M Tris, pH 6.8)	-	1.6 ml
10% SDS	300 µl	125 µl
10% APS	150 µl	63 µl
TEMED	15 µl	6.3 µl

To prepare samples for gel loading, 5 µl 4 X protein loading dye (250 mM Tris-HCl, pH 6.8, 20% Glycerol, 4% SDS, 10% mercaptoethanol, 0.025% bromophenol blue) was added to 15 µl of each sample. When preparing concentrated samples (e.g. cell pellet or cell lysate) 3 µl sample was added to 12 µl of the appropriate lysis buffer and then 5 µl 4 X loading dye added. Samples were then heated to 95 °C for 5 min. Samples and 10 µl Precision Plus Protein Standard (BioRad) were loaded onto the gel and run in 1 X Tris-Glycine SDS Running Buffer (25 mM Tris, 250 mM Glycine, 0.1% SDS) at 70 V until samples entered the resolving gel. Voltage was then increased to 100 V and ran until samples reached the end of the resolving gel.

Gels were post-stained with Fairbanks A Staining Solution (0.05% Coomassie Blue, 25% isopropanol, 10% acetic acid). Solution was poured over protein gels and brought to the boil by heating for 30 sec in the microwave followed by shaking for 5 min at RT. To remove background staining, gels were destained with Fairbanks destaining solution (10% acetic acid) with the same heating and shaking procedure as above. Gels were imaged using an iBright imager (Invitrogen).

2.1.4.2 Native-PAGE

Native-PAGE gels were poured as for SDS-PAGE gels in section 2.1.4.1 above except with 12% acrylamide in the resolving gel and without the addition of SDS. Samples were prepared by adding 4 µl 5 X native loading dye (300 mM Tris-HCl,

pH 6.8, 50% Glycerol, 0.05% bromophenol blue) to 16 µl of each sample. Samples and 10 µl Precision Plus Protein Standard (BioRad) were loaded onto the gel and run in 1 X Tris-Glycine Running Buffer (25 mM Tris, 250 mM Glycine) at 70 V until samples entered the resolving gel. Voltage was then increased to 100 V and ran until samples reached the end of the resolving gel. Gels were stained and visualised as above in section 2.1.4.1.

2.1.5 Optimisation of FitB purification

FitB was purified using immobilized metal affinity chromatography (IMAC). Three different conditions were trialled to achieve FitB protein that was stable following purification.

2.1.5.1 IMAC purification with 1% Triton X-100

Triton X-100 was added to the Lysis buffer (50 mM $NaHPO_4$ pH 7.4, 200 mM NaCl, 20 mM Imidazole) and the Elution buffer (50 mM $NaHPO_4$ pH 7.4, 200 mM NaCl, 1 M Imidazole) to a final concentration of 1% Triton X-100.

A FitB expression culture cell pellet (see Section 2.1.2) was thawed at RT. The cell pellet was resuspended in 25 ml Lysis Buffer including Triton X-100 and sonicated on ice using a Misonix sonicator with a 5-50 ml microtip, setting 4, for 2.5 min in 30 sec intervals with 30 sec on ice in between intervals to keep sample temperature low. The cell lysate was centrifuged at 13,000 *g* for 20 min at 4°C to separate soluble and insoluble fractions. The supernatant (soluble fraction) was filtered through 1.2 µm, 0.45 µm, and 0.2 µm Minisart filters.

The filtered supernatant was loaded onto a pre-equilibrated 5 ml Ni HisTrap HP column (GE Healthcare Life Science) on a BioRad NGC system using the sample pump at a flow rate of 1 ml min^{-1}. The column was washed with 15 ml Lysis Buffer with Triton X-100 at a flow rate of 2 ml min^{-1} to remove any unbound proteins. These were collected for analysis. Bound proteins were eluted into collection tubes by running a gradient of 0% to 50% of the Elution buffer with Triton X-100 over 50 ml, at a flow rate of 2 ml min^{-1}. The eluted fractions (peak fractions) corresponding to a peak on the resulting 280 nm chromatogram were collected and stored on ice. Proteins that were unbound and eluted from the column during the wash step (flow through) and those eluted with elution buffer (peak fractions) were assessed by SDS-PAGE (section 2.1.4.1) and Native-PAGE (section 2.1.4.2).

2.1.5.2 IMAC purification with 5% glycerol

A FitB cell pellet was prepared for purification as in section 2.1.5.1 except glycerol was added to the Lysis and Elution buffers to a final concentration of 5%. IMAC purification was carried out as above (section 2.1.5.1) but an AKTA Basic (GE) chromatography system was used instead of the BioRad NGC system. Samples were analysed by SDS-PAGE (section 2.1.4.1) and Native-PAGE (section 2.1.4.2).

2.1.5.3 IMAC purification on ice

A FitB cell pellet was prepared and purified as in section 2.1.5.1, except no Triton X-100 was added to buffers. IMAC purification was performed using a BioRad NGC system (as in section 2.1.5.1) with fraction collection tubes situated on ice. The peak fractions were analysed by SDS-PAGE (section 2.1.4.1) and Native-PAGE (section 2.1.4.2) immediately following elution from the nickel column. When used in ribonuclease activity assays, eluted protein was taken immediately following elution and added to the reactions.

2.1.6 IMAC purification of FitAB

FitAB was Ni purified as for FitB (section 2.1.5.1) except no Triton X-100 was added to the buffers.

2.1.7 Expression and purification of CysE

CysE was expressed and purified by Keely Oldham as for FitB (refer to section 2.1.2 and 2.1.5.3).

2.1.8 Methods used for FitB mutagenesis

Two mutants of *fitB* were designed with point mutations in the PIN-domain active site. The mutation in one mutant was aspartate (position 104) to asparagine, the other was glutamate (position 42) to glutamine. Two different PCR based mutagenesis methods were performed to introduce the desired mutation into the *fitB* plasmid.

2.1.8.1 Two-halves mutagenesis method

Mutagenesis by two-halves involves creating each half of the gene from the plasmid individually before annealing these halves together to generate the full mutated gene, which is inserted back into the plasmid. The halves are generated by two PCR

reactions, one using the forward mutant primer with the reverse *fitB* primer, the other using the reverse mutant primer and the forward *fitB* primer.

The mutant primers were designed for the *E. coli* optimised version of *fitB* with the mutated codon in the centre of each primer (Table 2-2) using the Quikchange Primer Design software (Agilent Technologies, USA).

Table 2-2. Primer sequences used to generate *fitB* D104N mutant and *fitB* E42Q mutant using the two-halves mutagenesis method. The mutated codons are bold.

Name	Sequence (5'-3')
fitB D104N forward	CCACGGTAAAGAAATTGCAGCAGCA**AAC**GGTTATATTG CAGCAAC
fitB D104N reverse	GTTGCTGCAATAT**AAC**CGTTTGCTGCTGCAATTTCTTTA CCGTGG
fitB E42Q forward	CGCAATTACCGTTGCA**CAG**CTGCGTCTGGGTGTTG
fitB E42Q reverse	CAACACCCAGACG**CAG**CTGTGCAACGGTAATTGCG

The PCR reactions to generate two halves were set up using HOT FIREPol® DNA polymerase Blend Master mix with the *fitB* pET28b-pstI plasmid as the DNA template. Reactions were set up as in Table 2-3 with the following primer combinations:

fitB D104N forward: *fitB* PstI forward and *fitB* D104N reverse primers

fitB D104N reverse: *fitB* D104N forward and *fitB* XhoI reverse primers

fitB E42Q forward: *fitB* PstI forward and *fitB* E42Q reverse primers

fitB E42Q reverse: *fitB* E42Q forward and *fitB* XhoI reverse primers

PCR reactions were performed in replicates of four with one negative control in which the DNA template was omitted. The PCR cycling protocol was based on HOT FIREPol® DNA polymerase manufacturer recommendations (Table 2-4).

Table 2-3. Two-halves mutagenesis PCR reaction conditions.

Component	Concentration
5 X Master Mix	1 X
10 µM forward primer	0.3 µM
10 µM reverse primer	0.3 µM
Plasmid DNA template	0.6 ng

Table 2-4. Two-halves mutagenesis PCR cycling protocol.

PCR Cycles	Step	Temperature	Time (min:sec)
1	Initial denaturation	95°C	15:00
	Denature	95°C	0:20
30	Anneal	57°C	0:30
	Extend	72°C	1:00
1	Final extension	72°C	10:00

Following PCR amplification, the 20 µl reactions were loaded onto a 1% agarose gel pre-stained with 1 X SYBR Safe DNA gel stain (Invitrogen). Agarose gels were run at 100 V for 40 min. Gels were visualised using a blue light box and PCR products of the correct size were cut out of the gel and purified using the MoBio Ultraclean 15 DNA purification kit according to manufacturer's instructions.

Purified PCR products were used in a subsequent PCR reaction to generate the full-length gene. A PCR reaction was set up for each mutant using two corresponding half products as the DNA template. Each PCR product was added in a 1:1 molar ratio in the combination as follows:

> *fitB* D104N reaction: *fitB* D104N forward with *fitB* D104N reverse PCR products
>
> *fitB* E42Q reaction: *fitB* E42Q forward with *fitB* E42Q reverse PCR products

The reactions were prepared as in Table 2-5 in replicates of four and one negative control with no DNA template. PCR reactions were performed as for the first round of PCR above (Table 2-4).

Table 2-5. Two-halves mutagenesis PCR reaction conditions using the forward and reverse PCR products as DNA templates.

Component	Concentration
5 X Master Mix	1X
10 mM forward primer	0.3 mM
10 mM reverse primer	0.3 mM
Forward PCR product	5 ng
Reverse PCR product	5 ng

The four replicate PCR reactions for each mutant were pooled (total volume of 80 µl) and loaded on a 1% agarose gels pre-stained with 1 X SYBR Safe DNA gel stain (Invitrogen). Gels were run at 100 V for 40 min. PCR products of the correct size were cut from the gel and purified using the MoBio UltraClean 15 DNA purification kit and resuspended in 20 µl nuclease free water.

A restriction digest was carried out on each PCR product using the restriction enzymes PstI-HF and XhoI in CutSmart buffer (NEB). All reaction components (Table 2-6) were combined and incubated at 37 °C, 300 rpm for 2 hours. The restriction enzyme digest reactions were purified using the MoBio UltraClean 15 DNA purification kit.

Table 2-6. Composition of double restriction digest reaction.

Component	Volume (50 µl reaction)
XhoI	1 µl
PstI-HF	1 µl
DNA	1 µg
10 X CutSmart buffer	5 µl
Water	to 50 µl

The digested PCR products were ligated using T4 DNA ligase (NEB) into pET28b-PstI, in a 3:1 insert:plasmid molar ratio, following the T4 DNA ligation (NEB) protocol. All components were combined (Table 2-7) and incubated at 4 °C for 48 hours. To transform the plasmids into chemically competent *E. coli* DH5α, 10 µl

ligation reaction was added to 100 µl chemically competent *E. coli* DH5α and incubated on ice for 30 min. The bacteria were heat shocked at 42 °C for 45 secs and then placed on ice for 2 min. One millilitre of LB broth was added and incubated at 37 °C, shaking at 300 rpm, for 1 hour. One hundred microliters of bacteria were spread onto a LB agar plate with 50 µg ml^{-1} kanamycin and incubated overnight at 37 °C. Colonies from the plates were screened for successful transformation by colony PCR using T7 forward and reverse primers. A PCR reaction was set up for each colony (Table 2-8) and carried out using an Eppendorf PCR machine (Table 2-9) then assessed on a 1% TAE agarose gel as described previously. The colonies that contained the plasmid with the desired gene insert were grown in 5 ml LB broth with 50 µg ml^{-1} kanamycin overnight at 37 °C. The plasmid was extracted using the Qiagen Miniprep kit as per manufacturer's instructions and sequenced by the Massey Genome Sequencing Service with T7 forward and reverse primers.

Table 2-7. Ligation reaction of full length gene PCR product and pET28b-pstI.

Component	Volume (20 µl reaction)
10 X T4 DNA ligase buffer	2 µl
pET28b-PstI plasmid	1.1 µl
fitB D104N PCR product	0.84 µl
T4 DNA ligase	1 µl
Water	to 20 µl

Table 2-8. Colony PCR conditions.

Components	Volume (25 µl reaction)	Final concentration
10 X PCR buffer	2.5 µl	1 X
50 mM $MgCl_2$	0.75	1.5 mM
10 mM dNTPs	0.5	0.2 mM
10 µM T7 forward primer	1.25 µl	0.5 µM
10 µM T7 reverse primer	1.25 µl	0.5 µM
Taq polymerase	0.1 µl	
Water	to 25 µl	-

Table 2-9. Colony PCR cycling protocol.

PCR Cycles	Step	Temperature	Time (min:sec)
1	Initial denaturation	95°C	15:00
	Denature	94°C	0:45
30	Anneal	55°C	0:30
	Extend	72°C	3:00
1	Final extension	72°C	10:00

2.1.8.2 Site-directed mutagenesis method

The site-directed mutagenesis method introduces a point mutation directly into circular plasmid DNA. Template DNA is removed by DpnI digestion and the mutated plasmid is directly transformed into *E. coli*.

For this method of mutagenesis, Platinum Superfi^{TM} DNA polymerase (Invitrogen) was used and the mutant primers were designed differently than those used for two-halves mutagenesis method above (section 2.1.8.1). Mutant primers were designed using Geneious (Biomatters) with a 21-nucleotide complementary region containing the targeted mutation, followed by nine non-overlapping bases at the 3'-terminus (Table 2-10).

The primer annealing temperatures were calculated using the T_m calculator online, specifically designed for site-directed mutagenesis using Platinum Superfi^{TM} DNA polymerase (thermofisher.com/tmcalculator). The site-directed mutagenesis PCR reaction was carried out following the manufacturer's protocol (Table 2-11 and Table 2-12) using an Eppendorf PCR machine and *fitB* pET28b-pstI plasmid as the DNA template.

Table 2-10. Primer sequences for site-directed mutagenesis of fitB. The non-overlapping region is underlined and the mutated codon is in bold.

Name	Sequence (5'-3')
fitB E42Q forward	ACCGTTGCA**CAG**CTGCGTCTGGGTGTTGCA
fitB E42Q reverse	CAGACG**CAG**CTGTGCAACGGTAATTGCGCT

Table 2-11. Site-directed mutagenesis PCR reaction.

Component	Volume (50 µl reaction)	Final concentration
Nuclease free water	To 50 µl	-
5 X Superfi Buffer	10 µl	1X
dNTP mix (10 mM each)	1 µl	0.2 mM each
10 µM forward primer	2.5 µl	0.5 µM
10 µM reverse primer	2.5 µl	0.5 µM
Plasmid DNA template	10 ng	10 ng
Platinum SuperFi DNA Polymerase (2 U μl^{-1})	0.5 µl	0.02 U μl^{-1}

Table 2-12. Site-directed mutagenesis PCR cycling protocol.

PCR Cycles	Step	D104N		E42Q	
		Temperature (°C)	Time (min:sec)	Temperature (°C)	Time (min:sec)
1	Initial denaturation	98	0:30	98	0:30
30	Denature	98	0:10	98	0:10
	Anneal	67.7	0:10	72	0:10
	Extend	72	3:00	72	3:00
1	Final extension	72	5:00	72	5:00

Upon completion of the PCR reaction, template DNA was removed by addition of 1.5 µl DpnI (NEB) and incubated at 37 °C for 1 hour. DpnI was inactivated by heating the reaction to 80 °C for 20 min. Five microliters of the PCR product was directly transformed into chemically competent *E. coli* DH5α following the same protocol as described above in section 2.1.8.1. Colonies were selected from a LB agar plate including 50 µg ml^{-1} kanamycin and used to inoculate 5 ml LB broth with 50 µg ml^{-1} kanamycin then incubated overnight at 37 °C, shaking at 180 rpm. The plasmid was extracted using the Qiagen Miniprep kit as per manufacturer's instructions and sequenced by the Massey Genome Sequencing Service with T7 forward and reverse primers.

2.1.9 The Pentaprobe System

2.1.9.1 Preparation of DNA pentaprobes

The pentaprobe system was obtained from Joel McKay, School of Molecular Bioscience, University of Sydney. The system consists of 12 plasmids each containing a pentaprobe strand in the forward or reverse direction. Pentaprobes in the forward direction are termed 922, 923, 924, 925, 926, and 927, and the corresponding complementary strands are termed 928, 929, 930, 931, 932, and 933, respectively.

Pentaprobe inserts 922, 923, 924, 925, 926, 927 and 932 (Appendix B.1.) were PCR amplified using the *Pfx*® DNA polymerase system (Invitrogen) with forward and

reverse primers flanking the pentaprobe insert and including the T7 promoter in pcDNA3. See Table 2-13 and Table 2-14 for reaction concentrations and conditions.

Table 2-13. Reaction concentrations for Platinum *Pfx*® PCR reaction.

Component	Concentration
Pfx amplification buffer	1 X
Deoxynucleotide mix (dATP, dCTP, dTTp & dATP)	0.3 mM
$MgSO_4$	1 mM
Enhancer solution	1 X
Platinum Pfx® DNA polymerase	2 U
Forward & reverse primers	0.2 µM
Template DNA	20-120 ng

Table 2-14. Platinum *Pfx*® PCR reaction cycling conditions for amplification of pentaprobe inserts.

PCR Cycles	Step	Temperature	Time (min:sec)
1	Initial denaturation	94°C	2:00
30	Denature	94°C	0:15
	Anneal	55°C	0:30
	Extend	68°C	0:45
1	Final extension	68°C	7:00

2.1.9.2 Transcription of Pentaprobe RNA transcripts

The RNA Pentaprobes (922, 923, 924, 925, 926, 927, 932) were transcribed from the pentaprobe PCR products (Section 2.1.9.1 above) using T7 MEGAscript® kit (Ambion) according to manufacturer's instructions (Table 2-15). Transcription reactions were incubated at 37 °C for 2 hours followed by the addition of 1 µl TURBO DNase to remove template DNA and further incubated at 37 °C for 15 min. RNA was precipitated by sodium acetate and ethanol precipitation (section 2.1.10.1 below) RNA was resuspended in 30 µl nuclease free H_2O and concentration

determined by NanoDrop™. A working stock was made in nuclease-free water to a final concentration of 1 mg ml^{-1} and stored at -80 °C.

Table 2-15. Reaction composition for the transcription reaction of Pentaprobes using the T7 Megascript kit.

Component	Volume (20 µl reaction)
Water, nuclease free	to 20 µl
rNTP mix (10 mM each)	8 µl
10 X reaction buffer	2 µl
DNA template	200 ng
T7 transcriptase enzyme mix	2 µl

2.1.10 Ribonuclease activity screens

2.1.10.1 Sodium acetate and ethanol precipitation

To purify RNA from activity assays, 1/10th of the volume of 3 M sodium acetate, pH 5.2, was added to the sample, followed by 2.5 volumes of ice-cold 200 proof ethanol. Samples were mixed gently by inverting several times then incubated at -20 °C overnight. Following incubation, samples were centrifuged at 13,000 *g* for 15 min at 4 °C to pellet the RNA. All supernatant was removed and the pellet washed with 800 µl 70% ethanol. Samples were centrifuged at 13,000 *g* for 10 min at 4 °C. All traces of ethanol were removed and the RNA pellet was air dried for 5 min before being resuspended in 10 - 20 µl nuclease-free water.

2.1.10.2 Ribonuclease activity assays with pentaprobe RNA substrates

Ribonuclease activity assays using pentaprobe RNA transcripts were set up in a 5 X assay buffer (50 mM $NaHPO_4$ pH 7.4, 200mM NaCl, 25 mM $MgCl_2$) with 1 mg ml^{-1} (20.2 pmol) Pentaprobe RNA. For each Pentaprobe RNA transcript tested, five reactions were set up:

(i) RNA only
(ii) addition of FitB
(iii) addition of FitB and 10 mM EDTA
(iv) addition of FitAB
(v) addition of CysE

All assays were prepared on ice with 5 X assay buffer, water and RNA (Table 2-16). FitAB was purified (section 2.1.6) and added to reaction iv, CysE was purified (section 2.1.7) and added to reaction v. FitB was purified (section 2.1.5.3) and added to reaction ii once all other reactions had been prepared to avoid degradation of FitB during the assay.

In preliminary assays, FitB activity was evaluated over a time course by stopping reactions by the addition of 10 µl 2 X formamide RNA loading dye after 5, 15 and 30 min. RNA only and EDTA control reactions were stopped after 30 min. Reactions were then stored at -20 °C. In subsequent assays, all reactions were stopped after 30 min. Ribonuclease activity was evaluated by urea-denaturing polyacrylamide gel electrophoresis (urea-PAGE) (section 2.1.10.3).

Table 2-16. Composition of pentaprobe assay 10 µl reactions.

Component	RNA Only	FitB	FitB & EDTA	FitAB	CysE
5 X Assay Buffer	2 µl	2 µl	-	2 µl	2 µl
5 X Assay Buffer + 50 mM EDTA	-	-	2 µl	-	-
Water	to 10 µl	to 10 µl	to 10 µl	to 10 µl	to 10 µl
Pentaprobe RNA (1 mg ml^{-1} = 20.2 pmol)	2 µl	2 µl	2 µl	2 µl	2 µl
FitB protein (approx. 0.10 mg ml^{-1} = 6.1 pmol $µl^{-1}$)	-	6 µl.	6 µl	-	-
FitAB protein (0.151 mg ml^{-1} = 6.09 pmol $µl^{-1}$)	-	-	-	6 µl	-
CysE protein (1.425 mg ml^{-1} = 44.12 pmol $µl^{-1}$)	-	-	-	-	0.6 µl

2.1.10.3 Urea-denaturing polyacrylamide gel electrophoresis.

Ten percent urea-PAGE gels were made fresh (Table 2-17) with ten-well combs. The PAGE gel solution (8 M urea, 1 X TBE, 10% acrylamide and water) was heated to 55 °C with a stirring rod to dissolve all the urea before APS and TEMED were

added. Gels were poured into a Hoeffer multi gel-caster and left to set at RT for approximately 1 hour. Gels were pre-run in 1 X TBE buffer for 30 min at 100 V. Wells were flushed with 1 X TBE to remove any remaining urea. Ribonuclease activity assay samples were thawed on ice then heated to 75 °C for 5 min and returned to ice. Low range ssRNA ladder (NEB) was loaded (0.5 µg) on the gel alongside 20 µl of each sample. Gels were run at 150 V for approximately 1 hour. Gels were post-stained with 1 X SYBR Safe DNA gel stain (Invitrogen) in 1 X TBE Buffer and visualised using an iBright imager (Invitrogen). Band sizes were determined by comparison with the low range ssRNA ladder (NEB).

Table 2-17. Composition of 10% urea-PAGE gels (to make five mini-gels).

Component	Quantity (50 ml total)	Final concentration
Urea	22 g	8 M
10 x TBE	5 ml	1 X
30% Acrylamide	16.7 ml	10 %
Diethyl pyruvate carbonate (DEPC) treated water	to 50 ml	-
10% APS	150 µl	0.3%
TEMED	30 µl	

2.1.10.4 Ribonuclease activity assays with oligonucleotides

Short RNA oligos, 20 - 30 nucleotides (nt) long, were designed in Geneious (Biomatters) based on the 923 Pentaprobe sequence. The oligos were designed to have ten overlapping nucleotides at each end to ensure all sequence combinations from pentaprobe 923 were still present. They were labelled 'Oligo 1-5' (Appendix B.3.) and ordered from IDT.

To screen activity of FitB against these oligos, assays were prepared with 5 X Assay Buffer (as in section 2.1.10.2 above) and 1 mg ml^{-1} (100 pmol) each RNA oligo. For each RNA oligo tested, three reactions were set up:

(i) RNA only
(ii) addition of FitB
(iii) addition of FitB and 10 mM EDTA

As with the Pentaprobe assays above, all assays were set up on ice to a final volume of 10 µl with nuclease free water. Reactions were incubated at 37 °C for 30 min and stopped by the addition of 10 µl 2 X formamide RNA loading dye. Reactions were analysed by urea-PAGE as above (section 2.1.10.3) except 15% urea-denaturing gels were used by adding 25 ml of 30% acrylamide instead of 16.7 ml when preparing the gels.

2.1.11 High Performance Liquid Chromatography and Mass Spectrometry

We worked in consultation with Grant Smolenski at MS3 Solutions to develop a new method using High Performance Liquid Chromatography (HPLC) followed by MS to deduce cut site(s) of the RNA pentaprobes. RNA pentaprobes cut by FitB were analysed by this approach.

2.1.11.1 Preparation of RNA for HPLC-MS

To prepare assay reactions for HPLC-MS, modifications were made to the purification of FitB and the pentaprobe ribonuclease activity assays. FitB was purified as in section 2.1.5.3 except a Tris Lysis buffer (50 mM Tris pH 7.4, 200 mM NaCl, 20 mM Imidazole) and a Tris Elution buffer (50 mM Tris pH 7.4, 200 mM NaCl, 1 M Imidazole) were used. The pentaprobe assay buffer was changed to a 5 X ammonium phosphate buffer (50 mM NH_4PO_4 pH 7.4, 200mM NaCl, 25 mM $MgCl_2$). The ribonuclease activity reactions were stopped with 4 µl 5 M ammonium acetate and 2 volumes of ice-cold 200 proof ethanol and stored at -20 °C overnight. Samples were centrifuged at 13,000 *g* for 20 min at 4 °C. The supernatant was removed and the RNA pellet washed with 70% ethanol and centrifuged for a further 20 min as above. All traces of ethanol were removed and the RNA was resuspended in 10 µl nuclease-free water. All samples were stored at -80 °C until taken to MS3 solutions for analysis.

2.1.12 Reverse transcription and cDNA sequencing

This method was developed for sequencing cut RNA pentaprobes from the ribonuclease activity assays to deduce the cut site(s) targeted by FitB.

RNA was prepared for cDNA analysis in the same way as for HPLC-MS (section 2.1.11.1).

2.1.12.1 Circularisation of RNA fragments

The fragmented pentaprobes from each reaction were circularised using T4 RNA Ligase I (NEB) according to manufacturer's instructions (Table 2-18). Reactions were incubated at 25 °C, shaking at 300 rpm for 1.5 hours and stopped by heat inactivation at 65 °C, shaking at 300 rpm for 15 min. RNA was precipitated by sodium acetate and ethanol precipitation (as in section 2.1.10.1) and resuspended in 10 µl nuclease free H_2O.

Table 2-18. T4 RNA ligase reaction for circularisation of RNA.

Component	Volume (20 µl reaction)	Final concentration
10 X Reaction Buffer	2 µl	1 X
RNA (1 µg)	10 µl	
T4 RNA Ligase	1 µl	10 units
RNase Inhibitor (40 µ μl^{-1})	0.5 µl	
PEG8000 (50%)	4 µl	10%
ATP (1 mM)	0.6 µl	30 µM
Water	to 20 µl	

2.1.12.2 First-strand cDNA synthesis.

The circular RNA was used as a template to synthesise the first cDNA strand using qScript XLT cDNA Supermix (QuantaBio). The reaction was prepared on ice following manufacturer's instructions (Table 2-19). All Components were combined and vortexed briefly to mix. The reaction was centrifuged for 3 sec before incubation at a series of temperatures: 25 °C for 5 min, 42 °C for 1 hour, 85 °C for 5 min followed 4 °C indefinitely. The RNA:cDNA hybrid was precipitated from the reaction via a sodium acetate and ethanol precipitation as in section 2.1.10.1and resuspended in 10 µl water.

Table 2-19. Q-script XLT cDNA Supermix reaction composition.

Component	Volume (20 µl reaction)	Final concentration
qScript XLT cDNA Supermix (5 X)	4 µl	1 X
RNA	10 µl	varies
Water	to 20 µl	

2.1.12.3 Second-strand cDNA synthesis.

The second cDNA strand was generated by nick translation using the RNA:cDNA hybrid from the first-strand cDNA synthesis reaction. The 10 X Second-strand Buffer was composed of 10 X NEB-Buffer 2 (50 mM NaCl, 10 mM Tris-HCl, 10 mM $MgCl_2$, 1 mM DTT), 10 X T4 DNA Ligase Reaction Buffer (NEB) (50 mM Tris-HCl, 10 mM $MgCl_2$, 10 mM DTT, 1 mM ATP) and 10 X RNase H Reaction Buffer (NEB) (75 mM KCl, 50 mM Tris-HCl, 3 mM $MgCl_2$, 10 mM DTT) in a 1:1:1 ratio. All the second strand reaction components (Table 2-20) were added in order to the RNA:cDNA hybrid and vortexed gently to mix. The reaction was incubated at 16 °C for 2 hours then placed on ice before the addition of 25 µl 0.25 M sodium EDTA, pH 7.5. The cDNA was precipitated out of solution by adding ammonium acetate (final concentration of 1 M) and ethanol (final concentration 75%) and incubating at -20 °C for 2 hours. The reaction was then centrifuged at 13,000 *g* for 20 min at 4 °C to pellet cDNA and supernatant was removed. The pellet was resuspended in 20 µl NEB-buffer 2 and the cDNA concentration measured by NanoDrop™.

Table 2-20. Composition of second-strand cDNA synthesis reaction.

Component	Concentration
RNA:cDNA hybrid	1 µg
DEPC-treated water	-
10 mM dNTP mix	250 µM each (dATP, dCTP, dGTP, dTTP)
10 X Second-strand Buffer	1 X
E. coli DNA Pol I (NEB)	250 U ml^{-1}
E. coli RNase H (NEB)	8.5 U ml^{-1}
E. coli T4 DNA Ligase (NEB)	30 U ml^{-1}

2.1.12.4 Generation of blunt ends

Blunt ends were generated on cDNA strands using DNA Polymerase I (DNA Pol I), Large (Klenow) Fragment (NEB). A mix of dNTPs, containing 33 µm dATP, dCTP, dGTP and dTTP, were added to cDNA followed by 1 unit of Klenow per µg cDNA. The reaction was incubated at 25 °C for 15 min and stopped by addition of EDTA to a final concentration of 10 mM and heating to 75 °C for 20 min. The cDNA was precipitated out of solution as before by addition of ammonium acetate (final concentration of 1 M) and ethanol (final concentration 75%) and incubation at -20 °C for 2 hours. The reaction was centrifuged at 13,000 *g* for 20 min at 4 °C to pellet the cDNA and all supernatant removed. The cDNA was resuspended in 10 µl nuclease-free water.

2.1.12.5 Sequence preparation

The cDNA product with blunt ends was ligated into the pGEM®-T Easy Vector (Promega) as per the manufacturer's instructions (Table 2-21). The molar ratio of 1:1, insert:vector, has been optimised in the pGEM®-T Easy Vector system. All components were mixed and incubated at RT for 1 hour.

Table 2-21. Composition of the ligation reaction using the cDNA product and pGEM®-T Easy Vector.

Component	Quantity (10 µl reaction)
2 X Rapid ligation buffer, T4 DNA Ligase	5 µl
pGEM®-T Easy Vector (50 ng)	1 µl
cDNA insert	0.8 – 1 ng *
T4 DNA Ligase (3 Weiss units μl^{-1})	1 µl
Nuclease-free water	to 10 µl

*based on a 1:1 molar ratio of insert:vector.

The ligation reaction was directly transformed into chemically competent *E. coli* DH5α as in section 2.1.1. Transformants were screened for the insert by colony PCR as in section 2.1.8.1. Plasmids containing the insert were extracted using the Qiagen Miniprep kit as per manufacturer's instructions and sequenced by the Massey Genome Sequencing Service.

2.2 Results & Discussion

2.2.1 Purification of FitB

To biochemically characterise activity of FitB we needed to stabilise purified protein to avoid degradation before or during ribonuclease activity assays. Previous attempts in our lab to stabilise FitB by purifying with 10% glycerol resulted in relatively stable but inactive FitB (Joanna Hicks, unpublished, 2017). We tested the stabilisation effects of 1% Triton X-100 and 5% glycerol by adding these to the FitB purification buffers. As the addition of detergents has the potential to interfere with activity we also tested the stability of FitB when kept at low temperatures for the duration of the purification steps.

FitB was successfully purified by IMAC with the addition of 1% Triton X-100 and 5% glycerol in the purification buffers. The chromatogram of the IMAC purifications under each condition and the corresponding SDS-PAGE gels (Figure 2-2) show FitB elutes at approximately 30 - 35% elution buffer, corresponding to 300 – 350 mM imidazole. Non-specific, unbound proteins elute early in the elution gradient (flow through). The 280 nm trace of these proteins (at 0 – 20 ml) was cropped out of the chromatogram for scaling purposes to emphasise the peak of interest (peak fraction). To assess if FitB was in its native, folded form, the peak fraction was run on a Native-PAGE gel which, unlike SDS-PAGE, does not denature the proteins. There appeared to be a small amount of FitB in its native form from the purification with 1% Triton X-100 as indicated by faint bands on the Native-PAGE gel (Figure 2-2d), however, it could not be used in ribonuclease activity assays as the protein precipitated out of solution after a very short time. No bands corresponding to folded FitB could be seen on the Native-PAGE gel of the purification with 5% glycerol (Figure 2-2d) signifying FitB was unfolded and thus of no use in ribonuclease activity assays.

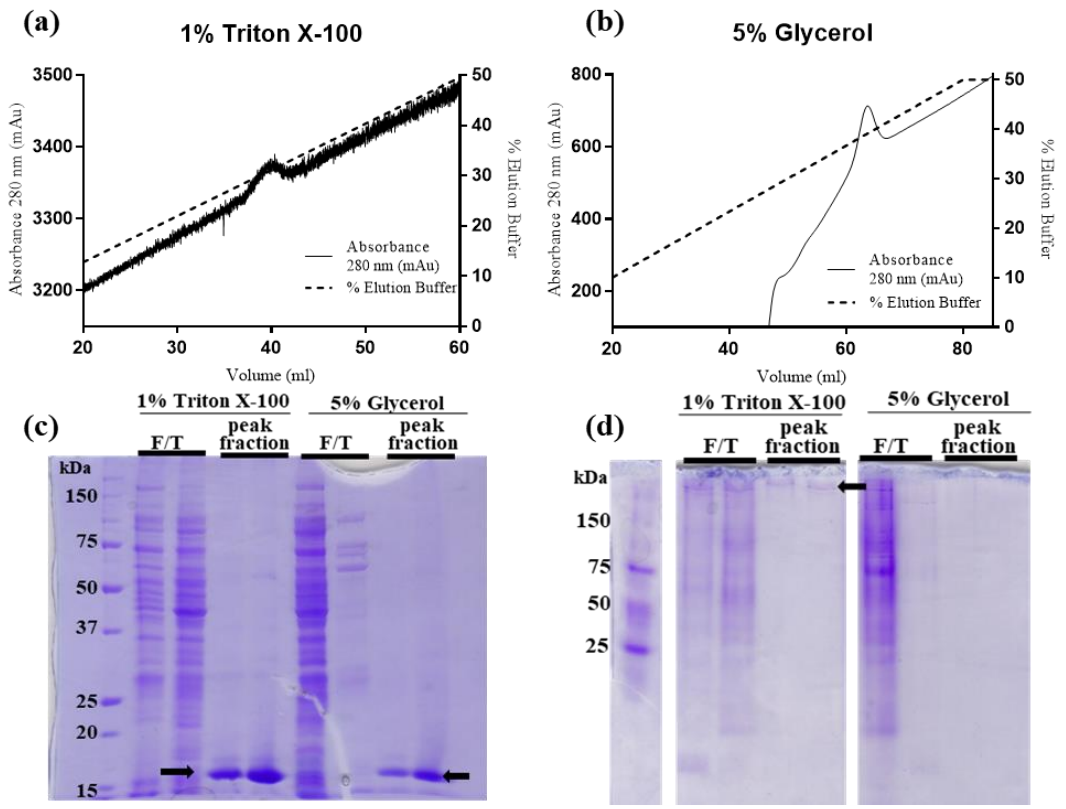

Figure 2-2. IMAC purification and protein analysis of FitB purified with 1% Triton X-100 and 5% glycerol. (a, b) Chromatograms from purification with 1% Triton X-100 (a) and 5% glycerol (b) depict the UV absorbance (280 nm) and elution of FitB under each condition. The flow through fractions (0 – 20 ml) are cropped out for scaling purposes. (c) 15% SDS-PAGE gel shows non-specific proteins (flow through, F/T) and protein eluted at 30 – 35% elution buffer (peak fraction). (d) 12% Native-PAGE gel of proteins in the F/T and peak fraction. (c, d) FitB is indicated by a black arrow. Molecular weight of each band is determined from a Precision Plus Protein Standard ladder. Molecular weight (kDa) values are labelled.

The third method trialled to stabilise FitB was keeping the protein at a low temperature before and after purification. This was achieved by keeping the cell lysate on ice or at 4 °C during sonication and centrifugation prior to purifying (see Section 2.1.3 for details). The fraction collection tubes were set up on ice so FitB was exposed to low temperatures once eluted from the column. The chromatogram of this IMAC purification and the corresponding SDS and Native-PAGE gels (Figure 2-3) show under these conditions FitB elutes from the column with approximately 20% elution buffer (corresponding to 200 mM imidazole). Interestingly, on the SDS-PAGE gel there is a band corresponding to FitB (approx. 16 kDa), suggesting some FitB expressed in the *E. coli* expression host is insoluble (Figure 2-3b). As the concentration of soluble FitB in the peak fraction was sufficient for our requirements we did not investigate the insoluble protein further.

Native-PAGE analysis revealed FitB was in its native, folded form (Figure 2-3c). When attempting to concentrate FitB using spin concentrators it rapidly precipitated out of solution. Unconcentrated FitB stored on ice appeared to precipitate after approximately 2 hours. To avoid precipitation of FitB by concentration, the maximum possible volume of FitB (6 µl), after buffer and substrate were accounted for, was added to the ribonuclease activity assays (see Section 2.1.10.2).

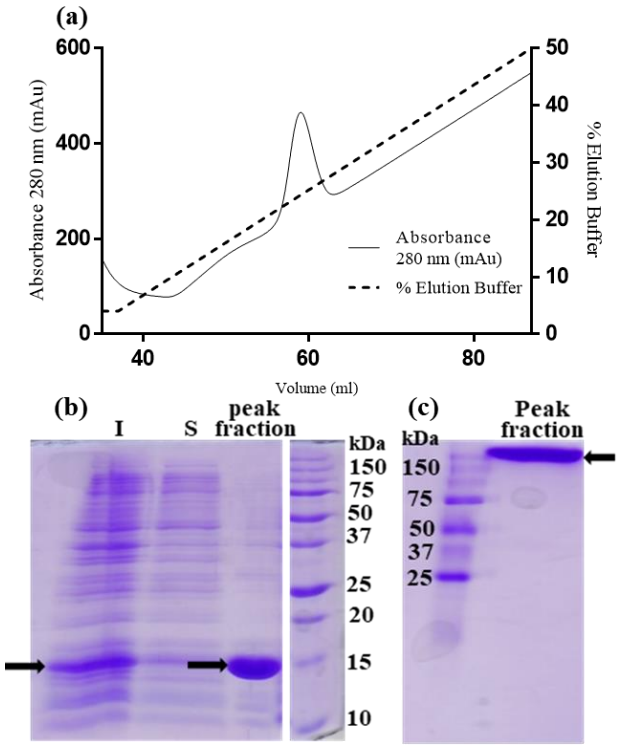

Figure 2-3. IMAC purification of FitB on ice and protein analysis. (a) Chromatogram depicts the UV absorbance (280 nm) and elution of FitB. 0 - 35 ml at the beginning of the chromatogram has been cropped for scaling purposes. (b) 15% SDS-PAGE gel shows insoluble protein (I), soluble protein (S) and protein eluted at approx. 20% elution buffer (peak fraction). (c) 12% Native-PAGE gel of protein eluted in the peak fraction. (b, c) FitB is indicated by a black arrow. Molecular weight of each band is determined from a Precision Plus Protein Standard ladder. Molecular weight (kDa) values are labelled.

Out of the three methods trialled, both the addition of Triton X-100 and maintaining the protein at low temperatures resulted in protein in its native, folded form, however this folded form was short lived as both methods resulted in precipitated, unfolded protein after short time periods. Maintaining FitB at low temperatures kept FitB soluble for longer so this method was selected for future purifications. This method also had the advantage of not adding components, such as detergents, that could interfere with the ribonuclease activity assays.

Many VapC proteins are insoluble when expressed in *E. coli* and purified without VapB. Mycobacterial VapC proteins are only soluble when expressed and purified as the VapBC complex (McKenzie *et al.*, 2012a; Robson *et al.*, 2009). Robson *et al.* (2009) attempted to express and purify VapB and VapC from *M. smegmatis* individually in an *E. coli* expression system but found neither were soluble. Similarly, VapC from *M. tuberculosis* could not be purified on its own so was obtained by expressing and purifying the VapBC complex followed by a trypsin digest to degrade VapB and anion exchange chromatography to isolate VapC (McKenzie *et al.*, 2012a). The insolubility of VapC during expression is presumably due to its toxicity to the host. $VapC_{PAE0151}$ protein from *P. aerophilum* is an exception as it can be expressed and purified on its own using an *E. coli* expression and purification system (Bunker *et al.*, 2008). However, $VapC_{PAE0151}$ is only soluble at pH 9.2 which would negate any toxicity issues to *E. coli*. FitB is also an exception as it is soluble when expressed on its own in *E. coli*, at neutral pH, although it is very unstable in solution following purification. We took advantage of this by using an *E. coli* expression system and stabilising FitB during purification to prolong protein integrity for the duration of the ribonuclease activity assays.

2.2.2 Producing a negative control for ribonuclease assays

A negative control was required for the ribonuclease activity assays to ensure any cleavage of the RNA substrates was due to ribonuclease activity of FitB and not an artefact of the pentaprobe system or a result of contaminating ribonucleases from the purification step or in the assay buffers.

2.2.2.1 FitAB toxin-antitoxin complex

FitAB was purified by IMAC (see section 2.1.4) and eluted from the column at 20% elution buffer, corresponding to approx. 200 mM imidazole (Figure 2-4). Both FitA and FitB were present in the peak fraction (Figure 2-4b). On the SDS-PAGE gel, a prominent band at approximately 8.4 kDa in the insoluble fraction indicated a large portion of FitA was insoluble. Analysis by Native-PAGE indicated there was disproportionately more FitB protein in its native, folded form than there was FitA (Figure 2-4c). Due to the large presence of FitA in the insoluble fraction and the instability of antitoxins in TA systems it is probable FitA unfolded during the purification process.

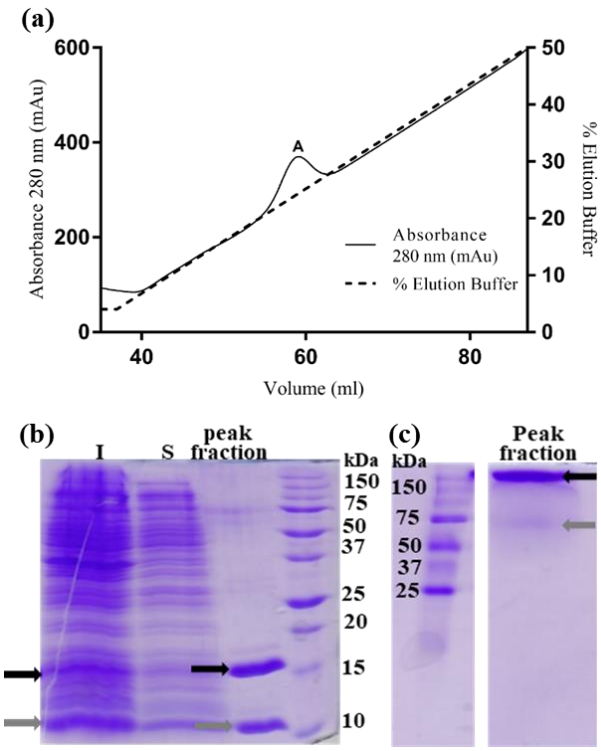

Figure 2-4. IMAC purification of FitAB and protein analysis. (a) Chromatogram depicts the UV absorbance (280 nm) and elution of FitAB. 0- 35 ml at the beginning of the chromatogram has been cropped for scaling purposes. (b) 15% SDS-PAGE gel shows insoluble protein (I), soluble protein (S) and protein eluted at approx. 20% elution buffer (peak fraction). (c) 12% Native-PAGE gel of protein eluted in the peak fraction. (b, c) FitB is indicated by a black arrow, FitA is indicated by a grey arrow. Molecular weight of each band is determined from a Precision Plus Protein Standard ladder. Molecular weight (kDa) values are labelled.

Unexpectedly, when FitAB was added to the ribonuclease activity reactions, the RNA pentaprobes were cleaved in the same way as the FitB ribonuclease activity reactions (Figure 2-5). This would have been a consequence of FitA degradation during purification, leaving active FitB. FitAB was therefore not an appropriate negative control for the ribonuclease activity assays.

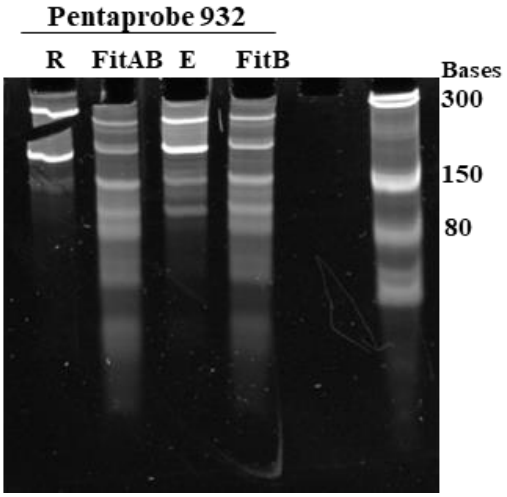

Figure 2-5. Ribonuclease activity assays with FitAB control on a 10% urea-denaturing PAGE gel. The RNA substrate is labelled at the top (Pentaprobe 932). Reactions consist of RNA only control (R), FitAB negative control (FitAB), FitB with EDTA (E) and FitB (FitB). Size of bands are indicated by a Low range ssRNA ladder on right side of gel, bases are labelled.

2.2.2.2 FitB mutant

Previously in our lab, ribonuclease activity of $VapC_{PAE0151}$ from *Pyrobaculum aerophilum* was abrogated by mutating aspartic acid (Asp^{92}) to asparagine and glutamic acid (Glu^{38}) to glutamine (Duyvestyn, 2012). These residues are highly conserved in the catalytic site of PIN-domains (Arcus *et al.*, 2011) so mutation to positively charged residues alters the charge of the catalytic pocket, preventing cations from binding and subsequently preventing magnesium-dependent ribonuclease activity. We attempted to inhibit the ribonuclease activity of FitB by mutating the homologous PIN-domain residues, Asp^{104} and Glu^{42}. Using inactive FitB as a negative control would ensure the ribonuclease activity is due to the PIN-domain active site of FitB and not an artefact of the purification system or the buffers.

The first method used to generate the FitB mutants was the two-halves mutagenesis method. For each mutant, the forward and reverse half of the gene is amplified individually with primers containing the desired mutation. Each half is annealed in a single PCR reaction to generate the complete mutated gene. Agarose gel electrophoresis showed the PCR reactions were successful as the PCR products seen on the gel were the correct size (Figure 2-6). The *fitB* D104N mutagenesis forward reaction generated a 329 base-pair (bp) product and the reverse reaction generated a 133 bp product (Figure 2-6a). *FitB* E42Q mutagenesis forward reaction

generated a 142 bp product and the reverse reaction generated a 310 bp product (Figure 2-6c). The subsequent PCR reaction, using each half reaction, resulted in complete gene products, 417 bp long, for both *fitB* D104N and *fitB* E42Q mutagenesis (Figure 2-6).

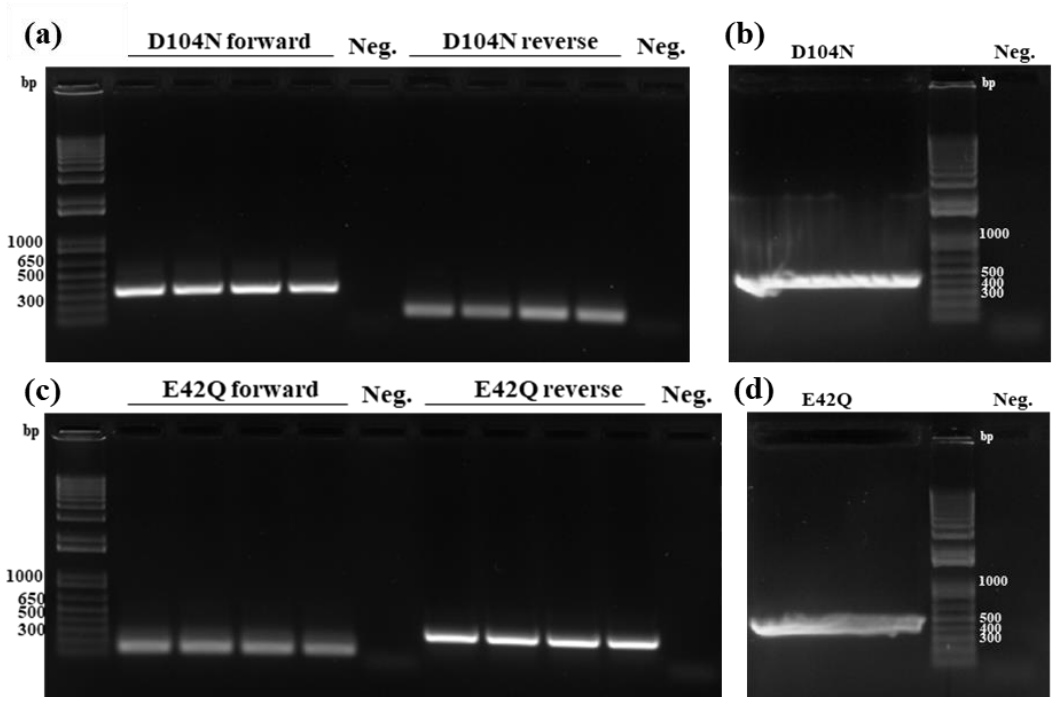

Figure 2-6. PCR products of the two-halves mutagenesis reactions on 1% TAE agarose gels. (a) *FitB* D104N forward and reverse half sequences. (b) *FitB* D104N complete gene product. (c) *FitB* E42Q forward and reverse half sequences. (d) *FitB* E42Q complete gene product. Negative controls (Neg.) show no amplification. The size of the bands are indicated by a 1 kb$^+$ ladder, number of bases are labelled.

The PCR products were ligated into the pET28b-pstI plasmid, between PstI and XhoI restriction sites, and transformed into chemically competent *E. coli* DH5α. Transformed colonies were screened for the presence of plasmid with the gene insert by colony PCR followed by agarose gel electrophoresis of the PCR product (Figure 2-7). There were no more than four colonies from each of the transformations so they were all taken for screening by colony PCR. Two of the colonies from the D104N transformation contained plasmids with the insert, represented by a 620 bp band on the agarose gel (Figure 2-7). The third colony contained plasmid without the insert, represented by a faint band at 362 bp on the agarose gel (Figure 2-7). All four colonies from the E42Q transformation contained plasmid with no insert (Figure 2-7) suggesting the *fitB* E42Q gene was not ligated into the plasmid.

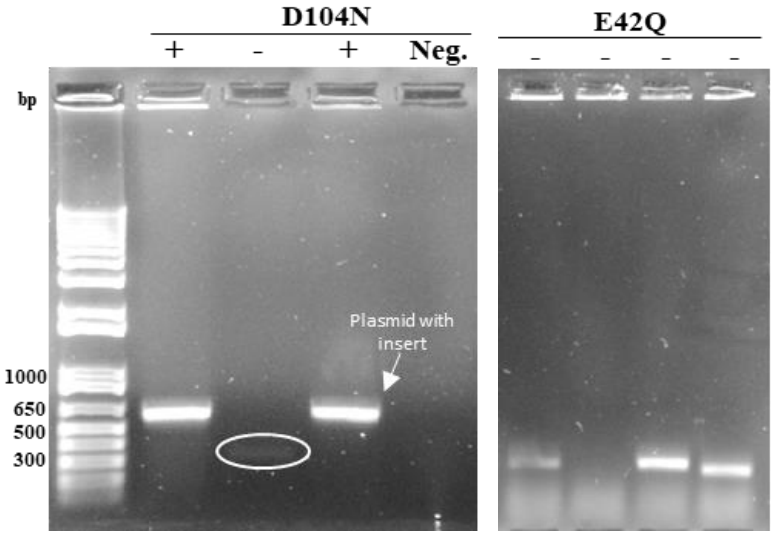

Figure 2-7. Colony PCR reactions on a 1% TAE agarose gel screening for plasmids containing mutated *fitB* genes following transformation into E. coli DH5α. Each lane contains PCR amplified plasmid from a single colony transformed with *fitB* D104N plasmid (D104N) or *fitB* E42Q plasmid (E42Q). Each lane is labelled + (plasmid with gene insert) or – (no or empty plasmid). Plasmid containing the gene insert is indicated by a white arrow and labelled. Empty plasmid is indicated by a white circle. The PCR negative control (Neg.) has no plasmid DNA. The size of the bands are indicated by a 1 kb$^+$ ladder, number of bases are labelled.

Sequencing of the plasmids with the *fitB* D104N gene mutation from the two positive transformants revealed the aspartic acid codon was successfully mutated to the arginine codon (Figure 2-8). However, two adenine bases in the gene sequence had been deleted (Figure 2-8), causing a frame shift in the codon sequence so the protein would be incorrectly translated.

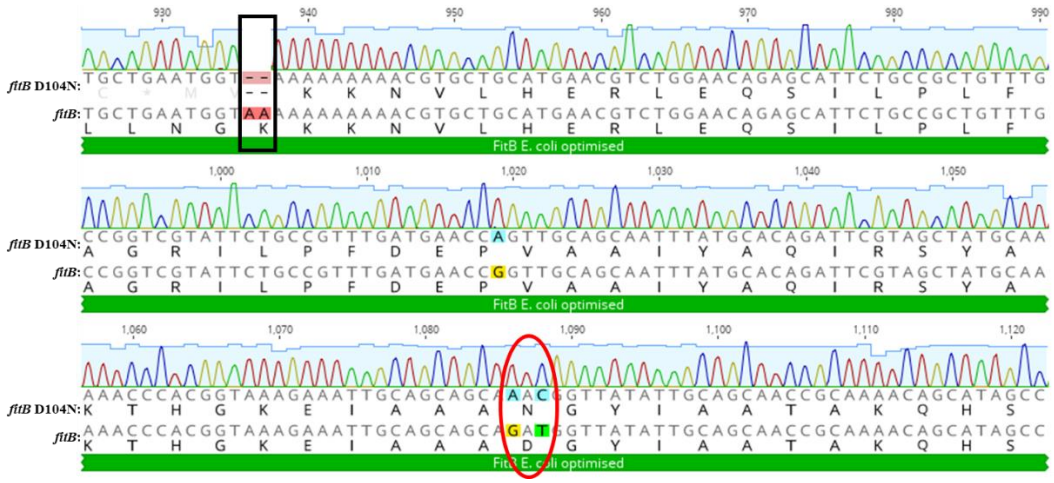

Figure 2-8. Pairwise alignment of *fitB* pET28b-pstI with *fitB* D104N plasmid synthesised by two-halves mutagenesis. Only the alignment from nucleotides 925 - 1122 is shown. The sequencing chromatogram shows the signal intensities of each nucleotide (A, red; T, green; C, blue; G, yellow). The nucleotide sequence is given for each sequence with the translated amino acid sequence immediately underneath. The deletion in *fitB* D104N sequence is indicated by a black box. The mutation from aspartic acid (D) to asparagine (N) is indicated by a red circle.

We were unable to generate the E42Q mutant by this protocol so we tried a site-directed mutagenesis method using Platinum Superfi^{TM} DNA polymerase. In contrast to mutagenesis by the two-halves method, where two halves of the sequence were mutated then joined together, the site-directed mutagenesis method introduces a point mutation directly into circular plasmid DNA. Template DNA is removed by DpnI digestion, as this targets methylated DNA, leaving plasmid containing the desired mutation.

To confirm the presence of mutated plasmid following PCR and DpnI digestion, the PCR reaction for E42Q mutagenesis was run on an agarose gel (Figure 2-9). The high-molecular weight band seen on the gel corresponds to full-length plasmid, *fitB* pET28b-pstI (Figure 2-9). The negative control did not contain plasmid template so the low-molecular weight band on the gel is most likely primer-dimers (Figure 2-9). After transforming the PCR product into *E. coli* DH5α and extracting the plasmid, the plasmid DNA was sequenced. The glutamic acid residue had been correctly mutated to glutamine, however, the primer sequence was duplicated in the plasmid sequence (Figure 2-10) so the protein could not be expressed.

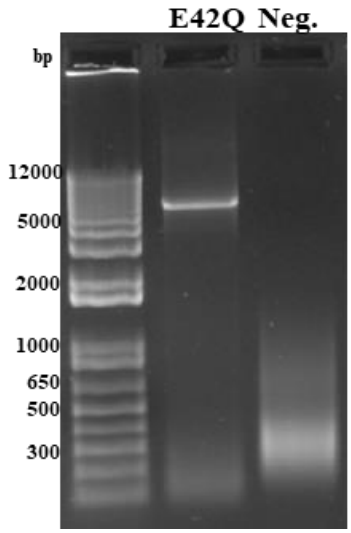

Figure 2-9. PCR product from the *fitB* E42Q site-directed mutagenesis reaction on a 1% TAE agarose gel. The PCR reaction (E42Q) contains a band at approx. 5600 bp corresponding to the plasmid DNA. The negative control (Neg.) contains a small band corresponding to primer-dimers. The size of the bands are indicated by a 1 kb^{+} ladder with bp values labelled.

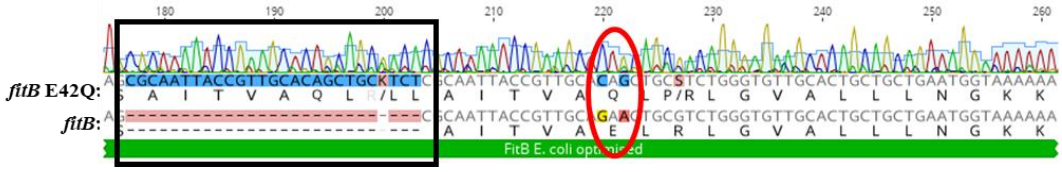

Figure 2-10. Pairwise alignment of *fitB* pET28b-pstI with *fitB* E42Q plasmid synthesised by site-directed mutagenesis. The alignment from nucleotides 175 -261 is shown. The sequencing chromatogram shows the signal intensities of each nucleotide (A, red; T, green; C, blue; G, yellow). The nucleotide sequence is given for each sequence with the translated amino acid sequence immediately underneath. The duplicated sequence in *fitB* E42Q and misalignment with *fitB* is denoted by a black box. The mutation from glutamic acid (E) to glutamine (Q) is indicated by a red circle.

Neither of the mutagenesis protocols used resulted in viable mutants to express and use in the ribonuclease activity assays as a negative control. Due to time constraints, we were unable to trouble-shoot and optimise the mutagenesis reactions so alternative avenues were investigated for a negative control.

2.2.2.3 Cysteine biosynthesis protein, CysE

Concurrently to this project, a protein involved in cysteine biosynthesis in *N. gonorrhoeae* was being expressed and purified in our lab using the same protocols as for FitB. This protein, CysE, is a serine acetyltransferase which catalyses the acetylation of L-serine to *O*-acetylserine, the first step in the synthesis of L-cysteine (Hicks & Mullholland, 2018; Kredich & Tomkins, 1966). The structure of CysE does not resemble that of ribonuclease proteins (Olsen *et al.*, 2004)

and functional studies have not shown any ribonuclease activity (Kredich & Tomkins, 1966; Pye *et al.*, 2004). Therefore, as CysE was cloned, expressed and purified the same as FitB it was chosen as a negative control for the ribonuclease activity assays. This ensures cleavage of pentaprobe RNAs by FitB is not an artefact of the pentaprobe system or due to contaminating ribonucleases from the purification step.

2.2.3 Ribonuclease activity of FitB

Pentaprobe RNAs differ in sequence and, over the suite of RNAs, cover every combination of five bases. FitB was screened for ribonuclease activity against pentaprobe RNA substrates 922, 923, 924, 925, 926, 927 and 932. Pentaprobe 932 is the complementary sequence of pentaprobe 926 so, presumably, if FitB is a sequence-specific ribonuclease, both pentaprobes would be cleaved in the same way. Nonetheless, Pentaprobe 932 was included in ribonuclease activity testing as, if it was cleaved well by FitB, we had the suite of RNA oligos already in the lab from *M. smegmatis* activity screens (McKenzie *et al.*, 2012a).

Preliminary assays were stopped by the addition of formamide loading dye after five, 15 and 30 minutes incubation to determine the length of time for optimal activity of FitB. FitB exhibited ribonuclease activity after a minimum of five minutes (Figure 2-11) but 30 minutes incubation allowed for more efficient fragmentation of all the pentaprobes.

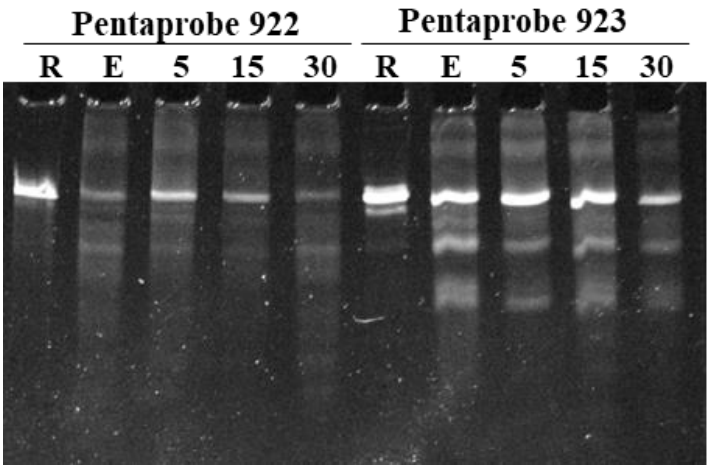

Figure 2-11. Ribonuclease activity time-course assay on a 10% urea-denaturing PAGE gel. Each set of reactions are labelled with the name of the RNA pentaprobe substrate (Pentaprobe 922 and Pentaprobe 923) accordingly. All reactions with FitB are labelled with the time at which they were stopped (five min, 5, 15 min, 15, 30 min, 30). Negative controls consisted of RNA only, R, and FitB with EDTA, E. Each band corresponds to an RNA fragment in the reaction, with lower molecular weight bands appearing lower on the gel.

Based on these ribonuclease activity assays all subsequent activity screens were carried out for 30 minutes. FitB displayed ribonuclease activity against all the pentaprobes tested (Figure 2-12). Each pentaprobe was cleaved at different positions yielding different sized RNA fragments (Figure 2-12). The differing banding patterns across different pentaprobe RNA transcripts suggests FitB targets a specific sequence and/or secondary structure. The number of bands on the urea-PAGE gel is indicative of the amount of times FitB cuts the RNA substrates. Some pentaprobes have a few prominent bands while others have multiple small bands (Figure 2-12). It is likely that FitB has an optimal cut site and other suboptimal cut sites that are present in these pentaprobe sequences, consistent with the ribonuclease activity seen for other VapC proteins (McKenzie *et al.*, 2012a; McKenzie *et al.*, 2012b). The banding patterns for all the pentaprobes tested are different from that seen by VapC proteins from *M. smegmatis* (McKenzie *et al.*, 2012b), *P. aerophilum* (McKenzie *et al.*, 2012a) and *M. tuberculosis* (Sharrock *et al.*, 2018) indicating the sequence-specific activity of FitB is unique to this protein and is not an artefact of the pentaprobe assay.

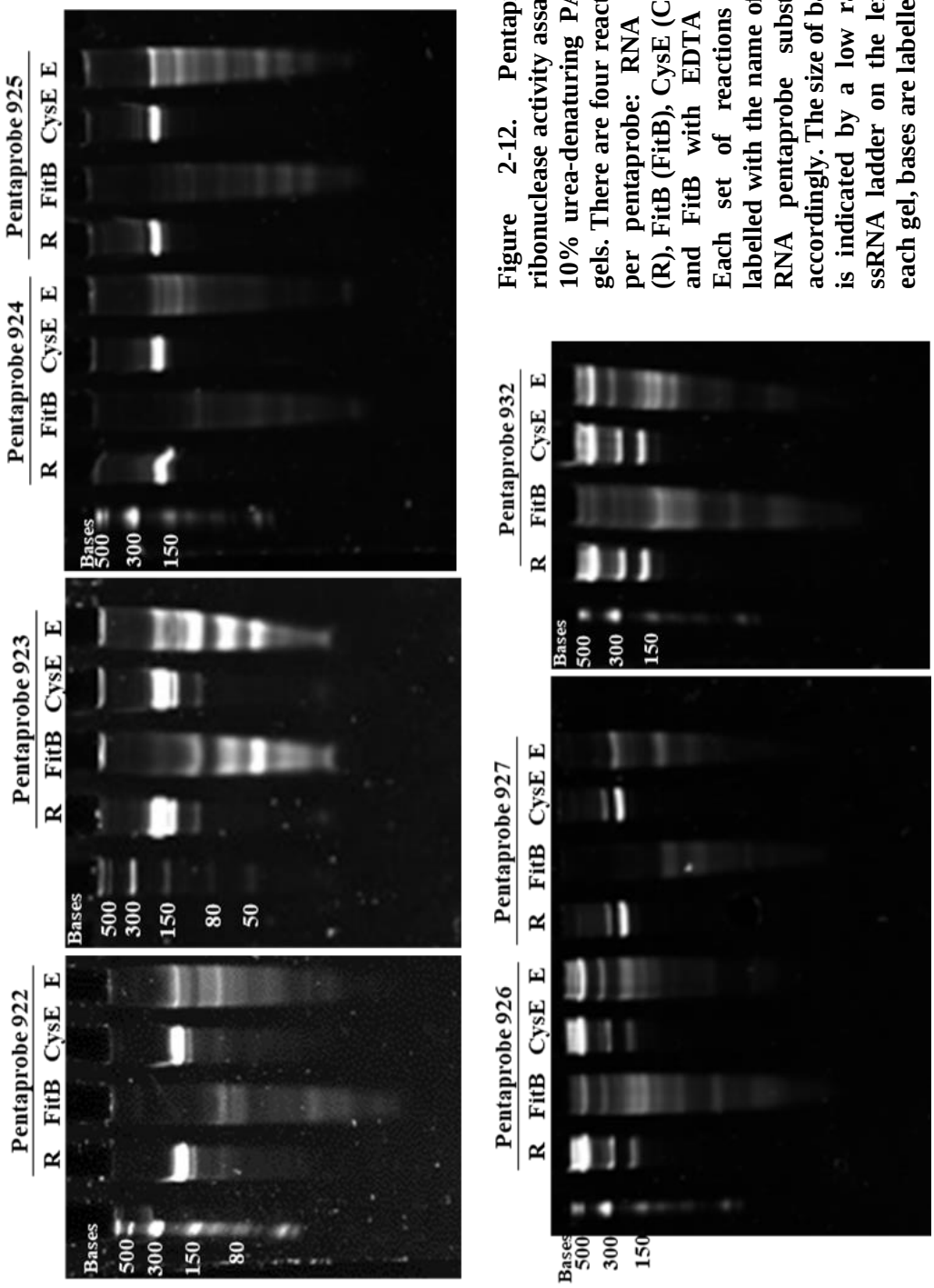

Figure 2-12. Pentaprobe ribonuclease activity assay on 10% urea-denaturing PAGE gels. There are four reactions per pentaprobe: RNA only (R), FitB (FitB), CysE (CysE) and FitB with EDTA (E). Each set of reactions are labelled with the name of the RNA pentaprobe substrate accordingly. The size of bands is indicated by a low range ssRNA ladder on the left of each gel, bases are labelled.

The EDTA reaction is used as a negative control as it chelates Mg^{2+} ions to inhibit the Mg^{2+}-dependent ribonuclease activity of FitB. Ribonuclease activity of FitB was greatly reduced with the addition of EDTA but not inhibited completely (Figure 2-12). This could be due to carryover of Mg^{2+} or other divalent cations when purifying FitB. As FitB was expressed on its own (without FitA) it is possible that FitB coordinated a metal-cation present in *E. coli* and maintained the ion in its catalytic centre during purification. Consequently, when FitB was added to the ribonuclease reactions, some of the protein would be in its active state without needing Mg^{2+} from the assay buffer. If the interaction between Mg^{2+} and the catalytic residues of FitB is stronger than the attraction of Mg^{2+} to EDTA then this would explain why there is some residual activity in the EDTA control reactions. In this scenario, free cations in the buffer would be chelated but the active FitB proteins from the purification would be able to act on the substrate. When the same reactions were tested with other VapC proteins (McKenzie *et al.*, 2012a; McKenzie *et al.*, 2012b; Sharrock *et al.*, 2018) the EDTA control inhibited total activity of VapC. In these assays, VapC was expressed and purified with its cognate VapB antitoxin followed by a trypsin digest to degrade VapB (McKenzie *et al.*, 2012a; McKenzie *et al.*, 2012b; Sharrock *et al.*, 2018). By purifying VapC in this way, the catalytic centre where Mg^{2+} is coordinated would have been blocked by an arginine residue of VapB, preventing VapC from coordinating Mg^{2+} when expressed in *E. coli*. Therefore, when VapC was added to the pentaprobe reactions it only became active once coordinating Mg^{2+} from the assay buffer, or in the case of the EDTA control, remained inactive as all the Mg^{2+} would have been chelated by EDTA.

The cysteine biosynthesis protein, CysE, was used as a control to ensure cleavage was a result of FitB activity and not ribonuclease contamination from the expression or purification steps. The pentaprobe RNA transcripts showed no fragmentation upon incubation with CysE in place of FitB (Figure 2-12), confirming ribonuclease activity is specific to FitB.

Of all the RNA pentaprobes screened, Pentaprobe 923 showed the simplest banding pattern when cleaved by FitB, with three prominent RNA fragments on a urea-PAGE gel, approximately 100-nt, 75-nt and 50-nt long (Figure 2-12). There are also some fainter bands present on the gel, less than 50-nt long, suggesting the

pentaprobe is further fragmented into smaller stands which could be due to multiple cut sites on the pentaprobe.

To further investigate the cut site(s) targeted by FitB on pentaprobe 923 we designed shorter oligos, approximately 30-nt long, based on the pentaprobe sequence. Five oligos were designed with ten bases overlapping at each end to ensure all possible nucleotide combinations within the sequence were covered. Based on the results from the pentaprobe assay, we hypothesised at least one of the shorter oligos would contain a cut site so would be cleaved by FitB, provided the ribonuclease activity was sequence-specific. The results of the oligonucleotide assays were assessed on a urea-denaturing PAGE gel (Figure 2-13).

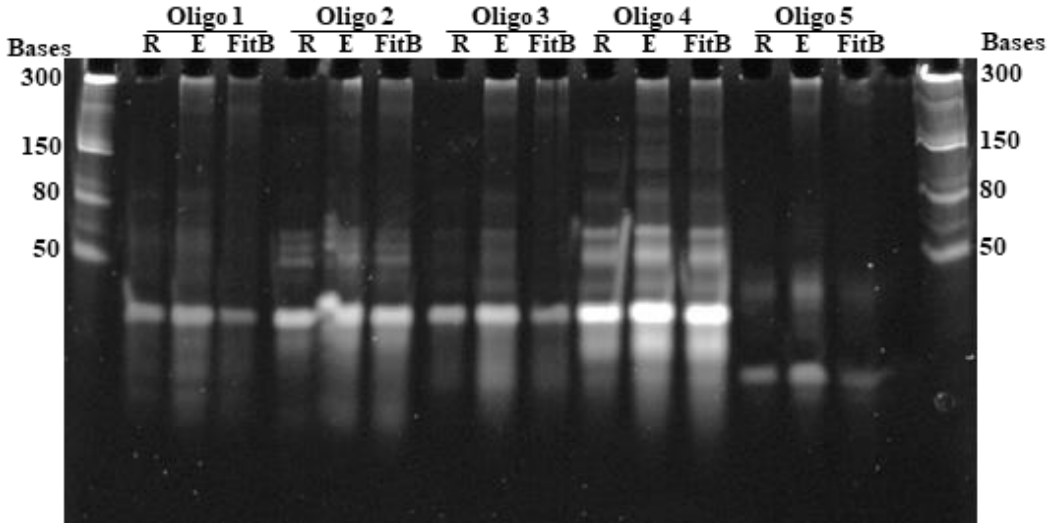

Figure 2-13. Oligonucleotide ribonuclease activity assay on a 15% urea-denaturing PAGE gel. There are three reactions per oligo: RNA only (R), FitB with EDTA (E) and FitB (FitB). Each set of reactions are labelled with the name of the RNA oligonucleotide substrate accordingly. The set of oligonucleotides is based on the RNA Pentaprobe 923 sequence. The size of bands is indicated by a low range ssRNA ladder on the left of the gel, bases are labelled.

Contrary to our hypothesis, none of the oligos were cleaved by FitB. Intriguingly, there appears to be a band in the wells and more 'smearing' of higher molecular weight products higher on the urea gel for the assays that contained FitB (FitB and the FitB with EDTA control) but not in the RNA only controls (Figure 2-13). The same feature is seen in the pentaprobe assays (Figure 2-12). This is likely FitB bound to RNA, which would be too large to migrate through the gel so remains in the wells or runs higher on the gel due to its increased molecular weight.

RNA binding has been seen for *M. smegmatis* VapC (McKenzie *et al.*, 2012b) and *M. tuberculosis* VapC4 (Sharp *et al.*, 2012) but not for other *M. tuberculosis* VapCs,

Rv0065 and Rv0617 (Ahidjo *et al.*, 2011) suggesting this characteristic is unique to certain VapC proteins. It is evident, FitB can bind RNA without cleaving it. This is also seen for VapC4 which binds short RNA oligos, 30-nt long, at specific sequences (ACGC or AC(A/U)GC) without cleaving them (only 2% of the bound RNA was cleaved) (Sharp *et al.*, 2012). RNA binding by VapC4 was proposed to be a mechanism of translation inhibition *in vivo*, more-so than the actual cleavage of RNA (Sharp *et al.*, 2012). Due to structural homology, it is possible FitB also binds mRNA transcripts at a specific sequence to inhibit translation in *N. gonorrhoeae*.

The lack of ribonuclease activity against RNA oligos by FitB differs from the activity seen by VapC proteins from *M. smegmatis* (McKenzie *et al.*, 2012b), *P. aerophilum* (McKenzie *et al.*, 2012a) and *M. tuberculosis* (Sharrock *et al.*, 2018). Each of these VapC proteins cleaved shorter oligos that corresponded to a cut pentaprobe. Interestingly, the ribonuclease activity displayed by *M. smegmatis* VapC against the oligos was much less efficient than the cleavage of the full length pentaprobe (McKenzie *et al.*, 2012b). Further investigation into this revealed the importance of secondary structure in conjunction with the target sequence for optimal RNA cleavage by *M. smegmatis* VapC (McKenzie *et al.*, 2012b).

McKenzie *et al.* (2012b) found *M. smegmatis* VapC cleaves the RNA sequence AUA(U/A) where there is a hairpin structure immediately downstream (Figure 2-14). Secondary structures associated with three experimentally cut sequences were predicted using RNAfold as part of the Vienna RNA secondary structure server (Hofacker, 2003) and aligned with 39 genes to build a consensus model of the most probably sequence and structure motif targeted by VapC (Figure 2-14). Based on comparison between RNA substrates with variations of the predicted target motif it was concluded that VapC cuts RNA most efficiently at the predicted cut site, and will cut substrates without the complete motif but to a lesser extent (Figure 2-14).

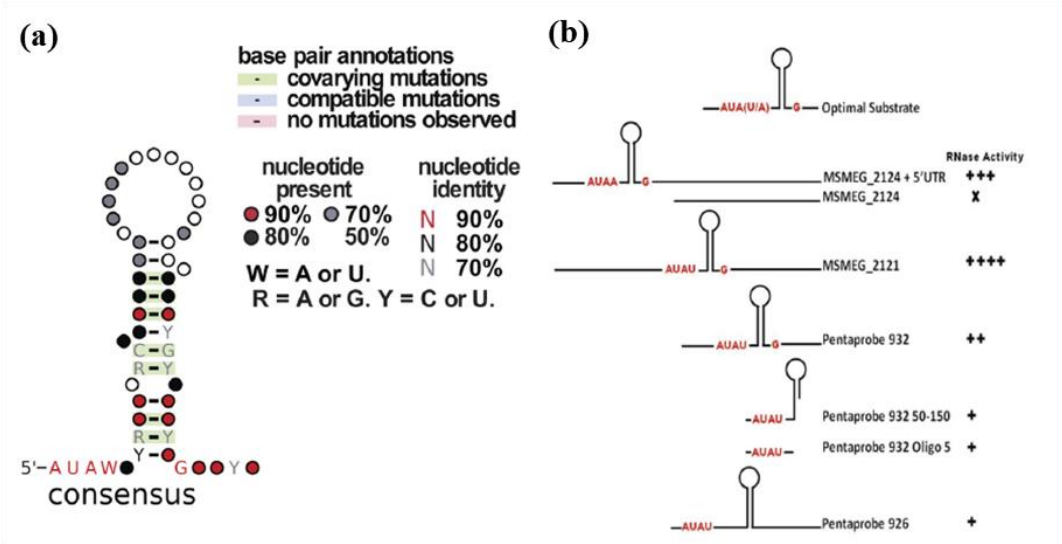

Figure 2-14. Models of RNA secondary structure targeted by *M. smegmatis* VapC. (a) Secondary structure consensus model. (b) Schematic diagrams of RNA substrates showing the presence or absence of the consensus model motif. MSMEG_2124 and MSMEG_2121 are genes downregulated by VapC. The extent of ribonuclease (RNase) activity is scored from +, weak activity, to ++++, strong activity, and X, no activity. Figures retrieved from (McKenzie *et al.*, 2012b).

Secondary structure is also important for RNA cleavage by other *M. tuberculosis* VapC proteins (Winther *et al.*, 2016; Winther *et al.*, 2013). The secondary structure of the Sarcin-Ricin loop of 23S rRNA is important for VapC20 cleavage as activity is abolished when the stem is modified or removed (Winther *et al.*, 2013). Given structural homology, it is likely that FitB recognises specific secondary structures as do the VapC proteins described above. Based on the results from our ribonuclease activity assays, we compared the secondary structures of the pentaprobes and the oligos to assess whether this could have affected activity of FitB. The secondary structures were predicted using RNAfold (Figure 2-15 & Appendix B.2.) (Hofacker, 2003).

The secondary structures of the oligos are distinct from that in the parent 923 pentaprobe (Figure 2-15). Pentaprobe 923 forms several hairpin structures with an open strand of nucleotides on the 5' end (Figure 2-15), much like the secondary structure motif targeted by *M. smegmatis* VapC (McKenzie *et al.*, 2012b). The oligos, however, do not possess a similar structure. Despite having a secondary structure preference, other VapC proteins still cleaved the shorter oligos. As FitB

did not cleave the oligos at all, secondary structure targets might be strictly limited suggesting FitB is highly specific toward certain cellular targets.

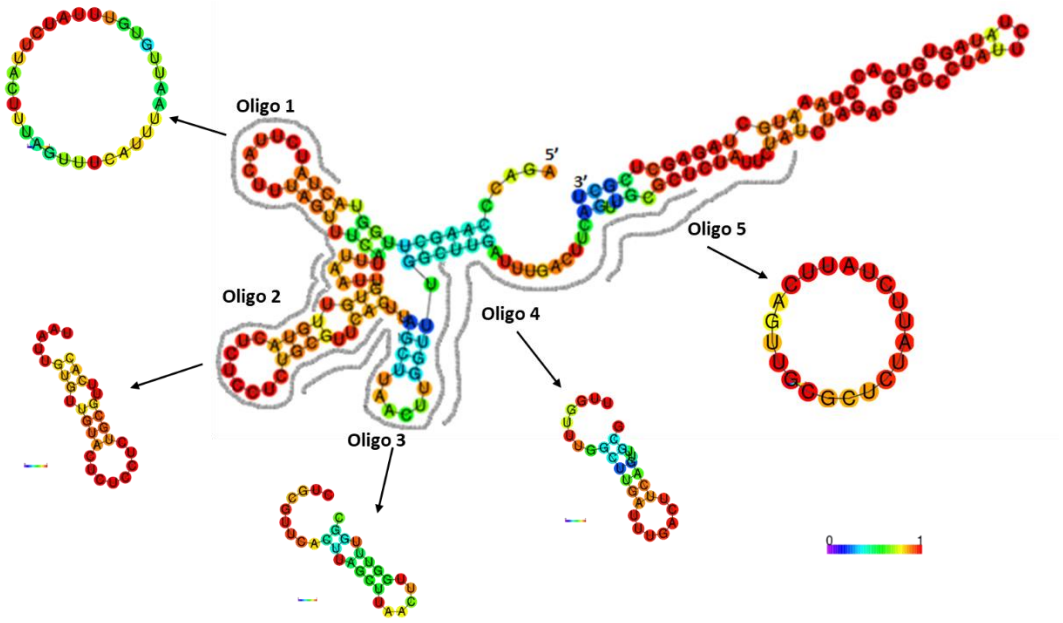

Figure 2-15. Secondary structures of Pentaprobe 923 and oligos predicted using RNAfold. Grey lines around the pentaprobe represent the portion of the pentaprobe that the labelled oligo matches. Nucleotide colours indicate the probability of base-pair folding as shown on the colour scale (purple, zero, red, one).

To characterise the sequence-specificity of VapC proteins from *M. smegmatis* (McKenzie *et al.*, 2012b), *P. aerophilum* (McKenzie *et al.*, 2012a) and *M. tuberculosis* (Sharrock *et al.*, 2018) the sequence of the cut oligonucleotides was determined using MALDI-TOF MS. By this method, the masses of each cut fragment from the oligonucleotide activity assays (like above) were determined and the VapC cut site(s) was deduced (McKenzie *et al.*, 2012a; Sharrock *et al.*, 2018). We were unable to use this method to determine the cut site of FitB as the short oligonucleotides were not cut by FitB and the longer pentaprobes are too long for MALDI-TOF MS analysis. MALDI-TOF MS is a highly sensitive method when using small RNA, however, the mass resolution decreases with an increase in RNA length (Kirpekar *et al.*, 1994).

We aimed to develop a similar MS approach to analyse the larger pentaprobe sequences. We worked in consultation with Grant Smolenski at MS3 Solutions and began developing a method using HPLC followed by MS. HPLC is important for separating the cut fragments before measuring their mass by electrospray ionisation mass spectrometry (ESI-MS).

To prepare the RNA for HPLC and MS analysis, the buffers for purification and for the activity assays needed to be altered to contain no sodium ions. Sodium ions tend to form adducts with RNA which interferes with the masses measured by MS (Thomas & Akoulitchev, 2006). The purification buffer was changed to a Tris buffer and the assay buffer was changed to ammonium phosphate. This did not affect the purification of FitB nor did it affect the activity of FitB in pentaprobe assays. We have taken 2 µg purified pentaprobe 923 RNA and pentaprobe 923 RNA fragments after cleavage by FitB to MS3 solutions and are currently waiting for analysis to see if this method is feasible.

An alternative approach to determining putative target cut sites of FitB is sequencing cDNA synthesised from the cut RNA fragments. The protocol for obtaining cDNA was designed using a combination of different protocols and enzymes (Farrell Jr, 2009; Gubler & Hoffman, 1983). It is not a straight forward reverse-transcription reaction because we do not know where the pentaprobes are cut which means we cannot design sequence-specific primers.

The first cDNA strand is synthesised by circular reverse-transcription PCR (RT-PCR) with random-hexamer primers. Each RNA fragment is circularised to ensure the full length sequence is reverse-transcribed, regardless of where the random-hexamer primers bind. If the primers were to bind randomly along the linear fragments we would not be able to identify if the cDNA was synthesised from the full length RNA fragment or partially synthesised due to misplacement of the primers. Circular RT-PCR produces an RNA:cDNA hybrid with the first cDNA strand bound to the RNA template.

The second cDNA strand is synthesised from the RNA:cDNA hybrid by nick translation. This involves a cocktail of enzymes each with a different role in the reaction. RNase H nicks the RNA strand in the RNA:cDNA hybrid in several places to form short segments that act as primers (Farrell Jr, 2009). DNA Pol I adds nucleotides to the end of the ‘primers’ using cDNA as a template for transcription. RNA fragments downstream of active DNA Pol I are digested by the enzyme as it transcribes the DNA. T4 DNA ligase repairs breaks in the second cDNA strand following DNA Pol I transcription to produce a complete double-stranded DNA product.

For sequencing, blunt ends are generated on each end of the DNA product and the product is inserted into an annotated plasmid vector, pGEM®-T Easy. The plasmid can be sequenced using primers flanking the insertion region so the sequence of DNA can be determined.

To date, we have tested this method twice, however, have not been successful in obtaining DNA sequences. The reaction to synthesise the second cDNA strand requires optimisation as the RNA:cDNA hybrid is degraded during this step. Due to the complex nature of this reaction it is unsurprising that the conditions need optimising to ensure all enzymes are working efficiently. This protocol is currently being optimised.

2.3 Conclusions

FitB can be expressed and purified on its own without its cognate antitoxin, FitA. This is unlike many other VapC proteins which must be purified as the VapBC complex, followed by a trypsin digest to remove VapB (McKenzie *et al.*, 2012a; Robson *et al.*, 2009). Despite being soluble, purified FitB is unstable in solution making it difficult to characterise its activity. We have developed a method to stabilise FitB during purification to ensure the protein remains in its native, folded form for the duration of ribonuclease activity assays.

FitB is a ribonuclease with sequence and structural specificity. FitB cuts RNA pentaprobes, approx. 160-nt long, but does not cleave short, 30-nt RNA oligos of the same sequence. We, therefore, predict secondary structure is important for RNA cleavage by FitB. The secondary structures of the RNA oligos is significantly different to that of the pentaprobes which would explain why activity is seen with one substrate but not the other. Intriguingly, FitB displays RNA binding properties by binding both the RNA pentaprobes and oligos. RNA binding by FitB occurs regardless of RNA cleavage suggesting both are important functions of FitB.

Methods to determine the target cut site sequence(s) of FitB have been established and are currently under development.

2.4 Future Research

The HPLC-MS approach described in this chapter will continue to be developed to determine the cut site sequence(s) of FitB. If it is too difficult to analyse the pentaprobe ribonuclease activity assays using this approach, cDNA from the cut

RNA fragments will be synthesised and sequenced, as discussed, and the cut sites will be deduced by comparing sequences of the cut RNA fragments with the original pentaprobe sequence. The secondary structure targeted by FitB will also be characterised by further ribonuclease activity assays using RNA substrates with known secondary structures. RNA binding by FitB will be investigated by gel electrophoretic mobility shift assays, as reported by Sharp *et al.* (2012), to assess sequence specificity and evaluate the importance of binding in relation to RNA cleavage.

Chapter Three

The Role of FitAB in Intracellular Replication

3.1 Introduction

During infection of the human urogenital tract, *N. gonorrhoeae* invades human epithelial cells and traffics through to the other side, exiting into the subepithelial layer (Billker *et al.*, 2002; Evans, 1977; Wang *et al.*, 1998). Although the mechanism of adherence and invasion is well understood, little is known about the intracellular lifecycle of *N. gonorrhoeae* or the molecular mechanisms driving intracellular trafficking.

A study by Hopper *et al.* (2000) investigated molecular mechanisms of intracellular trafficking using a transposon mutagenesis screen. Hopper *et al.* (2000) identified fast intracellular traffickers with mutations in a single locus containing two open reading frames, *fitA* and *fitB*. One transposon was inserted upstream of both genes, the other inserted within the *fitB* gene (Figure 1-4). Further investigation into the effects of these mutations revealed an increase in intracellular growth rate associated with the faster trafficking phenotype (Figure 3-1) (Hopper *et al.*, 2000).

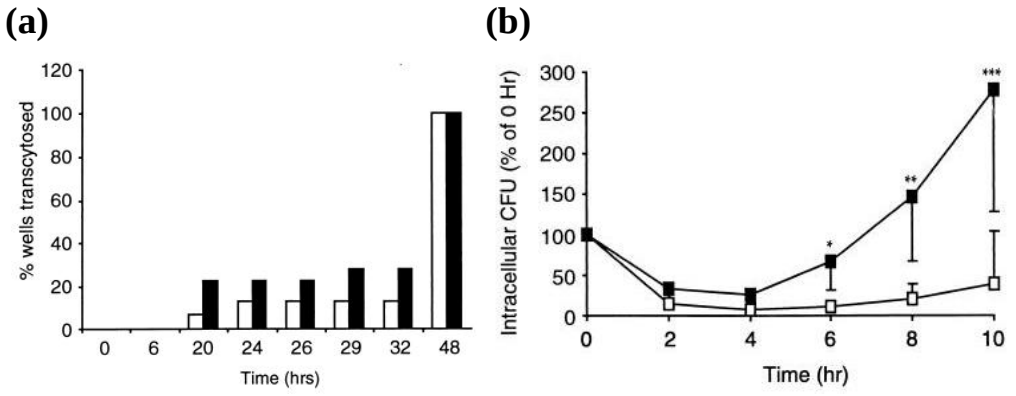

Figure 3-1. Graphs showing transepithelial trafficking and intracellular replication by *N. gonorrhoeae* WT and *N. gonorrhoeae fitAB* gene deletion strains. (a) Rate of epithelial trafficking depicted by percent of T84 monolayers transcytosed at various time-points (hours, hrs) and (b) intracellular growth rate in A431 human epithelial cells represented by percent of CFU present at zero hour (hr) for *N. gonorrhoeae* MS11 wild-type (white bars/boxes) and *N. gonorrhoeae* MS11 *fitAB* gene deletion strain (black bars/boxes). Retrieved from (Hopper et al., 2000).

Although *fitA* and *fitB* were identified as being translationally coupled (Hopper *et al.*, 2000), it was not known at the time that they constituted the FitAB toxin-antitoxin (TA) system, belonging to the VapBC superfamily (Arcus *et al.*, 2011; Mattison *et al.*, 2006). In other bacteria, VapBC TA systems have been implicated in the regulation of intracellular growth to generate bacteriostatic/persistent cell populations (McKenzie *et al.*, 2012b; Sharrock *et al.*, 2018; Winther & Gerdes, 2011). *N. gonorrhoeae* has the ability to enter a state of persistence, causing asymptomatic infection (Workowski & Berman, 2007). We hypothesise that the VapBC TA system, FitAB, is important for generation of this persistent state.

In *M. smegmatis*, VapC regulates cell growth by cleaving mRNA transcripts involved in carbon transport and glycerol metabolism (McKenzie *et al.*, 2012b). To understand how FitAB regulates growth of *N. gonorrhoeae* we must determine its biological targets, which can be elucidated by comparing intracellular replication of *N. gonorrhoeae* wild-type (WT) and *N. gonorrhoeae fitAB* gene deletion strains (*ΔfitAB*) and analysing gene expression during infection.

In this chapter, we characterise the role of FitAB in *N. gonorrhoeae* by extending the intracellular growth experiment conducted by Hopper *et al.* (2000) and extract RNA from *N. gonorrhoeae* at different time-points throughout the experiment in preparation for transcriptome analysis.

3.2 Materials & Methods

3.2.1 Human epithelial cell culture

3.2.1.1 Culturing A549 human lung epithelial cells

Stocks of A549 human lung epithelial cells were stored in Freezing Media (80% 1 X DMEM/F12 (Gibco), 10% fetal calf serum (FCS, Gibco) and 10% dimethyl sulfoxide (DMSO)) at -80 °C. To establish a cell culture, a stock of cells was thawed at 37 °C with 5% CO_2 for 10 min and centrifuged at 3000 *g* for 5 min. All DMSO was removed, with caution not to disrupt the cell pellet, and the cell pellet was resuspended in 1 ml 10% Cell Culture Media (1 X DMEM/F12, 10% FCS, 2.5 µg ml^{-1} vancomycin, 1 µg ml^{-1} amphotericin B) by gentle pipetting and transferred to a vented cell culture flask containing 4 ml of pre-warmed 10% Cell Culture Media. The flask was then incubated at 37 °C with 5% CO_2 for approximately 15 hours. Following incubation, the Cell Culture Media was

replaced with fresh, pre-warmed 10% Cell Culture Media. Once the cells had grown to approximately 80% confluency, media was replaced with pre-warmed 1% Cell Culture Media (1 X DMEM/F12, 1% FCS, 2.5 µg ml^{-1} vancomycin, 1 µg ml^{-1} amphotericin B) to maintain cell cultures. Media was then refreshed every three days.

3.2.1.2 Detaching A549 cells from culture flasks

To detach epithelial cells from cell culture flasks, all media was removed and cells were washed with 2 ml Washing Media (1 X DMEM/F12, 2.5 µg ml^{-1} vancomycin, 1 µg ml^{-1} amphotericin B). Washing Media was removed before addition of 1 ml 0.25% Trypsin-EDTA (TE) including Phenol Red (Gibco) to cover the base of the flask. Cell cultures were then incubated at 37 °C for 3 min to detach cells.

3.2.1.3 Splitting A549 cell cultures

A549 cells were detached from the flasks as above (section 3.2.1.2). Suspended cells (in TE) were transferred to pre-warmed 10% Cell Culture Media. The volume of cell culture media depended on how many new cell cultures were required. Cells were dispersed through the cell culture media by gently inverting before transferring into new cell culture flasks in 5 ml aliquots. Cultures were incubated at 37 °C with 5% CO_2 for 15 hours. The media was replaced with fresh pre-warmed 10% Cell Culture Media and returned to incubate at 37 °C with 5% CO_2 until cells became confluent.

3.2.1.4 Freezing A549 cell cultures

Cells were detached (section 3.2.1.2) and transferred into 9 ml 10% Cell Culture Media. Cells were pelleted by centrifugation at 2000 *g* for 30 min. All supernatant was removed and cells were resuspended in 4 ml Freezing Media. Cells were transferred into cryovials in 1 ml aliquots and placed in a controlled rate freezing apparatus for cell culture. This was placed in a -80 °C freezer overnight. The following day, cells were transferred to a freezer box for long-term storage at -80 °C.

3.2.2 Bacteria cell culture

Glycerol stocks of *N. gonorrhoeae* FA1090 WT and *N. gonorrhoeae* FA1090 *ΔfitAB* were stored at -80 °C.

3.2.2.1 Growth on solid media

N. gonorrhoeae was cultured on either supplemented chocolate agar plates (Fort Richard Laboratories) or GCB agar plates.

GCB-agar plates were poured fresh according to the method in (Dillard, 2011). In brief, 36.25 g GC Medium Base (Difco) and 1.25 g agar was added to 1 L water. The solution was autoclaved and cooled to 50 - 60 °C. Immediately before pouring into plates, 10 ml (per 1 L) Iso Vitalex supplement (BD Biosciences) was added to the agar. Plates were poured with approximately 20 ml agar per plate and set at room temperature (RT). GCB-agar plates were stored at 4 °C for up to a week.

N gonorrhoeae glycerol stocks were streaked onto agar plates and incubated upside-down at 37 °C with 5% CO_2.

3.2.2.2 Growth in liquid media

A sterile loop was used to transfer colonies from agar plates (section 3.2.2.1) to 5 ml pre-warmed 10% Cell Culture Media in a vented cell culture flask. Flasks were incubated overnight at 37 °C with 5% CO_2.

3.2.3 Intracellular replication experiment

Two A549 cell cultures were grown from cell culture stocks as described in section 3.2.1.1. Once confluent, each culture was split into ten new cultures using the method described in section 3.2.1.2. For each culture, 1 ml of cells in TE buffer was added to 49 ml 10% Cell Culture Media and aliquoted into ten flasks in 5 ml aliquots, giving a total of 20 new cell cultures. These cultures were incubated for 36 hours at 37 °C with 5% CO_2 until cells were 80% confluent. Each cell culture was split again into two new cultures to yield 40 A549 cell cultures which were returned to 37 °C with 5% CO_2 until confluent.

Prior to infection with *N. gonorrhoeae*, A549 cell cultures were counted using a BioRad Cell Counter. Cells were detached from the flasks as in section 3.2.1.2 and transferred into 1.5 ml tubes. BioRad cell counter slides for each culture were loaded with 10 µl of cells and placed in the BioRad cell counter for automatic

counting. The remaining cells were centrifuged at 13,000 *g* for 1 min. The supernatant was removed from each tube and the cell pellets were resuspended in 1 ml pre-warmed 10% Cell Culture Media. This was transferred to individual cell culture flasks containing 4 ml 10% Cell Culture Media. Cells were incubated for 1 hour at 37 °C with 5% CO_2 to allow cells to adhere to the flasks.

Three *N. gonorrhoeae* FA1090 WT and three *N. gonorrhoeae* FA1090 Δ*fitAB* cultures were set up as in Section 3.2.2.2. After incubation for 15 hours at 37 °C with 5% CO_2 the optical density (OD) at 600 nm was measured using a spectrophotometer blanked with 10% Cell Culture Media. The cultures were considered ready for infection when cell growth was high (OD_{600} > 1.0). Each A549 culture was infected with 100 - 150 µl bacterial cells (the inoculation volume was adjusted to account for variations in OD of each culture). Each culture of *N. gonorrhoeae* was used to infect six A549 cell cultures. After inoculation, flasks were returned to 37 °C with 5% CO_2 for 14 hours to allow bacteria to invade the cells. After 14 hours, 10 µl of 20 mg ml^{-1} gentamicin was added to each flask containing A549 cells and *N. gonorrhoeae*, and mixed by swirling. Flasks were returned to 37 °C with 5% CO_2 for 1 hour. Following incubation, media was removed and cells washed with pre-warmed Washing Media twice to remove any extracellular bacteria and gentamicin. Fresh 10% Cell Culture Media was added to each flask and all were returned to 37 °C with 5% CO_2, except for six flasks (one of each inoculum) which were processed as the zero hour time-point.

At zero, six, eight, ten, 14 and 24 hours post-gentamicin treatment six cell cultures (one of each *N. gonorrhoeae* inoculum) were removed from incubation to harvest the intracellular bacteria. To harvest the bacteria, all media was removed and each culture was washed twice with 3 ml Washing Media. Cells were detached from flasks (section 3.2.1.2) and transferred to a 1.5 ml tube. Cells were pelleted by centrifugation at 5000 *g* for 2 min. All supernatant was removed and the cells washed with Washing Media before further centrifugation. The supernatant was removed and cell pellets were resuspended in 500 µl of 0.5% Saponin, made up fresh in 1 X phosphate-buffered saline (PBS), vortexed briefly and gently mixed for 7 to 8 min by inversion until the solution was less opaque (indicating epithelial cells lysis). Lysed epithelial cells were centrifuged as above and the supernatant was removed. Cell pellets were resuspended in Washing Media and centrifuged to

pellet as above. All Washing Media was removed and the cell pellet resuspended in 200 µl Washing Media.

Intracellular replication of *N. gonorrhoeae* was calculated by measuring colony forming units (CFUs) grown on agar plates. The bacteria harvested from A549 cells were resuspended in 200 µl Washing Media (undiluted), and a dilution series prepared including a 10^{-2} dilution, and 10^{-4} dilution with Washing Media. The dilution series was prepared by transferring 2 µl undiluted bacteria to 198 µl Washing Media and vortexing to mix. This was repeated again, transferring 2 µl of the diluted sample to another tube of 198 µl Washing Media and vortexing to mix. Five microliters of each dilution was pipetted three times (technical replicate) onto pre-warmed chocolate agar or GCB-agar plates. Plates were incubated upside-down at 37 °C with 5% CO_2 overnight and colonies counted the following morning (see section 3.2.3.1).

The undiluted bacteria from above were centrifuged at 13,000 g for 2.5 min. Cell pellets were resuspended in 500 µl 5 M guanidinium thiocyanate (GITC), made up fresh in DEPC-treated water, and transferred to 1.5 ml screw cap tubes containing 0.3 g of 0.1 mm and 4 x 2.5 mm zirconia beads, prebaked at 120 °C overnight (bead-beating tubes). These were immediately transferred to -80 °C freezer for storage.

3.2.3.1 Data analysis of CFU measurements

The colony forming units (CFUs) counted from the agar plates were analysed in Excel. CFUs were converted to cells ml^{-1} using Equation 1.

Equation 1. Conversion from CFU to cells ml^{-1}

$$CFU \times dilution\ factor \times 0.005\ ml = cells\ ml^{-1}$$

These values were normalised by converting to a percentage of the amount of cells present at zero hour using Equation 2 for each mutant.

Equation 2. Normalisation of cell counts at each time-point in relation to cells present at zero hour.

$$\left(\frac{cells\ ml^{-1}}{0\ hr\ cells\ ml^{-1}}\right) \times 100\% = \%\ of\ 0\ hr$$

The average of each technical replicate was plotted as a scatter plot (time vs percent of intracellular CFU) using GraphPad Prism 7.04. A trendline based on the mean values was fit for each mutant. A multiple t-test was performed using the Holm-Sidak method (alpha = 0.05) in GraphPad Prism 7.04 to determine statistical significance. The P value for each time-point was marked statistically significance if $p < 0.05$.

3.2.4 General methods used for RNA extraction

3.2.4.1 Sodium acetate and ethanol precipitation

To purify RNA from other contaminating phenols or salts, $1/10^{th}$ of the volume of 3 M sodium acetate, pH 5.2, was added to RNA suspended in water, followed by 2.5 volumes of ice-cold 200 proof ethanol. Samples were mixed gently by inverting several times then incubated at -20 °C overnight. Following incubation, samples were centrifuged at 13,000 *g* for 15 min at 4 °C to pellet the RNA. All the supernatant was removed and the pellet was washed with 1 ml of 70% ethanol. Samples were centrifuged at 13,000 *g* for 5 min at 4 °C. All traces of ethanol were removed and the RNA pellet air dried for 5 min before resuspension in 10 - 20 µl nuclease-free water.

3.2.4.2 DNase treatment

Contaminating DNA was removed using PerfeCTa DNase I (QuantaBio) as per manufacturer's instructions. A 30 µl reaction was set up (Table 3-1). All reagents were added to the 1.5 ml tube of RNA while on ice. The reaction was vortexed gently to mix and centrifuged briefly to collect components at the bottom of the tube. The reaction was incubated at 37 °C, shaking at 300 rpm for 30 min. Following incubation, the reaction was stopped by addition of 3 µl 10 X Stop Buffer. The reaction was vortexed again and centrifuged briefly before incubation at 65 °C for 10 min. The reaction was returned to ice and RNA purified by sodium acetate and ethanol precipitation (section 2.1.10.1) and resuspended in 20 µl water.

Table 3-1. Composition of the PerfeCta DNase I (QuantaBio) reaction.

Composition	Quantity (30 µl reaction)	Concentration
RNA Template	10 µl	
10X reaction buffer	3 µl	1 X
PerfeCta DNase I (2 U μl^{-1})	3 µl	0.2 U μl^{-1}
RNase/DNase free water	to 30 µl	

3.2.4.3 Agarose gel electrophoresis

Agarose gels were made up to 1% agarose with TAE buffer and 1 X SYBR safe DNA gel stain (Invitrogen). RNA samples were mixed 1:1 with 2 X formamide loading dye and heated to 75 °C for 5 min before loading onto the gels. Gels were run at 100 V for 40 min and visualised using an iBright imager (Invitrogen). Band sizes were determined based on comparison with a 1 Kb plus DNA ladder (Invitrogen).

3.2.4.4 Qubit® RNA Broad-Range (BR) assay

RNA concentration was measured using a Qubit® RNA BR assay kit (Invitrogen) and a Qubit® Fluorometer (Invitrogen). The Qubit® RNA BR assay kit measures RNA concentrations between 0.05 ng μl^{-1} and 6 ng μl^{-1} after dilution. All samples were prepared and measured in thin-wall, clear 0.5 ml PCR tubes (Axygen® PCR-05-C tubes). Qubit® working solutions were set up by diluting the Qubit® RNA BR Reagent 1:200 in Qubit® RNA BR Buffer as per manufacturer's instructions. Two standards and RNA samples were prepared as in Table 3-2, vortexed briefly and incubated at RT for 2 min. The Qubit® Fluorometer was calibrated with the standards, and samples were read. All measurements were corrected for the 200 fold dilution. Where the RNA concentration was outside the measurement range for this kit, a result of > 6 ng μl^{-1} (after dilution) was given.

Table 3-2. Composition of Qubit® RNA standard and sample assays.

Composition	Standards (200 µl reaction)	Samples (200 µl reaction)
Qubit® working solution	190 µl	199 µl
Standard (from kit)	10 µl	-
RNA sample	-	1 µl

3.2.5 Methods used to optimise RNA extraction

RNA extraction methods were tested and optimised using 5 ml of *N. gonorrhoeae* culture grown in 10% Cell Culture Media (section 3.2.2.2). The yield and quality of the RNA extracted by each method was assessed by NanoDrop™, agarose gel electrophoresis (refer to section 3.2.4.3) and Qubit® RNA analysis (refer to section 3.2.4.4).

3.2.5.1 TRIzol® Reagent with bead-beating

N. gonorrhoeae FA1090 WT was cultured as in section 3.2.2.2. Cultures were transferred to 1.5 ml tubes and centrifuged at 13,000 *g* for 2 min to pellet cells. The supernatant was removed and the pellet was resuspended in 1 ml TRIzol® Reagent (Invitrogen) and transferred to bead-beating tubes as in section 3.2.3. Samples were frozen at -80 °C.

Samples were removed from the -80 °C freezer and thawed at RT. Cells were lysed by bead beating using a FastPrep cell disrupter (FP120 Thermo Savant) for 30 sec at setting 6.5, left to cool for 30 sec, and repeated three more times at setting 6.0, 5.5 and 5.0 respectively. Two hundred microlitres of chloroform was added and samples were mixed on a rotating wheel for 3 min at RT. Samples were then centrifuged at 13,000 *g* for 15 min at 4 °C to separate the aqueous and organic phases. The upper aqueous phase containing RNA was transferred to a new tube and 500 µl isopropanol was added before incubating at -20 °C overnight to precipitate the RNA.

Samples were then spun at 13,000 *g* for 20 min at 4 °C to pellet the RNA. All isopropanol was removed and the RNA pellet washed with 1 ml 70% ethanol. Samples were vortexed briefly before spinning at 7500 *g* for 10 min at 4 °C. All traces of ethanol were removed. RNA was air dried briefly and resuspended in 20 µl

of nuclease free water. RNA was purified by sodium acetate and ethanol precipitation (section 2.1.10.1). Contaminating DNA was removed by DNase treatment (section 3.2.4.2) followed by an additional sodium acetate and ethanol precipitation (section 2.1.10.1) and resuspended in 20 µl nuclease-free water.

3.2.5.2 TRIzol® Reagent with lysozyme

N. gonorrhoeae FA1090 WT was cultured as in section 3.2.2.2. Cultures were transferred to 1.5 ml tubes and centrifuged at 13,000 *g* for 2 min to pellet cells and all supernatant removed. Cell pellets were resuspended in 500 µl lysozyme buffer (30 mM Tris, 10 mM EDTA, 10 mg ml^{-1} lysozyme, pH 6.2) and incubated at 37 °C for 30 min. One millilitre of TRIzol® Reagent and 300 µl chloroform was added to samples and mixed well by pipetting before centrifugation at 13,000 *g* for 20 min at 4 °C. The upper aqueous phase was transferred to a new tube followed by addition of 300 µl saline solution (0.6 M NaCl, 0.4 M sodium citrate) and 300 µl isopropyl ethanol. Samples were then mixed by inverting and stored at -20 °C overnight to precipitate RNA. Samples were centrifuged at 13,000 *g* for 20 min at 4 °C and all supernatant removed. The RNA pellet was washed with 1 ml 70% ethanol and centrifuged for a further 10 min at 7500 *g*. All traces of ethanol were removed and the RNA pellet air dried. The RNA was dissolved in 50 µl nuclease-free water and contaminating DNA was removed by DNase treatment (section 3.2.4.2), followed by purification by sodium acetate and ethanol precipitation (section 2.1.10.1).

3.2.5.3 Lysis method

N. gonorrhoeae FA1090 WT was cultured as in section 3.2.2.2. Cultures were transferred to 1.5 ml tubes and centrifuged at 13,000 *g* for 2 min to pellet cells and all supernatant removed. The pellet was resuspended in 600 µl lysis buffer (TE buffer, 0.006% SDS, 0.12 mg ml^{-1} Proteinase K) and vortexed. The reaction was incubated for 1 hour at 37 °C, shaking at 300 rpm. Cells were lysed when the solution turned clearer. An equal volume of acid-phenol/chloroform (1:1, *v/v*) was added and mixed well by inverting until it appeared monophasic. Samples were centrifuged at 13,000 *g* for 5 min at RT to separate the phases. A distinct white layer containing protein was formed at the interface. The upper aqueous phase was transferred to a new tube and the phenol/chloroform phase separation steps repeated until no white interface was observed. To remove the phenol from the aqueous

phase an equal volume of chloroform was added and mixed by inverting. The solution was centrifuged at 13,000 *g* for 5 min and the upper aqueous phase transferred to a new tube. RNA was precipitated by adding 2.5 volumes of ice-cold 200 proof ethanol, mixed gently and incubated at -20 °C for a minimum of 30 min. RNA was centrifuged at 13,000 *g* for 15 min at 4 °C and all ethanol removed. The RNA pellet was washed with 1 ml 70% ethanol and centrifuged at 13,000 *g* for 2 min. All ethanol was removed and the pellet briefly air dried. The RNA was resuspended in 15 µl RNase free water and heated at 55 °C for 10 min to solubilise the RNA. Contaminating DNA was removed by DNase treatment (section 3.2.4.2), followed by purification by sodium acetate and ethanol precipitation (section 2.1.10.1).

3.2.5.4 GITC/phenol/bromo chloropropane isolation

N. gonorrhoeae FA1090 WT was cultured as in section 3.2.2.2. Cultures were transferred to 1.5 ml tubes and centrifuged at 13,000 *g* for 2 min to pellet cells and all supernatant removed. The pellets were resuspended in 500 µl 5 M GITC and transferred to bead-beating tubes (refer to section 3.2.3) and frozen at -80 °C.

Samples frozen in 5 M GITC were thawed at RT and lysed using a Precellys 24 New Generation tissue homogenizer. Cells were lysed by two rounds of bead beating for 20 sec at 4000 rpm, with a 1 min rest in between to allow the samples to cool. The homogenized samples were centrifuged at 13,000 *g* for 5 min at 4 °C to remove any foam. A phenol and bromo-chloropropane (BCP) phase separation was performed by addition of $1/10^{th}$ of the volume of 2 M sodium acetate, pH 4, and an equal volume of acid-phenol, pH 4, with a brief vortex to mix. The samples were placed on a rotating wheel for 10 min at RT followed by addition of 100 µl BCP. Samples were shaken for 1 min then incubated on ice for 5 min. Samples were centrifuged at 13,000 *g* for 1 min at 4 °C to separate the aqueous phase, interphase and organic phase. The upper aqueous phase containing the RNA was transferred into a new tube and the phenol and BCP phase separation was repeated until no white interface was present. An equal volume of isopropanol was added to the aqueous layer and incubated overnight at -20 °C to precipitate RNA.

Samples were then centrifuged at 13,000 *g* for 15 min at 4 °C to pellet the RNA. All traces of isopropanol were removed and the RNA pellet dissolved in 100 µl of 10 mM Tris-HCl, pH 7.0 and 0.5 mM $MnCl_2$. Samples were DNase treated by the

addition of 2.5 µl Promega RQ1 DNase. Reactions were incubated at 37 °C at 350 rpm for 30 min followed by the addition of 300 µl viral extraction solution (5.2 M guanidium thiocyantate, 2 M guanidine HCl, 2 M urea). Samples were incubated at RT for 5 min on a rotating wheel. Four hundred microliters of isopropanol was added, and samples were incubated for 10 min at RT and centrifuged at 13,000 *g* for 15 min at RT. All supernatant was removed and RNA pellets washed with 1 ml 70% ethanol and centrifuged at 13000 *g* for 5 min at RT. All traces of ethanol were removed and RNA pellets dissolved in 200 µl nuclease-free water and 200 µl of 5 M lithium chloride. Samples were incubated at -20 °C for 1 hour then centrifuged at 13,000 *g* for 15 min at 4 °C. RNA pellets were resuspended in 100 µl nuclease-free water, purified by sodium acetate and ethanol precipitation (section 2.1.10.1) and resuspended in 30 µl nuclease-free water.

3.2.5.5 Modified GITC/phenol/bromo chloropropane isolation

The GITC/phenol/BCP isolation method (section 3.2.5.4) was modified to optimise for extraction of RNA from *N. gonorrhoeae*. *N. gonorrhoeae* FA1090 WT cell cultures were grown and frozen in 5 M GITC as in section 3.2.5.4. Samples were thawed at RT and lysed using a Precellys 24 New Generation tissue homogenizer (two rounds of bead beating for 20 seconds at 4000 rpm with a 1 min rest). Homogenised samples were centrifuged at 13,000 *g* for 5 min at 4 °C followed by phenol and BCP phase separation and isopropanol precipitation (refer to section 3.2.5.4).

Samples were centrifuged at 13,000 *g* for 15 min at 4 °C to pellet RNA. All traces of isopropanol were remove, RNA was dissolved in 100 µl nuclease-free water, and 300 µl viral extraction solution was added. Samples were incubated at RT for 5 min on a rotating wheel. Four hundred microliters of isopropanol was added and samples were incubated for a further 10 min at RT before centrifugation at 13,000 *g* for 15 min at RT. All supernatant was removed and the RNA pellet washed with 1 ml 70% ethanol, followed by centrifugation at 13,000 *g* for 5 min at RT. All traces of ethanol were removed and the RNA pellet air dried for 5 min before dissolving in 10 µl nuclease free water. Contaminating DNA was removed by DNase treatment (section 3.2.4.2) followed by purification by sodium acetate and ethanol precipitation (section 2.1.10.1).

3.2.6 Preparation of RNA for sequencing

Total RNA to be sequenced was extracted from *N. gonorrhoeae* grown within epithelial cells during the intracellular replication experiment (refer to section 3.2.3) using the modified GITC/phenol/BCP method (refer to section 3.2.5.5). The RNA was stored in 75% ethanol at -80 °C. Samples were shipped frozen, on ice, to BGI Tech Solutions, Hongkong, for transcriptome analysis (RNA-Seq).

3.3 Results & Discussion

To assess the role of FitAB in persistence, we performed intracellular replication experiments. These involved infecting A549 human lung epithelial cells with *N. gonorrhoeae* WT and *N. gonorrhoeae* Δ*fitAB* strains and measuring intracellular bacterial growth over time. This experiment was originally carried out by Hopper *et al.* (2000) but only over a 10 hour time-course. Our aim was to repeat the experiment as in Hopper et al (2000) but extend the time course and extract RNA from various time-points for transcriptome analysis.

3.3.1 Intracellular replication experiment

Intracellular replication experiments using *N. gonorrhoeae* typically involve infection of human epithelial cells then, 14 hours post initial infection, treatment with gentamicin to remove extracellular bacteria. At specific time-points post gentamicin treatment (including a zero hour time-point immediately after treatment) epithelial cells are lysed to release intracellular bacteria. Bacteria are then plated onto agar plates and bacterial growth determined.

The intracellular replication experiment described in this chapter was first carried out in our lab by Dr. Joanna Hicks prior to the start of this MSc research. She optimised the lysis protocol using saponin for the extraction of bacteria from within epithelial cells and also checked for extracellular growth of bacteria post gentamicin treatment to ensure colonies counted were a true indicator of intracellular replication.

Upon beginning this MSc project the first aim was to optimise the intracellular replication experiment. We first conducted this experiment using some materials that differ from what is described in section 3.2.3; rather than GCB-agar, the

bacteria were cultured using supplemented chocolate agar plates, and 1 X PBS was used for the wash steps.

Each A549 epithelial cell culture contained on average 2.14 x 10^6 cells. The average OD_{600} of the inoculation cultures of *N. gonorrhoeae* was 1.46. Bacteria were harvested from the epithelial cells at six different time-points, zero, six, eight, ten, 14 and 24 hours following gentamicin treatment and CFUs were counted. Growth curves were generated from the CFU counts for *N. gonorrhoeae* FA1090 WT and *N. gonorrhoeae* FA1090 Δ*fitAB* (Figure 3-2). P-values were determined for each time-point (Table C-2).

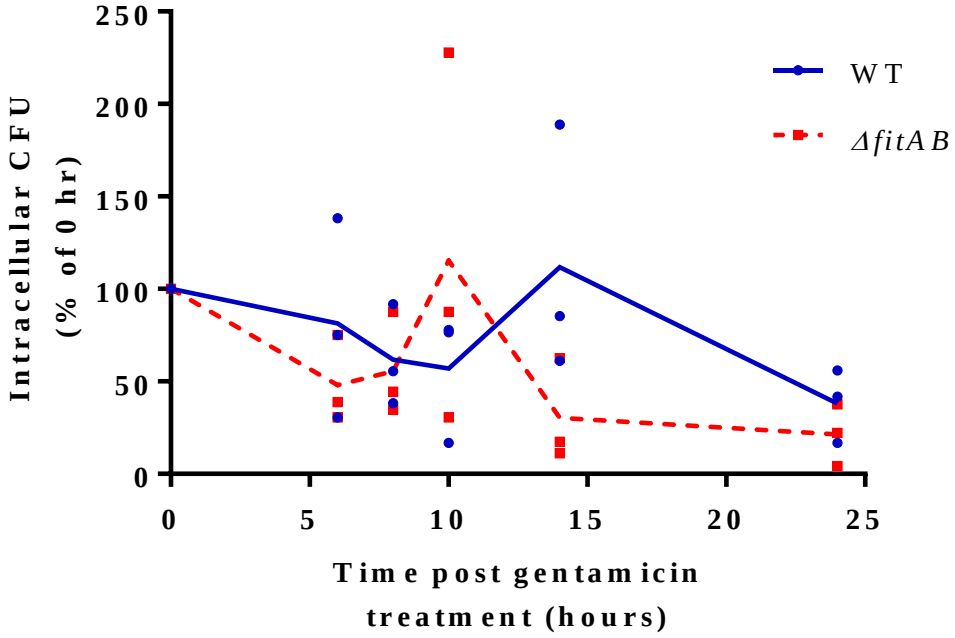

Figure 3-2. Comparison of intracellular growth of *N. gonorrhoeae* FA1090 WT strain (circles) and *N. gonorrhoeae* FA1090 Δ*fitAB* deletion strain (squares) from the first intracellular growth experiment. Growth is shown as percentage of CFU at zero hour verse time (hours). Each point represents a biological replicate. Trendlines were fit based on the means of each strain at each time-point. No time-points were determined as statistically significant (p > 0.05 for all time-points).

Following gentamicin treatment, to remove extracellular bacteria, the population of intracellular WT and *ΔfitAB* bacteria declines, until approximately six hours when the *ΔfitAB* population begins to replicate again (Figure 3-2). The WT bacteria are delayed at resuming replication as this population of bacteria does not increase until ten hours post-gentamicin treatment. This trend aligns with findings by Hopper *et al.* (2000), although in their experiment *ΔfitAB* bacteria began to replicate after just four hours following gentamicin treatment. The intracellular population of Δ*fitAB* bacteria more than doubles in size between six to ten hours then declines

dramatically at 14 hours while WT bacteria double in population between ten and 14 hours (Figure 3-2). Growth steadily declines for both Δ*fitAB* and WT between 14 and 24 hours. The rapid decline in population of Δ*fitAB* bacteria is suggestive of a sudden cell death event. This is intriguing because WT bacteria do not undergo the same rapid decline in population and there is only one reported event of another TA deletion system presenting the same phenotype (Frampton *et al.*, 2012). An *M. smegmatis* triple TA deletion mutant, in which three different TA loci, *mazEF*, *vapBC* and *phd/doc*, were deleted, displayed rapid cell death after a period of normal growth, while growth of single and double deletion mutants remained unchanged (Frampton *et al.*, 2012). It is interesting that *M. smegmatis* only displays this phenotype when three different TA systems are deleted whereas *N. gonorrhoeae* was affected by a single TA deletion. This suggests FitAB may be more important for intracellular survival of *N. gonorrhoeae* than the other TA systems.

As the dispersal of data at each time-point was broad, and none of the comparisons were statistically significant, we collated data from the first intracellular replication experiment with an independent experiment performed by Dr. Joanna Hicks (unpublished, 2017) (Figure 3-3). The experiment performed by Dr. Joanna Hicks did not contain CFU counts at 14 hours post-gentamicin treatment so, consequently, there are less data points on the graph at the 14 hour time-point. The trendlines show the average CFU at each time-point. The change in intracellular growth over the time course is consistent with the trend seen in the initial experiment (Figure 3-2). Statistical analysis resulted in p-values (Table C-3) greater than 0.05 for zero, six, eight and 14 hour time-points, suggesting the error in CFU counts at these time-points was too great to determine statistical significance.

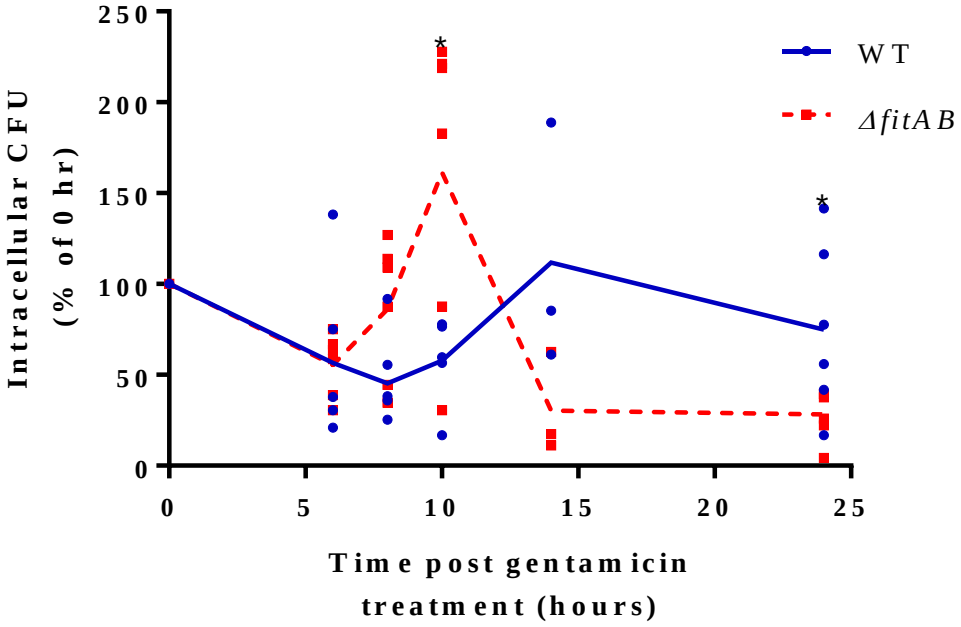

Figure 3-3. Comparison of intracellular growth of *N. gonorrhoeae* FA1090 WT strain (circles) and *N. gonorrhoeae* FA1090 Δ*fitAB* deletion strain (squares) grown in human A549 epithelial cells. Growth is shown as percentage of CFU at zero hour verse time (hours). Data is collated from two individual experiments and each point represents a biological replicate. Trendlines were fit based on the means of each strain at each time-point. Asterisks signify statistical significance at the corresponding time-point ($p < 0.05$).

In an attempt to reduce error in the CFU counts we consulted Prof. So whom we originally obtained the strains from and is an expert in *Neisseria* research. Based on her recommendations we made some modifications. In initial experiments, cell suspensions were washed with 1 X PBS, however, after consultation with Prof. So it was thought this may have been reducing *N. gonorrhoeae* cell viability as PBS is known to increase lysis of *N. gonorrhoeae*. Therefore, 1 X PBS was replaced with cell culture media without FCS (Washing Media) for all wash steps. This would reduce bacterial cell lysis and improve cell viability as bacteria would already be acclimatised to this media. The solid media on which *N. gonorrhoeae* was cultured was changed from supplemented chocolate agar plates to GCB-agar containing nutritional supplements. Unlike chocolate agar, GCB-agar is transparent so light microscopy can be used to evaluate the morphology and the presence of Type IV pili on bacterial colonies.

N. gonorrhoeae use Type IV pili to attach to and invade epithelial cells (Swanson *et al.*, 1987). Expression of pilus proteins is phase variable meaning expression can be switched on and off. Upon exposure to epithelial cells, the pilus proteins are switched on, however, by inoculating epithelial cell cultures with *N. gonorrhoeae*

already expressing pili, invasion would be more efficient. It was therefore important to identify colonies expressing pilus proteins versus colonies not expressing pili. Piliated colonies can be identified by a dark ring around the edge of the colony.

We identified colonies with dark rings and cultured these in liquid media. These cultures did not grow the same as in previous experiments. Previously, cultures of *N. gonorrhoeae* appeared yellow (due to a change in pH of the culture media) and opaque after overnight incubation (at 37 °C with 5% CO_2). Cultures grown from piliated colonies, however, formed numerous clumps without clouding the media. The clumping is due to the pili on the cells causing the bacteria to attach to each other and form microcolonies. To assess the difference this would make to invasion of epithelial cells, we repeated the intracellular replication experiment using these cultures as an inoculum. Due to clumping of the bacteria, measuring the OD was difficult but care was taken to ensure each epithelial cell culture was inoculated with the same amount of bacteria. As data are processed as a percent of the zero hour time-point, slight differences in the amount of bacteria used for inoculation would be accounted for.

This experiment resulted in the same trend of intracellular growth between zero and 14 hours as seen previously in that intracellular replication of the Δ*fitAB* deletion strain was faster compared to the WT strain (Figure 3-4). However, the overall change in growth over the course of the experiment was less than observed in previous experiments. This was surprising as we predicted the infection rate, and therefore intracellular CFU count, would be greater by inoculating the epithelial cells with piliated bacteria. This may have been due to the epithelial cells being inoculated with less bacteria compared to previous experiments. The OD_{600} values of *N. gonorrhoeae* cultures used in this experiment were approximately 0.5 ± 0.2 whereas in previous experiments cultures had an OD_{600} of approximately 1.2 ± 0.1. It is also possible that due to the bacteria clumping, the dispersal of bacteria was not even throughout the epithelial cell culture causing some cells to be more heavily invaded than others. Bacteria in heavily invaded epithelial cells would have a limit to their intracellular replication while epithelial cells not infected by bacteria would not have any intracellular growth. Therefore, the total CFU counts of intracellular growth would not be representative of the whole epithelial cell culture.

Interestingly, intracellular replication increased after 14 hours for both WT and Δ*fitAB* bacteria. Despite being a plausible growth curve for WT bacteria, this was unexpected for Δ*fitAB* bacteria as the population had already declined between ten and 14 hours and the opposite trend was seen in the previous experiments (Figure 3-3). It also goes against our understanding of intracellular growth when TA systems are deleted from other bacteria as replication tends to decrease and does not increase again (Frampton *et al.*, 2012). It is possible that this trend is a result of a low inoculum and not a true representation of intracellular growth, however further investigation is needed.

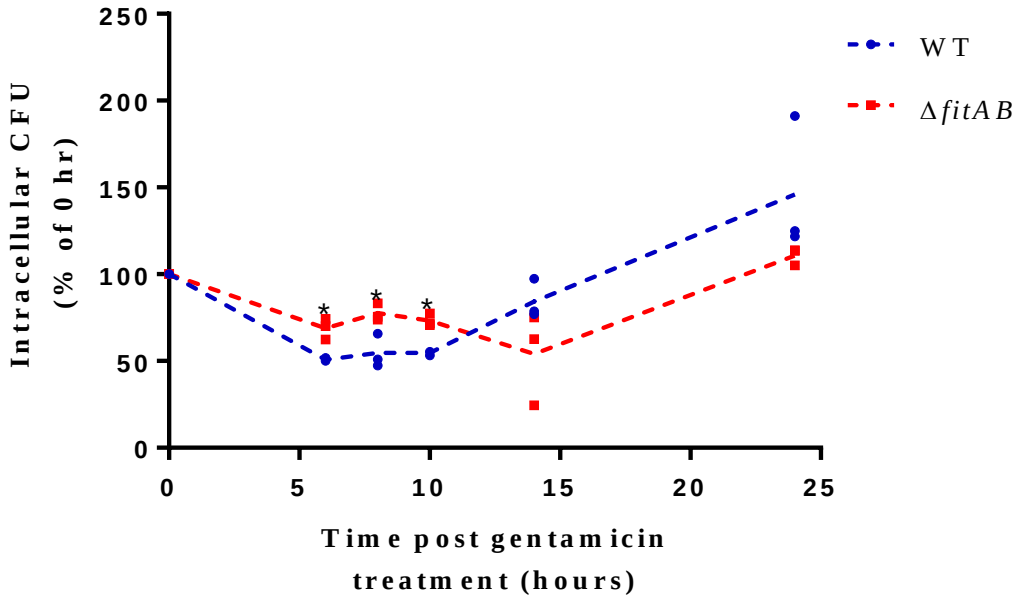

Figure 3-4. Comparison of intracellular growth of *N. gonorrhoeae* FA1090 WT strain (circles) and *N. gonorrhoeae* FA1090 Δ*fitAB* deletion strain (squares) grown from a low inoculum in human A549 epithelial cells. Growth is shown as percentage of CFU at zero hour verse time (hours). Each point represents a biological replicate. Trendlines were fit based on the means of each strain at each time-point. Asterisks signify statistical significance at the corresponding time-point ($p < 0.05$).

When cultured in media only, there is no difference in growth rate between *N. gonorrhoeae* WT and *N. gonorrhoeae* Δ*fitAB* strains over 24 hours (Figure 3-5) (Hopper *et al.*, 2000)(Joanna Hicks, unpublished, 2017). This indicates FitAB only regulates growth of *N. gonorrhoeae* within human epithelial cells. It is hypothesised that when growing extracellularly, the FitAB complex is in its stable, inert form bound to the *fitAB* operon (Mattison *et al.*, 2006; Wilbur *et al.*, 2005). Upon invasion of human epithelial cells, an as yet un-identified stimuli, such as cellular proteases, pH or nutritional deprivation, triggers the degradation of FitA causing dissociation of the complex, dysregulated transcription of the operon, and release

of active FitB (Mattison *et al.*, 2006). As with other VapC proteins (Sharrock *et al.*, 2018; Winther & Gerdes, 2011) FitB is toxic to the cell, thus active FitB causes cell growth to slow or cease altogether, resulting in slower intracellular replication.

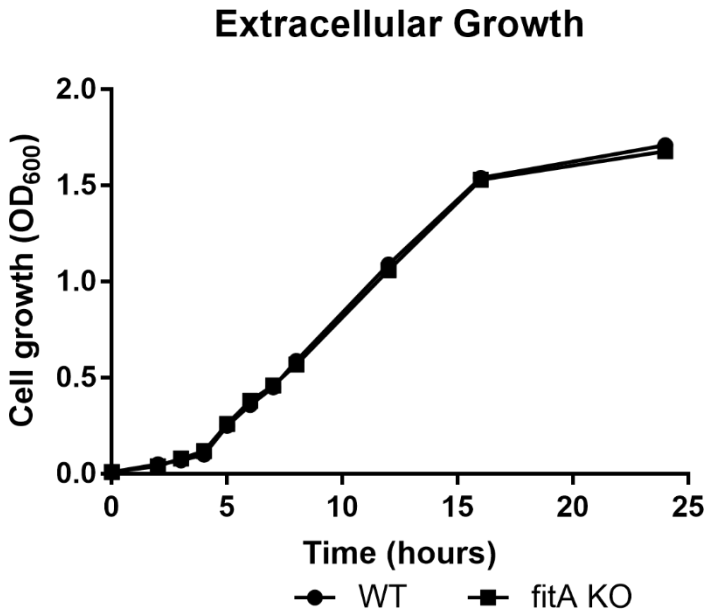

Figure 3-5. Comparison of growth in culture media of *N. gonorrhoeae* FA1090 WT strain (circles) and *N. gonorrhoeae* FA1090 Δ*fitAB* deletion strain (squares). Growth is shown as optical density at 600 nm verse time (hours). (Joanna Hicks, Unpublished, 2017).

3.3.2 Optimising RNA extraction

Extraction of RNA from *N. gonorrhoeae* was optimised for bacteria grown in culture prior to extraction of RNA from bacteria grown intracellularly. Several RNA extraction methods were trialled: TRIzol® Reagent with bead beating, TRIzol® Reagent with lysozyme, a Lysis method, GITC/phenol/BCP isolation, and a modified method of the GITC/phenol/BCP isolation. RNA extracted by each method underwent quantitative and qualitative analysis to determine which achieved RNA of a high enough quality and quantity for RNA sequencing.

The first RNA extraction method we trialled used TRIzol® Reagent with physical cell lysis by bead beating. TRIzol® is a pre-mixed reagent containing phenol and GITC (Farrell Jr, 2009) designed to isolate RNA, DNA and protein from cell or tissue samples (Simms *et al.*, 1993). Addition of chloroform aids phase separation, isolating RNA in the aqueous phase and DNA and proteins in the organic phase (Farrell Jr, 2009). We trialled RNA extraction using the TRIzol® method as it has

been successfully used in previous work to extract RNA from *N. gonorrhoeae* (Nudel *et al.*, 2018; Remmele *et al.*, 2014; Yu *et al.*, 2016).

This method yielded reasonable concentrations of RNA (Table 3-3) however the absorbance ratios at OD260/280 and OD260/230 were lower than 2.0 (Table 3-3), which is desired for pure RNA. The OD260/280 ratios of 1.7 - 1.9 suggested the presence of DNA, however these ratios did not improve after the DNase treatment. Prior to purification of the RNA by sodium acetate and ethanol precipitation (see section 2.1.10.1) the OD260/230 ratios were below 2.0 (Table 3-3) indicating potential contamination by phenols, peptides, or carbohydrates. This contamination was likely due to the high concentration of GITC in the TRIzol® Reagent (Cicinnati *et al.*, 2008; Luebbehusen) which increases the absorbance at 230 nm, lowering the OD260/230 ratio. Purification of RNA by sodium acetate and ethanol precipitation proved important for removing the GITC carry-over, indicated by an improvement in OD260/230 ratios to over 2.0 following this step (Table 3-3).

To assess the integrity of total RNA on an agarose gel, bands of 23S rRNA and 16S rRNA should be present in approximately a 2:1 ratio, respectively. In the RNA samples extracted using Trizol® and bead-beating, a high molecular weight band (23S rRNA) appeared to be present but fainter than the 16S rRNA band suggesting large RNA was degraded (Figure 3-6). Following DNase treatment, no bands of 23S or 16S rRNA were visible on the agarose gel (Figure 3-6) indicating complete degradation of the RNA.

Table 3-3. Comparison of total RNA extracted using each RNA extraction method. The success of each method was quantified based on RNA concentration and OD260/280 and OD260/230 ratios as determined by NanoDrop™. The extraction method used is labelled on the far left with sample numbers given for each replicate that correspond to sample numbers on agarose gel figures. The concentration of RNA was measured in ng µl^{-1}.

Method	Sample #	Concentration (ng µl^{-1})	OD260/280	OD260/230
TRIzol® with bead beating (before DNase and purification)	1	144.6	1.90	0.98
	2	67.6	1.74	0.66
TRIzol® with bead beating (after DNase and purification)	1	108.5	1.91	2.49
	2	41.3	1.85	2.38
TRIzol® with lysozyme	1	22.9	1.53	1.04
Lysis	1	82	1.8	2.12
GITC/phenol/BCP isolation	1	2.3	3.19	0.43
	2	11.6	1.72	1.17
Modified GITC/phenol/BCP isolation before DNase optimisation	1	55.9	1.87	0.53
	2	35.1	1.82	1.05
Modified GITC/phenol/BCP isolation with optimised DNase step	1	219	1.99	2.31

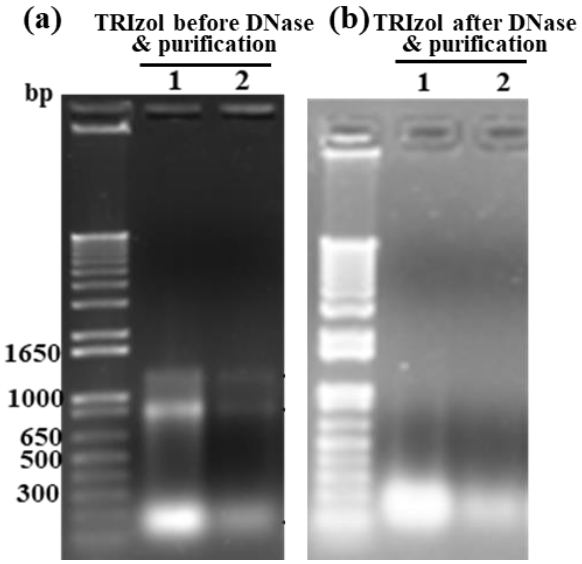

Figure 3-6. Total RNA extracted from *N. gonorrhoeae* using TRIzol® with bead beating, on 1% TAE agarose gels. (a) Two samples of RNA before DNase treatment and purification, sample numbers are labelled, 1 and 2. (b) The same two samples of RNA after DNase treatment and purification. The size of the bands are indicated by a 1 kb^{+} ladder on the left of each gel, number of bp are labelled.

To determine if physically lysing the cells via bead beating was contributing to RNA degradation we tested a second method using TRIzol® Reagent with chemical lysis. In this method, cells were lysed with lysozyme. This method yielded less RNA compared to the physical cell lysis method (Table 3-3) indicating lysozyme was not as efficient as bead beating for lysing bacterial cells. Agarose gel electrophoresis revealed no RNA bands for the lysozyme sample (Figure 3-7) suggesting the concentration of RNA detected by NanoDrop™ was in fact contamination and any extracted RNA was lost using this method.

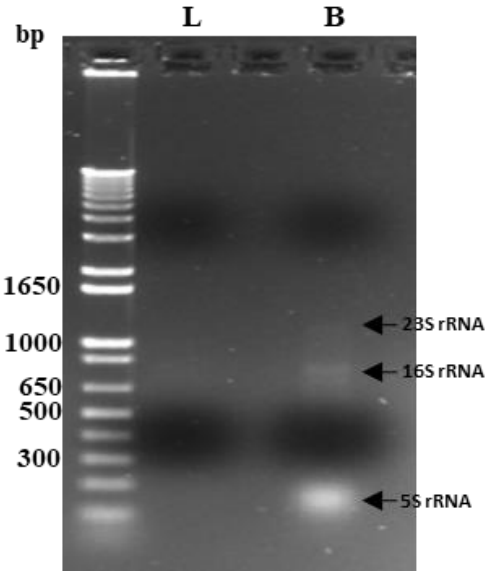

Figure 3-7. Total RNA extracted from *N. gonorrhoeae* using TRIzol® with lysozyme (L) or TRIzol® with bead beating (B), on a 1% TAE agarose gel. The size of rRNA bands are labelled on the right. The size of the bands are indicated by a 1 kb+ ladder on the left of each gel, number of bp are labelled.

The third method tested was a phenol-chloroform RNA extraction with chemical cell lysis using SDS and Proteinase K. This method yielded RNA with little phenol or salt contamination as indicated by the high OD260/230 ratio (Table 3-3), although the OD260/280 ratio suggested contaminating DNA was present, despite treating with DNase. The RNA concentration (Table 3-3) was comparable to the other methods tested. When visualised on an agarose gel the RNA was degraded and nucleotide smearing from a high molecular weight band confirmed the presence of contaminating DNA (Figure 3-8). Due to the absence of rRNA bands on the agarose gel, DNase treatment was not optimised for this method.

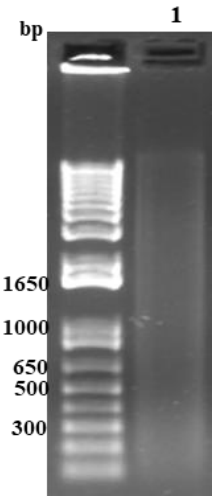

Figure 3-8. Total RNA extracted from *N. gonorrhoeae* by lysis RNA extraction, on a 1% TAE agarose gel. The size of the bands are indicated by a 1 kb^{+} ladder on the left of each gel, number of bp are labelled.

The fourth RNA extraction method tested was GITC/phenol/BCP isolation. This method has been successful in our laboratory for the extraction of RNA from *Mycobacteria*. This method uses the same principles as TRIzol® isolation except the extraction buffers are prepared in the laboratory. GITC and acidic phenol extract RNA from the bacteria cells into solution and BCP facilitates the phase separation, isolating RNA in the aqueous phase (Chomczynski & Mackey, 1995; Chomczynski & Sacchi, 1987). BCP is used in place of chloroform because it is less volatile and equally as efficient as chloroform for phase separation (Chomczynski & Mackey, 1995).

Initial attempts to extract RNA using this method resulted in very low concentrations of RNA (Table 3-3) which was heavily degraded (Figure 3-9a). The method was modified by removing the steps involving lithium-chloride. This was in part to remove lithium-chloride from the extraction procedure as this degrades small RNAs which may be important in the transcriptome analysis. The other reason for removing these steps was to reduce the amount of RNA precipitation and resuspension steps to minimise the amount of lost RNA. Removal of these steps improved the RNA yield (Table 3-3) and integrity (Figure 3-9b). The removal of contaminating DNA was optimised by moving the DNase treatment step from immediately after isopropanol precipitation to the end of the RNA extraction. This was a lot more efficient at removing contaminating DNA as evidenced by an OD260/280 ratio of 1.99 (Table 3-3) and the absence of smearing at high molecular weights on agarose gels (Figure 3-9c).

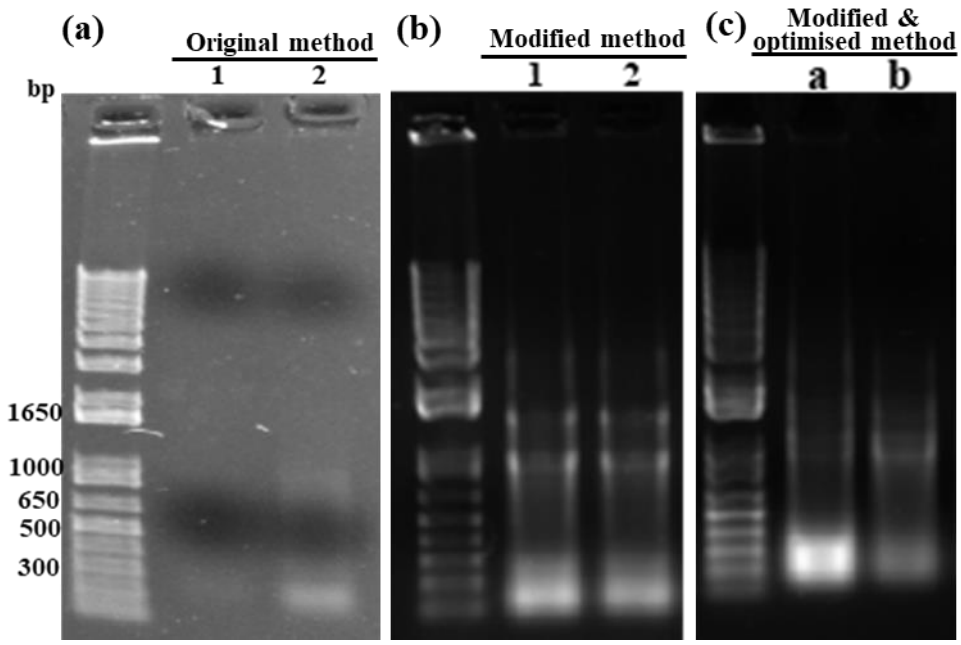

Figure 3-9. Total RNA extracted from *N. gonorrhoeae* using (a) the original GITC/phenol/BCP isolation method, (b) the modified GITC/phenol/BCP isolation method, and (c) the modified GITC/phenol/BCP isolation method with optimisation of the DNase step, visualised on a 1% TAE agarose gel. (a, b) Samples are numbered 1 and 2. (c) Sample a is RNA extracted before the addition of DNase, sample b is after. The size of the bands are indicated by a 1 kb^{+} ladder on the left of each gel, number of bp are labelled on the far left.

After comparing all RNA extraction methods the best quality RNA was obtained using the modified GITC/phenol/BCP isolation method with the optimised DNase treatment step. This method was used to extract RNA from *N. gonorrhoeae* harvested from the intracellular replication experiments (discussed in section 3.3.3).

3.3.3 Bacterial RNA extraction from the intracellular replication experiments

Samples of *N. gonorrhoeae* that had been harvested from the six, eight, ten and 24 hour time points during an intracellular replication experiment (method in section 3.3.1) performed by Dr Joanna Hicks, were frozen in 5 M GITC and stored at -80 °C. RNA was extracted from these samples using the modified GITC/Phenol/BCP isolation method (see section 3.2.5.5). The quality of the RNA was assessed by NanoDrop^{TM} (results from four samples are given in Table 3-4) and agarose gel electrophoresis (Figure 3-10), before and after the DNase treatment and purification by sodium acetate and ethanol precipitation.

Evaluation of the RNA prior to the DNase or purification reactions revealed the method yielded RNA of high concentration, at least 60 ng µl^{-1} per sample (Table

3-4), and reasonably good integrity based on the presence of 23S and 16S rRNA bands on the agarose gel (Figure 3-10a). High molecular weight nucleotide smearing on the agarose gel (Figure 3-10a), in conjunction with OD260/280 ratios of approximately 1.8 (Table 3-4), indicated contaminating DNA was present. OD260/230 ratios were lower than 1.8 (Table 3-4) indicating the presence of other contaminants such as phenol or salts.

To prevent loss of RNA, biological replicates for each time-point were pooled before the DNase was added. Analysis by agarose gel electrophoresis (Figure 3-10b) revealed large smearing patterns and bands of 23S or 16S rRNA were no longer visible suggesting the RNA had degraded during the clean-up process. The OD260/280 ratios remained predominantly unchanged suggesting the protocol for DNase treatment was not efficient at removing the DNA, despite the initial optimisation of the method (discussed in section 3.3.2). The OD260/230 ratio (Table 3-4) improved but remained less than 1.8 indicating phenol or salt contaminants were still present.

Table 3-4. NanoDrop™ values for four samples of RNA extracted from the intracellular replication experiment, before and after DNase treatment. (Note: the concentration is higher following DNase treatment because the RNA samples of biological replicates were pooled just prior to this step.)

	Before DNase			After DNase		
Sample ID	**Concentration (ng µl^{-1})**	**260/280**	**260/230**	**Concentration (ng µl^{-1})**	**260/280**	**260/230**
WT 6 hr	63.9	1.81	1.09	282.1	1.87	1.68
Δ*fitAB* 6 hr	61.1	1.84	0.62	173	1.79	1.56
WT 24 hr	65.9	1.77	0.43	99.4	1.84	1.37
Δ*fitAB* 24 hr	133.0	1.89	0.73	192.7	1.81	1.45

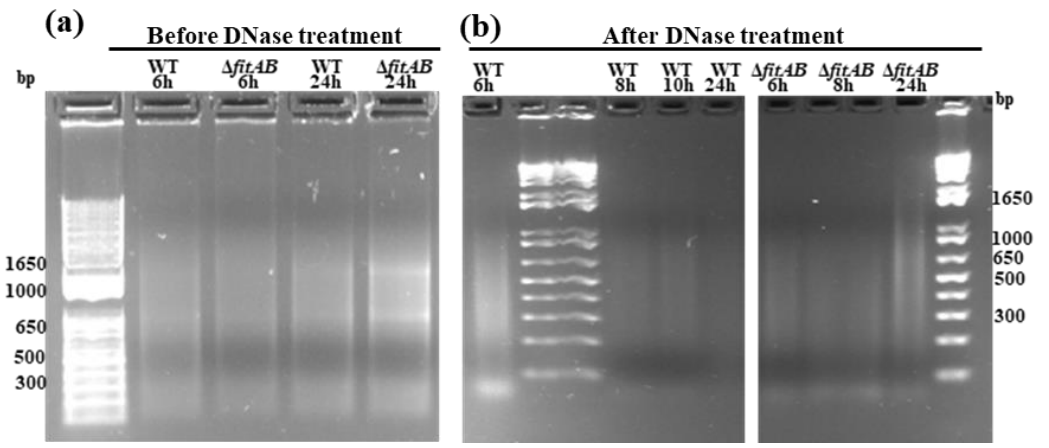

Figure 3-10. RNA extracted from *N. gonorrhoeae* from the intracellular replication experiment, visualised on 1% TAE agarose gels. Lanes are labelled with sample ID corresponding to those in Table 3-4. (a) Four RNA samples before DNase treatment. (b) Seven RNA samples after DNase treatment. The size of the bands are indicated by a 1 kb^{+} ladder on the left (a) and the right (b), number of bp are labelled.

In order for the extracted RNA to be sequenced by BGI Tech Solutions (BGI), the RNA must meet certain requirements of concentration and quality: concentration must be greater or equal to 40 ng µl^{-1}, there must be more than 1 µg, the RNA integrity number (RIN) value must be greater than 7.0, the ratio of 23S rRNA to 16S rRNA must be greater or equal to 1.0 and the absorbance ratios of OD260/280 and OD260/230 must be greater than 1.8. Due to the poor ratio values below 1.8 in the above RNA extraction, RNA was not sent to BGI for sequencing.

To improve the removal of contaminating DNA, the final concentration of DNase in the DNase reaction was increased from 0.1 U µl^{-1} to 0.2 U µl^{-1}. The intracellular replication experiment was repeated and RNA was extracted from these samples using the modified GITC/Phenol/BCP method and 0.2 U µl^{-1} DNase.

The concentration of RNA extracted from these samples was greater than that obtained in the previous extraction, with a minimum of 550 ng µl^{-1} RNA per sample of pooled biological replicates (results from four samples are given in Table 3-5). Absorbance ratios at OD260/280 were approximately 1.8 - 2.0 (Table 3-5) which is indicative of RNA and not DNA. This demonstrated the modified DNase reaction was efficient at removing contaminating DNA, more so than the method used previously. The OD260/230 ratios were greater than 2.0 indicating little to no contamination.

Table 3-5. RNA concentrations, OD260/280 and OD260/230 ratios, as measured by NanoDrop™ and Agilent 2100, of the first batch of samples sent to BGI.

	NanoDrop™			Agilent 2100 Bioanalyser	
Sample ID	**Concentration (ng µl^{-1})**	**OD 260/280**	**OD 260/230**	**Concentration (ng µl^{-1})**	**RIN**
WT 10hr	590.3	1.82	2.20	4.697	3.1
Δ*fitAB* 10hr	548.5	1.96	2.25	24	7.1
WT 14hr	1107.0	2.03	2.16	32	7.6
Δ*fitAB* 14hr	1415.6	2.05	2.18	210	8.4

Based on the NanoDrop™ results, the RNA samples met the requirements for RNA sequencing by BGI so four samples (listed in Table 3-5) were sent to BGI for sequencing. These samples were selected for RNA sequencing because the difference in intracellular growth between the WT and Δ*fitAB* strains was the greatest over the 24 hour time course (Figure 3-3) so would be the most informative samples when it came to comparing transcriptomes.

Prior to library prep, independent tests of the RNA samples were performed by BGI using an Agilent 2100 Bioanalyser (Table 3-5). The concentration of RNA for each sample was significantly lower than that measured by NanoDrop™ (Table 3-5). This could have been due to the NanoDrop™ measuring free ribonucleotides from degraded RNA whereas the Agilent 2100 Bioanalyser measures intact RNA. The RIN values were also determined, of which only three of the four samples (Table 3-5) met the RIN requirement (> 7.0) for sequencing. Sample Δ*fitAB* 14hr was the only sample to pass the BGI sequencing requirements with a concentration greater than 40.0 ng µl^{-1} and a RIN value greater than 7.0 (Table 3-5). For all other samples the concentration was too low and for WT 10hr the RIN value was also too low (Table 3-5). Consequently, none of the samples were sequenced.

To achieve a higher concentration of RNA for sequencing, the amount of bacteria from which the RNA was extracted from was increased. As this meant handling more cell culture flasks during the intracellular replication assay, this optimisation step was only carried out for ten and 14 hour time-points, and RNA was only

extracted from bacteria harvested at these time-points. The number of culture replicates at these time-points was increased to nine for each variant of *N. gonorrhoeae*. Starting with three biological replicates for each strain, each of these were used to inoculate three A549 cultures resulting in three technical replicates for each biological replicate. This provided a total of nine replicates for WT and nine replicates for Δ*fitAB* for extraction at both 10 hours and 14 hours post-gentamicin treatment (section 3.2.3). RNA was extracted from each of these samples (section 3.2.5.5) with 0.2 U μl^{-1} DNase in the DNase reaction. RNA from all the biological replicates was pooled at the end of the RNA extraction.

The increase in bacteria greatly improved the amount of RNA extracted (Table 3-6). As previous concentrations determined by NanoDrop™ differed greatly from that determined by the Agilent 2100 Bioanalyser, we measured the concentration using a Qubit® RNA BR assay kit (see section 3.2.4.4) as well. The Qubit® RNA BR analysis measures the concentration of intact RNA rather than free ribonucleotides. The concentration of RNA measured by this technique was outside the concentration range measureable by the Qubit® RNA BR assay (> 1200 ng μl^{-1}). Although an exact concentration could not be given by the Qubit® assay, this result indicated there was plenty of intact RNA that should meet BGI concentration requirements. The absorbance ratios at OD260/280 and OD260/230 were all greater than 2.0 (Table 3-6) indicating the RNA samples were pure with no contaminating DNA.

The samples were sent to BGI and independent tests using an Agilent 2100 Bioanalyser were carried out. The resulting concentrations were, again, lower than the NanoDrop™ measurements (Table 3-6) but still surpassed the RNA sequencing requirements. Unfortunately, the RIN values were all below 7.0 (Table 3-6) so sequencing was not recommended due to the possibility of library prep failure.

Table 3-6. RNA concentrations, OD260/280 and OD260/230 ratios, as measured by NanoDrop™ and Agilent 2100, of the second batch of samples sent to BGI.

	NanoDrop™			Agilent 2100 Bioanalyser	
Sample ID	**Concentration (ng µl^{-1})**	**OD 260/280**	**OD 260/230**	**Concentration (ng µl^{-1})**	**RIN**
WT 10hr	1560.5	2.06	2.01	620	5.9
Δ*fitAB* 10hr	2138.7	2.08	1.91	1340	4.2
WT 14hr	2791.1	2.09	2.12	1760	5
Δ*fitAB* 14hr	1634.0	2.06	2.01	1650	6.7

Subsequent intracellular replication assays and RNA extraction attempts failed to produce RNA that passed the sequencing requirements. After consultation with Prof. So and Dr Cherie Blenkrion, an expert in RNA sequencing, a decision was made to sequence the RNA from the last batch of samples sent to BGI (Table 3-6), despite the low RIN values. Unfortunately, the Illumina Ribo-zero rRNA Removal Kit used to deplete ribosomal RNA prior to library preparation was discontinued just prior to our decision to go ahead with sequencing. Other available rRNA depletion kits are yet to be trialled by BGI for sequencing *N. gonorrhoeae* RNA, so RNAseq is currently on hold.

3.4 Conclusion

The VapBC TA system, FitAB, decreases intracellular replication of *N. gonorrhoeae*. The population of *fitAB* gene deletion strains, within human epithelial cells, more than doubles in size over a four-hour period whilst WT bacteria remain at a slow, steady state of growth. Following rapid replication, *fitAB* gene deletion strains undergo a sudden cell death event, resulting in a dramatic decline in population. This is the most pronounced phenotype seen by a single TA mutant. In other bacteria, the difference in growth between *vapBC* deletion strains and the WT bacteria is much more subtle (McKenzie *et al.*, 2012b), and the sudden cell death event see for *N. gonorrhoeae* Δ*fitAB* has only been reported for an *M. smegmatis* triple TA deletion mutant (Frampton *et al.*, 2012). Despite having three other Type II TA systems, MazEF, RelBE and HicAB, it is evident FitAB

regulates growth of *N. gonorrhoeae* within human epithelial cells and is essential for sustaining long term survival of the population during infection.

An optimised method has been established for the extraction of RNA from *N. gonorrhoeae* grown within human epithelial cells. We have obtained RNA from WT and *fitAB* gene deletion strains of *N. gonorrhoeae* at different time-points during an intracellular replication experiment and this is currently awaiting sequencing and transcriptome analysis.

3.5 Future Research

The intracellular replication experiment will be repeated using cervical cells instead of A549 human lung epithelial cells to evaluate whether FitAB has the same effect in a cell line more relevant to *N. gonorrhoeae* infection.

The RNA will be sequenced to determine the transcriptomes of each strain of *N. gonorrhoeae* at different time-points. Transcriptomic analysis will determine differentially expressed genes between WT and *fitAB* gene deletion strains during different stages of intracellular growth. Transcripts that are up or down regulated will be applied to already established ribonuclease activity assays to determine if they are targeted by FitB. From these experiments we can determine the biological targets of FitB and determine how FitAB regulates intracellular growth of *N. gonorrhoeae.*

Chapter Four

Conclusion

N. gonorrhoeae, the causative agent of gonorrhoea, can cause asymptomatic infection by remaining within epithelial cells in a state of persistence (Workowski & Berman, 2007). The high rate of transmissible, asymptomatic infections in females and the acquisition of antibiotic resistance while in a persistent state are major contributing factors to the success of the pathogen. Little is known about the intracellular lifecycle of *N. gonorrhoeae* or the mechanisms of persistence. This thesis investigates the role of a toxin-antitoxin (TA) system in *N. gonorrhoeae* that regulates intracellular growth and produces a persistent phenotype.

TA systems consist of a stable toxin and a relatively unstable antitoxin, forming an inactive complex when both counterparts are expressed together. When the antitoxin degrades, the free toxin impedes cell growth and, in some cases, causes cell death. Despite being toxic to cells, TA systems are abundant in prokaryotes and archaea, which begs the question, what is the function of TA systems and why are they so important?

Several functions have been proposed for TA systems since they were first discovered over 30 years ago. The first TA systems described were encoded on plasmids (Gerdes *et al.*, 1986) and proposed to be plasmid maintenance modules. If segregants did not contain the plasmid, the antitoxin could not be expressed and replenished, leaving free toxin which would kill the cell. This function was questioned when TA loci were discovered on bacterial chromosomes (Gerdes *et al.*, 2005; Pandey & Gerdes, 2005). For some chromosomal TA systems, they were found within or linked to MGEs (Cambray *et al.*, 2010) and the proposed function was to maintain these MGEs in segregate cells (Hernández-Arriaga *et al.*, 2014). Many chromosomal systems, however, are not linked to MGEs and are often found in multiple copies throughout bacterial genomes, for example, *M. tuberculosis* has 80 chromosomal TA systems (Sala *et al.*, 2014). An abundance of these TA systems suggests they have more complex functions than initially thought.

Many chromosomal TA systems, particularly those belonging to the Type II family, have been characterised as stress-response elements (Christensen *et al.*, 2003; Gerdes, 2000). During periods of nutritional stress, chromosomal TA systems disrupt global translation of proteins and inhibit growth of the population (Christensen *et al.*, 2001; Gerdes, 2000; Jørgensen *et al.*, 2009). This response has been associated with the formation of persister cells to ensure the ultimate survival of bacterial populations (Amitai *et al.*, 2009; Coussens & Daines, 2016; Jørgensen *et al.*, 2009). As no TA system specific to *N. gonorrhoeae* has been characterised before, we wanted to characterise the function of FitAB, a Type II TA system found in the genome of *N. gonorrhoeae*, and assess whether it plays a role in persistence.

FitAB, is named after its fast intracellular trafficking phenotype (Hopper *et al.*, 2000) and belongs to the VapBC TA superfamily. Many VapC proteins have been characterised as sequence-specific ribonucleases (McKenzie *et al.*, 2012b; Sharrock *et al.*, 2018; Winther *et al.*, 2016; Winther & Gerdes, 2011). We have determined that FitB is a metal-dependent ribonuclease, targeting single-stranded RNA in a sequence-specific manner. FitB preferentially cuts RNA with a certain secondary structure but will bind to an array of single-stranded RNA fragments regardless of structure. FitB cuts RNA pentaprobes, which are approximately 160-nt long, but, unlike other VapC proteins, will not cut shorter RNA oligos of the same sequence. As FitAB is the only VapBC system in *N. gonorrhoeae*, it is likely the targeted sequence and secondary structure motif is highly specific to avoid off-target RNA cleavage.

We performed intracellular replication experiments to characterise the growth of *N. gonorrhoeae* wild-type and *fitAB* gene deletion strains within epithelial cells. In the *fitAB* deletion strain, intracellular replication is markedly faster than the wild-type strain. Between six and ten hours after gentamicin treatment the population of the *fitAB* deletion strain within the epithelial cells more than doubled, while growth of the wild-type population was delayed, doubling in size after 14 hours. This is the most pronounced difference in intracellular replication rate between wild-type and a single TA deletion mutant that has been characterised. In other bacteria, deletion of a VapBC system resulted in faster growth but the differences between that and wild-type were much more subtle (McKenzie *et al.*, 2012b).

Interestingly, by 14 hours, the population of the *fitAB* deletion strain had declined dramatically suggesting the occurrence of a sudden cell death event. This phenotype has only been reported once before, for an *M. smegmatis* triple TA mutant in which three different TA loci, *mazEF, vapBC* and *phd/doc*, were deleted (Frampton *et al.*, 2012). The mutant population experienced a sudden cell death event after a period of normal growth (Frampton *et al.*, 2012). This phenotype seen for *N. gonorrhoeae* suggests FitAB is important for regulating intracellular replication of *N. gonorrhoeae* and is essential for long term survival of the population during infection.

We extracted RNA from *N. gonorrhoeae* at different time-points during the intracellular replication experiment. This is awaiting sequencing and transcriptomic analyses. Once we have transcriptome data from the *fitAB* deletion mutant and wild-type strains, we can determine what transcripts are up or down regulated. Alignment of these transcripts with the biochemically determined FitB target cut site(s) will allow us to deduce the biological targets. We will apply the transcripts as substrates in the already established ribonuclease activity assays to confirm whether or not they are targets of FitB. This will help us determine the function of FitAB in *N. gonorrhoeae* during infection and contribute to our understanding of persistence.

Appendices

Appendix A: Gene & Protein Information

FitA (NGO0908) Information

FitA Gene Sequence (237 bp)

ATGGCTTCTGTTGTGATTAGAAATTTATCCGAGGCCACGCACAACGCA
ATCAAATTCCGTGCGCGAGCCGCAGGGCGCAGTACCGAAGCAGAAAT
CCGCTTAATTTTGGATAACATCGCCAAAGCACAACAAACTGTACGTTT
GGGGTCAATGTTGGCATCAATAGGGCAGGAAATCGGAGGTGTTGAGC
TGGAAGACGTACGCGGTCGTAATACTGATAACGAGGTTTCTTTGTGA

FitA *E. coli* optimised Gene Sequence (237 bp)

ATGGCTAGCGTTGTTATTCGTAATCTGAGCGAAGCAACCCATAACGCA
ATCAAATTTCGTGCACGTGCCGCAGGTCGTAGCACCGAAGCAGAAATT
CGTCTGATTCTGGATAATATTGCAAAAGCACAGCAGACCGTTCGTCTG
GGTAGCATGCTGGCAAGCATTGGTCAAGAAATTGGTGGTGTTGAACTG
GAAGATGTTCGTGGTCGTAATACCGATAATGAAGTTAGCCTGTGA

FitA Protein Sequence

MASVVIRNLSEATHNAIKFRARAAGRSTEAEIRLILDNIAKAQQTVRLGSM
LASIGQEIGGVELEDVRGRNTDNEVSL

78 amino acids
Molecular weight: 8.43 kDa
Theoretical pI: 6.57

FitB (NGO0907) Information

FitB Gene Sequence (420 bp)

ATGATTTTGCTGGACACGAATGTGATTTCCGAACCTTTGCGCCCACAA
CCCAATGAACGTGTGGTGGCATGGTTGGATAGTTTGATATTGGAAGAT
GTGTATTTGTCTGCCATTACTGTTGCAGAATTGCGTTTGGGTGTGGCGT
TGTTGCTCAATGGCAAGAAAAAGAATGTGCTGCACGAACGTTTGGAAC
AATCCATTTTGCCTTTATTTGCGGGGCGGATTCTGCCTTTTGATGAACC
GGTTGCCGCAATCTATGCGCAAATTCGTTCCTATGCCAAAACACATGG
CAAAGAGATTGCTGCCGCAGACGGCTATATTGCCGCCACTGCAAAACA
GCACAGTTTGACAGTTGCTACGCGTGATACCGGCTCATTTTTTGCGGCC
GATGTCGCGGTGTTCAATCCGTGGCACGATTAA

FitB Protein Sequence

MILLDTNVISEPLRPQPNERVVAWLDSLILEDVYLSAITVAELRLGVALLL
NGKKKNVLHERLEQSILPLFAGRILPFDEPVAAIYAQIRSYAKTHGKEIAA
ADGYIAATAKQHSLTVATRDTGSFFAADVAVFNPWHD

139 amino acids
Molecular weight: 15.3 kDa
Theoretical pI: 5.75

FitB *E. coli* Optimised Gene Sequence (417 bp)

ATGATTCTGCTGGATACCAATGTTATTAGCGAACCGCTGCGTCCGCAG
CCGAATGAACGTGTTGTTGCATGGCTGGATAGCCTGATTCTGGAAGAT
GTGTATCTGAGCGCAATTACCGTTGCAGAACTGCGTCTGGGTGTTGCA
CTGCTGCTGAATGGTAAAAAAAAAAACGTGCTGCATGAACGTCTGGA
ACAGAGCATTCTGCCGCTGTTTGCCGGTCGTATTCTGCCGTTTGATGAA
CCGGTTGCAGCAATTTATGCACAGATTCGTAGCTATGCAAAAACCCAC
GGTAAAGAAATTGCAGCAGCAGATGGTTATATTGCAGCAACCGCAAA
ACAGCATAGCCTGACCGTTGCAACCCGTGATACCGGTAGCTTTTTTGC
AGCCGATGTTGCAGTTTTTAATCCGTGGCATGAT

FitB Protein Sequence with His-tag

MILLDTNVISEPLRPQPNERVVAWLDSLILEDVYLSAITVAELRLGVALLL
NGKKKNVLHERLEQSILPLFAGRILPFDEPVAAIYAQIRSYAKTHGKEIAA
ADGYIAATAKQHSLTVATRDTGSFFAADVAVFNPWHDLEHHHHHH

147 amino acids
Molecular weight: 16.37 kDa
Theoretical pI: 6.17

FitAB Operon (NGO0907/8) Information

FitAB operon contains genes *fitA* and *fitB* as above with an overlapping nucleotide (highlighted green).

FitAB Operon (653 bp)

ATGGCTTCTGTTGTGATTAGAAATTTATCCGAGGCCACGCACAACGCA
ATCAAATTCCGTGCGCGAGCCGCAGGGCGCAGTACCGAAGCAGAAAT
CCGCTTAATTTTGGATAACATCGCCAAAGCACAACAAACTGTACGTTT
GGGGTCAATGTTGGCATCAATAGGGCAGGAAATCGGAGGTGTTGAGC
TGGAAGACGTACGCGGTCGTAATACTGATAACGAGGTTTCTTTGTGAT
GATTTTGCTGGACACGAATGTGATTTCCGAACCTTTGCGCCCACAACC
CAATGAACGTGTGGTGGCATGGTTGGATAGTTTGATATTGGAAGATGT
GTATTTGTCTGCCATTACTGTTGCAGAATTGCGTTTGGGTGTGGCGTTG
TTGCTCAATGGCAAGAAAAAGAATGTGCTGCACGAACGTTTGGAACA
ATCCATTTTGCCTTTATTTGCGGGGCGGATTCTGCCTTTTGATGAACCG
GTTGCCGCAATCTATGCGCAAATTCGTTCCTATGCCAAAACACATGGC
AAAGAGATTGCTGCCGCAGACGGCTATATTGCCGCCACTGCAAAACAG
CACAGTTTGACAGTTGCTACGCGTGATACCGGCTCATTTTTTGCGGCCG
ATGTCGCGGTGTTCAATCCGTGGCACGAT

FitAB Complex Protein Sequence

MASVVIRNLSEATHNAIKFRARAAGRSTEAEIRLILDNIAKAQQTVRLGSM
LASIGQEIGGVELEDVRGRNTDNEVSLMILLDTNVISEPLRPQPNERVVAW
LDSLILEDVYLSAITVAELRLGVALLLNGKKKNVLHERLEQSILPLFAGRIL
PFDEPVAAIYAQIRSYAKTHGKEIAAADGYIAATAKQHSLTVATRDTGSFF
AADVAVFNPWHD

271 amino acids
Molecular weight: 23.72 kDa
Isoelectric point: 5.97

FitAB Complex Protein Sequence with His-tag

MASVVIRNLSEATHNAIKFRARAAGRSTEAEIRLILDNIAKAQQTVRLGSM
LASIGQEIGGVELEDVRGRNTDNEVSLMILLDTNVISEPLRPQPNERVVAW
LDSLILEDVYLSAITVAELRLGVALLLNGKKKNVLHERLEQSILPLFAGRIL
PFDEPVAAIYAQIRSYAKTHGKEIAAADGYIAATAKQHSLTVATRDTGSFF
AADVAVFNPWHDLEHHHHHH

225 amino acids
Molecular weight: 24.79 kDa
Isoelectric point: 6.25

Appendix B: RNA Pentaprobe and Oligonucleotide Information

B.1. Pentaprobe Sequences with Flanking Vector Sequence

DNA sequence including flanking regions from pcDNA3 plasmid. The pentaprobe sequence is highlighted yellow.

Pentaprobe 922 + flanking sequences

AGACCCAAGCTTGGTACCGGAATTCTACGAATTTTTCTTTTGTTTATTTCCTTTCGCTTTGCTTCTCTTCCCTTCGGTTCTGTTCCGTTTTACCTTGTCTTGCCTTATCTTACTTTATCTAGAGGGCCCTATTCTATAGTGTCACCTAAATGCTAGAGCTCGCT

Pentaprobe 923 + flanking sequences

AGACCCAAGCTTGGTACTATCTTACTTTAGTTTCATTTAATTGTGTTGTACTCTCCTCTGCGTTCACTTAGCTTAACTTGGTTTGGCTTGATTTGACTTCAGTTGCGCTCTATTCTATCTAGAGGGCCCTATTCTATAGTGTCACCTAAATGCTAGAGCTCGCT

Pentaprobe 924 + flanking sequences

AGACCCAAGCTTGGTACCGCTCTATTCTACTGTCCTGTGCATTCAATCGTTGAGTTCGATCTAGTCTCGTCTAACCCTCCCCTGCTCCGCTGGTCTGGCCTCGCCTATCCTACCCATTCTAGAGGGCCCTATTCTATAGTGTCACCTAAATGCTAGAGCTCGCT

Pentaprobe 925 + flanking sequences

AGACCCAAGCTTGGTACTATCCTACCCATTGGGCTCATCTGATCCATCCGGTCCCGTCCACTCGGCTATGTTATGCTGTATTGCAGTCGTGTCGCGTCGAGCTGCCCTAATCCCACCTCTAGAGGGCCCTATTCTATAGTGTCACCTAAATGCTAGAGCTCGCT

Pentaprobe 926 + flanking sequences

AGACCCAAGCTTGGTACCCTAATCCCACCTAGCGTATCGGGTCATGTAGTGCTACGTTACGGCCCCCGCCCGGCATCATATTATATCACCCCAGTGTAATGTGGTGTGAGGTTGGAGTCTAGAGGGCCCTATTCTATAGTGTCACCTAAATGCTAGAGCTCGCT

Pentaprobe 927 + flanking sequences

AGACCCAAGCTTGGTACGTGAGGTTGGAGTCCGACCTGGAATCTCAGCCTGACGTGCCATGCGGTGCGATGTCACGCCGCGCCACGGTATAGTATGGTACGGGATCCCGTCTAGAGGGCCCTATTCTATAGTGTCACCTAAATGCTAGAGCTCGCT

Pentaprobe 932 + flanking sequences (reverse complement of 926)

AGACCCAAGCTTGGTACCGAGCTCGGATCCACTAGTAACGGCCGCCAGTGTGCTGGAATTCTGCAGATCTCCAACCTCACACCACATTACACTGGGGTGATATAATATGATGCCGGGCGGGGGCCGTAACGTAGCACTACATGACCCGATACGCTAGGTGGGATTAGGCATCACACTGGCGGCCGCTCGAGCATGCATCTAGAGGGCCCTATTCTATAGTGTCACCTAAATGCTAGAGCTCGCT

B.2. Pentaprobe Secondary Structures

Pentaprobe secondary structures were predicted for the pentaprobe sequence including the flanking sequence using RNAfold from the Vienna RNA Secondary Structure Server. Nucleotide colours indicate the probability of base-pair folding based on a colour spectrum:

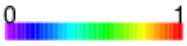

Pentaprobe 922

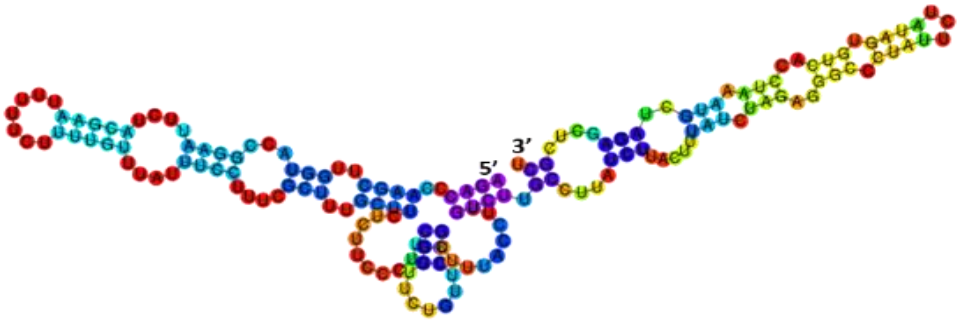

Pentaprobe 924

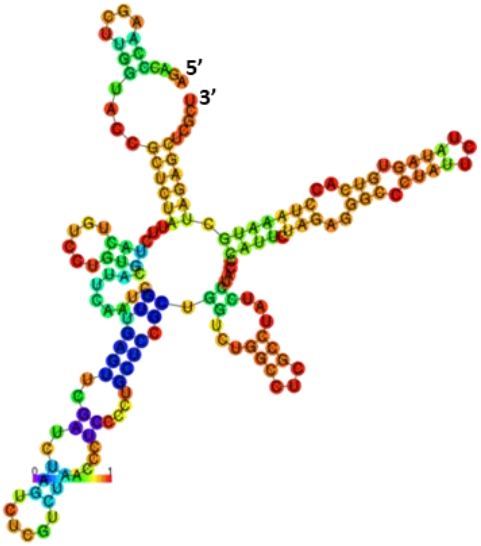

Pentaprobe 925

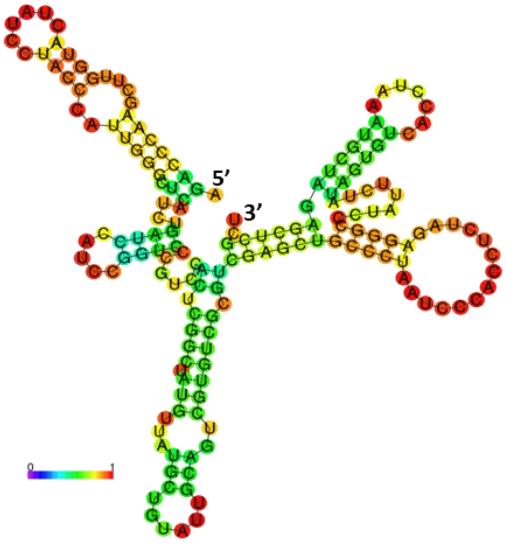

Pentaprobe 926

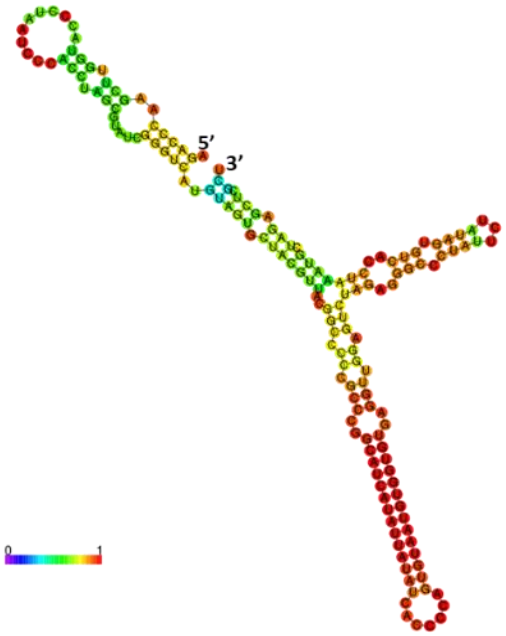

Pentaprobe 927

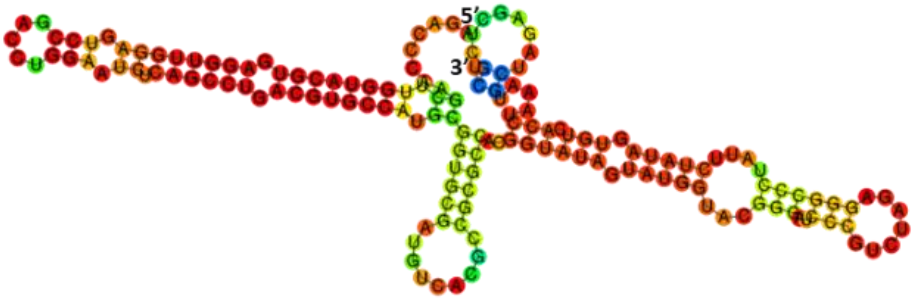

Pentaprobe 932

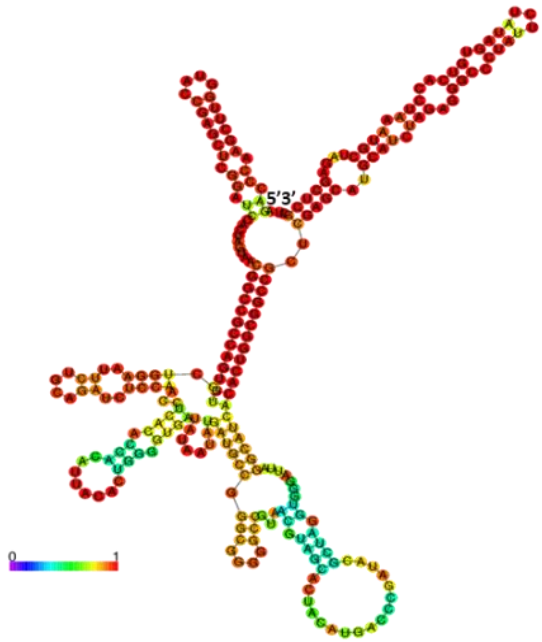

B.3. Oligonucleotide Sequences

RNA oligo sequences are based on parent pentaprobe 923 sequence.

Oligo 1

TATCTTACTTTAGTTTCATTTAATTGTGTT

Oligo 2

TAATTGTGTTGTACTCTCCTCTGCGTTCAC

Oligo 3

CTGCGTTCACTTAGCTTAACTTGGTTTGGC

Oligo 4

TTGGTTTGGCTTGATTTGACTTCAGTTGCG

Oligo 5

TTCAGTTGCGCTCTATTCTA

Appendix C: Raw Data

The following is raw data relating to Chapter Three.

Table C-1. Intracellular bacteria cell counts in cells.ml^{-1} for each biological replicate (numbered 1-3) at each time point (hours post-gentamicin treatment), corresponding to figure 3-2.

	WT			**Δ*fitAB***		
Time (hours)	**1**	**2**	**3**	**1**	**2**	**3**
0	240000	240000	226667	1533333	53333	120000
6	73333	180000	313333	46667	40000	46667
8	133333	220000	86667	53333	46667	53333
10	186667	40000	173333	46667	46667	273333
14	453333	146667	193333	26667	33333	13333
24	100000	40000	126667	6667	20000	26667

Table C-2. Intracellular bacteria cell counts normalised as percent of zero hour for each biological replicate (numbered 1-3) at each time point (hours post-gentamicin treatment) and P values, corresponding to figure 3-2. P values are recorded as calculated using the Holm-Sidak method in Prism.

	WT			**Δ*fitAB***			
Time (hours)	**1**	**2**	**3**	**1**	**2**	**3**	**P value**
0	100.00	100.00	100.00	100.00	100.00	100.00	
6	30.56	75.00	138.24	30.43	75.00	38.89	0.39
8	55.56	91.67	38.24	34.78	87.50	44.44	0.80
10	77.78	16.67	76.47	30.43	87.50	227.78	0.40
14	188.89	61.11	85.29	17.39	62.50	11.11	0.13
24	41.67	16.67	55.88	4.35	37.50	22.22	0.33

Table C-3. Intracellular bacteria cell counts normalised as percent of zero hour for each biological replicate (numbered 1-3) at each time point (hours post-gentamicin treatment) and P values, corresponding to figure 3-3. P values are recorded as calculated using the Holm-Sidak method in Prism.

Time (hours)	WT						Δ*fitAB*						
	1	**2**	**3**	**4**	**5**	**6**	**1**	**2**	**3**	**4**	**5**	**6**	**P value**
0	100.00	100.00	100.00	100.00	100.00	100.00	100.00	100.00	100.00	100.00	100.00	100.00	
6	20.90	37.74	37.50	30.56	75.00	138.24	58.62	63.64	66.67	30.43	75.00	38.89	0.96
8	25.37	35.85	25.37	55.56	91.67	38.24	113.79	109.09	127.08	34.78	87.50	44.44	0.05
10	59.70	56.60	59.70	77.78	16.67	76.47	182.76	221.21	218.75	30.43	87.50	227.78	0.01
14	-	-	-	188.89	61.11	85.29	-	-	-	17.39	62.50	11.11	0.13
24	77.61	141.51	116.42	41.67	16.67	55.88	25.86	39.39	39.58	4.35	37.50	22.22	0.04

Table C-4. Intracellular bacteria cell counts in cells.ml^{-1} for each biological replicate (numbered 1-3) at each time point (hours post-gentamicin treatment), corresponding to figure 3-4.

	WT			Δ*fitAB*		
Time (hours)	**1**	**2**	**3**	**1**	**2**	**3**
0	7466.67	9666.67	9533.33	11133.3	10333.3	10466.6
6	3733.33	5000.00	4800.00	7800.00	7666.67	6533.33
8	3533.33	4933.33	6266.67	9266.67	7800.00	7733.33
10	4133.33	5400.00	5066.67	8000.00	8000.00	7400.00
14	7266.67	7600.00	7333.33	2733.33	6466.67	7866.67
24	14266.67	12066.67	11600.00	12666.6	10866.6	11866.6

Table C-5. Intracellular bacteria cell counts normalised as a percent per zero hour for each biological replicate (numbered 1-3) at each time point (hours post-gentamicin treatment) and P values, corresponding to figure 3-4. P values are recorded as calculated using the Holm-Sidak method in Prism.

	WT			Δ*fitAB*			
Time (hours)	**1**	**2**	**3**	**1**	**2**	**3**	**P value**
0	100.00	100.00	100.00	100.00	100.00	100.00	
6	50.00	51.72	50.35	70.06	74.19	62.42	0.01
8	47.32	51.03	65.73	83.23	75.48	73.89	0.02
10	55.36	55.86	53.15	71.86	77.42	70.70	0.00
14	97.32	78.62	76.92	24.55	62.58	75.16	0.14
24	191.07	124.83	121.68	113.77	105.16	113.38	0.20

References

Ahidjo, B. A., Kuhnert, D., McKenzie, J. L., Machowski, E. E., Gordhan, B. G., Arcus, V., Abrahams, G. L., & Mizrahi, V. (2011). VapC toxins from *Mycobacterium tuberculosis* are ribonucleases that differentially inhibit growth and are neutralized by cognate VapB antitoxins. *PloS one, 6*(6), e21738.

Aizenman, E., Engelberg-Kulka, H., & Glaser, G. (1996). An Escherichia coli chromosomal "addiction module" regulated by guanosine [corrected] 3',5'-bispyrophosphate: a model for programmed bacterial cell death. *Proceedings of the National Academy of Sciences of the United States of America, 93*(12), 6059-6063.

Alirol, E., Wi, T. E., Bala, M., Bazzo, M. L., Chen, X.-S., Deal, C., Dillon, J.-A. R., Kularatne, R., Heim, J., Hooft van Huijsduijnen, R., Hook, E. W., Lahra, M. M., Lewis, D. A., Ndowa, F., Shafer, W. M., Tayler, L., Workowski, K., Unemo, M., & Balasegaram, M. (2017). Multidrug-resistant gonorrhea: A research and development roadmap to discover new medicines. *PLoS Medicine, 14*(7), e1002366.

Amitai, S., Kolodkin-Gal, I., Hananya-Meltabashi, M., Sacher, A., & Engelberg-Kulka, H. (2009). *Escherichia coli* MazF leads to the simultaneous selective synthesis of both "death proteins" and "survival proteins". *PLoS genetics, 5*(3), e1000390-e1000390.

Anantharaman, V., & Aravind, L. (2003). New connections in the prokaryotic toxin-antitoxin network: relationship with the eukaryotic nonsense-mediated RNA decay system. *Genome Biology, 4*(12), R81-R81.

Arcus, V. L., Backbro, K., Roos, A., Daniel, E. L., & Baker, E. N. (2004). Distant structural homology leads to the functional characterization of an archaeal PIN domain as an exonuclease. *Journal of Biological Chemistry, 279*(16), 16471-16478.

Arcus, V. L., McKenzie, J. L., Robson, J., & Cook, G. M. (2011). The PIN-domain ribonucleases and the prokaryotic VapBC toxin–antitoxin array. *Protein Engineering, Design & Selection, 24*(1-2), 33-40.

Arcus, V. L., Rainey, P. B., & Turner, S. J. (2005). The PIN-domain toxin–antitoxin array in mycobacteria. *Trends in microbiology, 13*(8), 360-365.

Balaban, N. Q. (2011). Persistence: mechanisms for triggering and enhancing phenotypic variability. *Current Opinion in Genetics & Development, 21*(6), 768-775.

Bibi-Triki, S., Li de la Sierra-Gallay, I., Lazar, N., Leroy, A., Van Tilbeurgh, H., Sebbane, F., & Pradel, E. (2014). Functional and structural analysis of HicA3-HicB3, a novel toxin-antitoxin system of Yersinia pestis. *Journal of bacteriology, 196*(21), 3712-3723.

Bigger, J. W. (1944). Treatment of staphylococcal infections with penicillin by intermittent sterilisation. *The Lancet, 244*(6320), 497-500.

Billker, O., Popp, A., Brinkmann, V., Wenig, G., Schneider, J., Caron, E., & Meyer, T. F. (2002). Distinct mechanisms of internalization of *Neisseria gonorrhoeae* by members of the CEACAM receptor family involving Rac1- and Cdc42-dependent and -independent pathways. *The EMBO journal, 21*(4), 560-571.

Bunker, R. D., McKenzie, J. L., Baker, E. N., & Arcus, V. L. (2008). Crystal structure of PAE0151 from Pyrobaculum aerophilum, a PIN-domain (VapC) protein from a toxin-antitoxin operon. *Proteins: Structure, Function, and Bioinformatics, 72*(1), 510-518.

Butt, A., Higman, V. A., Williams, C., Crump, M. P., Hemsley, C. M., Harmer, N., & Titball, R. W. (2014). The HicA toxin from Burkholderia pseudomallei has a role in persister cell formation. *The Biochemical journal, 459*(2), 333-344.

Cambray, G., Guerout, A.-M., & Mazel, D. (2010). Integrons. *Annual Review of Genetics, 44*(1), 141-166.

Chomczynski, P., & Mackey, K. (1995). Substitution of Chloroform by Bromochloropropane in the Single-Step Method of RNA Isolation. *Analytical Biochemistry, 225*(1), 163-164.

Chomczynski, P., & Sacchi, N. (1987). Single-step method of RNA isolation by acid guanidinium thiocyanate-phenol-chloroform extraction. *Analytical biochemistry, 162*(1), 156-159.

Christensen, S. K., & Gerdes, K. (2003). RelE toxins from Bacteria and Archaea cleave mRNAs on translating ribosomes, which are rescued by tmRNA. *Molecular Microbiology, 48*(5), 1389-1400.

Christensen, S. K., Mikkelsen, M., Pedersen, K., & Gerdes, K. (2001). RelE, a global inhibitor of translation, is activated during nutritional stress. *Proceedings of the National Academy of Sciences of the United States of America, 98*(25), 14328-14333.

Christensen, S. K., Pedersen, K., Hansen, F. G., & Gerdes, K. (2003). Toxin–antitoxin Loci as Stress-response-elements: ChpAK/MazF and ChpBK Cleave Translated RNAs and are Counteracted by tmRNA. *Journal of Molecular Biology, 332*(4), 809-819.

Cicinnati, V. R., Shen, Q., Sotiropoulos, G. C., Radtke, A., Gerken, G., & Beckebaum, S. (2008). Validation of putative reference genes for gene expression studies in human hepatocellular carcinoma using real-time quantitative RT-PCR. *BMC cancer, 8*, 350-350.

Clissold, P. M., & Ponting, C. P. (2000). PIN domains in nonsense-mediated mRNA decay and RNAi. *Current Biology, 10*(24), R888-R890.

Coussens, N. P., & Daines, D. A. (2016). Wake me when it's over - Bacterial toxin-antitoxin proteins and induced dormancy. *Experimental biology and medicine (Maywood, N.J.), 241*(12), 1332-1342.

Dienemann, C., Bøggild, A., Winther, K. S., Gerdes, K., & Brodersen, D. E. (2011). Crystal structure of the VapBC toxin-antitoxin complex from Shigella flexneri reveals a hetero-octameric DNA-binding assembly. *Journal of molecular biology, 414*(5), 713-722.

Dillard, J. P. (2011). Genetic Manipulation of *Neisseria gonorrhoeae*. *Current protocols in microbiology, 0 4*, Unit4A.2-Unit4A.2.

Duyvestyn, J. M. (2012). *Mechanism of RNase cleavage by VapC from Pyrobaculum aerophilum*. Masters thesis, University of Waikato, Hamilton, New Zealand.

Edwards, J. L., & Apicella, M. A. (2004). The molecular mechanisms used by *Neisseria gonorrhoeae* to initiate infection differ between men and women. *Clinical Microbiology Reviews, 17*(4), 965-981.

Edwards, J. L., & Butler, E. K. (2011). The Pathobiology of *Neisseria gonorrhoeae* Lower Female Genital Tract Infection. *Frontiers in Microbiology, 2*, 102.

ESR. (Compiler) (2014). *Sexually transmitted infections in New Zealand: Annual Surveillance Report 2014*. Porirua, New Zealand.

Evans, B. A. (1977). Ultrastructural Study of Cervical Gonorrhea. *Journal of Infectious Diseases, 136*(2), 248-255.

Eyre, D. W., Sanderson, N. D., Lord, E., Regisford-Reimmer, N., Chau, K., Barker, L., Morgan, M., Newnham, R., Golparian, D., Unemo, M., Crook, D. W., Peto, T. E. A., Hughes, G., Cole, M. J., Fifer, H., Edwards, A., & Andersson, M. I. (2018). Gonorrhoea treatment failure caused by a *Neisseria gonorrhoeae* strain with combined ceftriaxone and high-level azithromycin resistance, England, February 2018. *Eurosurveillance, 23*(27), 2-7.

Farrell Jr, R. E. (2009). *RNA Methodologies: laboratory guide for isolation and characterization*. Academic Press.

Fineran, P. C., Blower, T. R., Foulds, I. J., Humphreys, D. P., Lilley, K. S., & Salmond, G. P. C. (2009). The phage abortive infection system, ToxIN, functions as a protein–RNA toxin–antitoxin pair. *Proceedings of the National Academy of Sciences of the United States of America, 106*(3), 894-899.

Fisette, P. L., Ram, S., Andersen, J. M., Guo, W., & Ingalls, R. R. (2003). The Lip lipoprotein from *Neisseria gonorrhoeae* stimulates cytokine release and NF-kappa B activation in epithelial cells in a toll-like receptor 2-dependent manner. *Journal of Biological Chemistry, 278*(47), 46252-46260.

Frampton, R., Aggio, R. B. M., Villas-Bôas, S. G., Arcus, V. L., & Cook, G. M. (2012). Toxin-antitoxin systems of *Mycobacterium smegmatis* are essential for cell survival. *The Journal of biological chemistry, 287*(8), 5340-5356.

Gerdes, K. (2000). Toxin-Antitoxin Modules May Regulate Synthesis of Macromolecules during Nutritional Stress. *Journal of Bacteriology, 182*(3), 561.

Gerdes, K., Christensen, S. K., & Løbner-Olesen, A. (2005). Prokaryotic toxin–antitoxin stress response loci. *Nature Reviews Microbiology, 3*(5), 371.

Gerdes, K., Rasmussen, P. B., & Molin, S. (1986). Unique type of plasmid maintenance function: postsegregational killing of plasmid-free cells. *Proceedings of the National Academy of Sciences of the United States of America, 83*(10), 3116-3120.

Gubler, U., & Hoffman, B. J. (1983). A simple and very efficient method for generating cDNA libraries. *Gene, 25*(2), 263-269.

Gupta, A., Venkataraman, B., Vasudevan, M., & Gopinath Bankar, K. (2017). Co-expression network analysis of toxin-antitoxin loci in *Mycobacterium tuberculosis* reveals key modulators of cellular stress. *Scientific Reports, 7*(1), 5868.

Harms, A., Brodersen, D. E., Mitarai, N., & Gerdes, K. (2018). Toxins, Targets, and Triggers: An Overview of Toxin-Antitoxin Biology. *Molecular Cell, 70*(5), 768-784.

Hayes, F. (2003). Toxins-Antitoxins: Plasmid Maintenance, Programmed Cell Death, and Cell Cycle Arrest. *Science, 301*(5639), 1496.

Hazan, R., Sat, B., & Engelberg-Kulka, H. (2004). *Escherichia coli* mazEF-mediated cell death is triggered by various stressful conditions. *Journal of bacteriology, 186*(11), 3663-3669.

Hernández-Arriaga, A. M., Chan, W. T., Espinosa, M., & Díaz-Orejas, R. (2014). Conditional Activation of Toxin-Antitoxin Systems: Postsegregational Killing and Beyond. *Microbiology Spectrum, 2*(5).

Hicks, J. L., & Mullholland, C. V. (2018). Cysteine biosynthesis in Neisseria species. *Microbiology, 164*(12), 1471-1480.

Hill, S. A., Masters, T. L., & Wachter, J. (2016). Gonorrhea - an evolving disease of the new millennium. *Microbial Cell, 3*(9), 371-389.

Hofacker, I. L. (2003). Vienna RNA secondary structure server. *Nucleic acids research, 31*(13), 3429-3431.

Holmes, K. K., Counts, G. W., & Beaty, H. N. (1971). Disseminated gonococcal infection. *Annals of Internal Medicine, 74*(6), 979-993.

Hopper, S., Wilbur, J. S., Vasquez, B. L., Larson, J., Clary, S., Mehr, I. J., Seifert, H. S., & So, M. (2000). Isolation of *Neisseria gonorrhoeae* mutants that show enhanced trafficking across polarized T84 epithelial monolayers. *Infection and Immunity, 68*(2), 896-905.

Jørgensen, M. G., Pandey, D. P., Jaskolska, M., & Gerdes, K. (2009). HicA of *Escherichia coli* defines a novel family of translation-independent mRNA interferases in bacteria and archaea. *Journal of bacteriology, 191*(4), 1191-1199.

Kamada, K., Hanaoka, F., & Burley, S. K. (2003). Crystal structure of the MazE/MazF complex: molecular bases of antidote-toxin recognition. *Molecular cell, 11*(4), 875-884.

Keren, I., Minami, S., Rubin, E., & Lewis, K. (2011). Characterization and Transcriptome Analysis of *Mycobacterium tuberculosis* Persisters. *mBio, 2*(3), e00100-11.

Kim, D.-H., Kang, S.-M., Park, S. J., Jin, C., Yoon, H.-J., & Lee, B.-J. (2018). Functional insights into the Streptococcus pneumoniae HicBA toxin-antitoxin system based on a structural study. *Nucleic acids research, 46*(12), 6371-6386.

Kirpekar, F., Nordhoff, E., Kristiansen, K., Roepstorff, P., Lezius, A., Hahner, S., Karas, M., & Hillenkamp, F. (1994). Matrix assisted laser desorption/ionization mass spectrometry of enzymatically synthesized RNA up to 150 kDa. *Nucleic acids research, 22*(19), 3866-3870.

Kredich, N. M., & Tomkins, G. M. (1966). The enzymic synthesis of L-cysteine in *Escherichia coli* and *Salmonella typhimurium*. *Journal of Biological Chemistry, 241*(21), 4955-4965.

Kwan, A. H. Y., Czolij, R., Mackay, J. P., & Crossley, M. (2003). Pentaprobe: a comprehensive sequence for the one-step detection of DNA-binding activities. *Nucleic acids research, 31*(20), e124-e124.

Lee, K.-Y., & Lee, B.-J. (2016). Structure, Biology, and Therapeutic Application of Toxin–Antitoxin Systems in Pathogenic Bacteria. *Toxins, 8*(10).

Leplae, R., Geeraerts, D., Hallez, R., Guglielmini, J., Drèze, P., & Van Melderen, L. (2011). Diversity of bacterial type II toxin–antitoxin systems: a comprehensive search and functional analysis of novel families. *Nucleic Acids Research, 39*(13), 5513-5525.

Lewis, K. (2010). Persister Cells. *Annual Review of Microbiology, 64*(1), 357-372.

Lobato-Márquez, D., Díaz-Orejas, R., & García-del Portillo, F. (2016). Toxin-antitoxins and bacterial virulence. *FEMS Microbiology Reviews, 40*(5), 592-609.

Luebbehusen, H. (Compiler). *The Significance of the 260/230 Ratio in Determining Nucleic Acid Purity. 2004.*

Maisonneuve, E., & Gerdes, K. (2014). Molecular Mechanisms Underlying Bacterial Persisters. *Cell, 157*(3), 539-548.

Makarova, K. S., Grishin, N. V., & Koonin, E. V. (2006). The HicAB cassette, a putative novel, RNA-targeting toxin-antitoxin system in archaea and bacteria. *Bioinformatics, 22*(21), 2581-2584.

Maté, M. J., Vincentelli, R., Foos, N., Raoult, D., Cambillau, C., & Ortiz-Lombardía, M. (2012). Crystal structure of the DNA-bound VapBC2 antitoxin/toxin pair from Rickettsia felis. *Nucleic acids research, 40*(7), 3245-3258.

Matelska, D., Steczkiewicz, K., & Ginalski, K. (2017). Comprehensive classification of the PIN domain-like superfamily. *Nucleic acids research, 45*(12), 6995-7020.

Mattison, K., Wilbur, J. S., So, M., & Brennan, R. G. (2006). Structure of FitAB from *Neisseria gonorrhoeae* bound to DNA reveals a tetramer of toxin-antitoxin heterodimers containing pin domains and ribbon-helix-helix motifs. *Journal of Biological Chemistry, 281*(49), 37942-37951.

McKenzie, J. L. (2011). *The Biochemistry of VapBC Toxin-Antitoxins.* Doctoral thesis, University of Waikato, Hamilton, New Zealand.

McKenzie, J. L., Duyvestyn, J. M., Smith, T., Bendak, K., MacKay, J., Cursons, R., Cook, G. M., & Arcus, V. L. (2012a). Determination of ribonuclease sequence-specificity using Pentaprobes and mass spectrometry. *Rna, 18*(6), 1267-1278.

McKenzie, J. L., Robson, J., Berney, M., Smith, T. C., Ruthe, A., Gardner, P. P., Arcus, V. L., & Cook, G. M. (2012b). A VapBC toxin-antitoxin module is a posttranscriptional regulator of metabolic flux in mycobacteria. *Journal of bacteriology, 194*(9), 2189-2204.

Mhlanga-Mutangadura, T., Morlin, G., Smith, A. L., Eisenstark, A., & Golomb, M. (1998). Evolution of the major pilus gene cluster of Haemophilus influenzae. *Journal of bacteriology, 180*(17), 4693-4703.

Miallau, L., Faller, M., Chiang, J., Arbing, M., Guo, F., Cascio, D., & Eisenberg, D. (2009). Structure and proposed activity of a member of the VapBC family of toxin-antitoxin systems. VapBC-5 from *Mycobacterium tuberculosis. The Journal of Biological Chemistry, 284*(1), 276-283.

Min, A. B., Miallau, L., Sawaya, M. R., Habel, J., Cascio, D., & Eisenberg, D. (2012). The crystal structure of the Rv0301-Rv0300 VapBC-3 toxin-antitoxin complex from *M. tuberculosis* reveals a Mg^{2+} ion in the active site and a putative RNA-binding site. *Protein science : a publication of the Protein Society, 21*(11), 1754-1767.

Mittenhuber, G. (1999). Occurence of mazEF-like antitoxin/toxin systems in bacteria. *Journal of molecular microbiology and biotechnology, 1*(2), 295-302.

Miyamoto, T., Kato, Y., Sekiguchi, Y., Tsuneda, S., & Noda, N. (2016). Characterization of MazF-Mediated Sequence-Specific RNA Cleavage in

Pseudomonas putida Using Massive Parallel Sequencing. *PloS one, 11*(2), e0149494-e0149494.

Newman, L., Rowley, J., Vander Hoorn, S., Wijesooriya, N. S., Unemo, M., Low, N., Stevens, G., Gottlieb, S., Kiarie, J., & Temmerman, M. (2015). Global Estimates of the Prevalence and Incidence of Four Curable Sexually Transmitted Infections in 2012 Based on Systematic Review and Global Reporting. *PLoS ONE, 10*(12), e0143304.

Nudel, K., McClure, R., Moreau, M., Briars, E., Abrams, A. J., Tjaden, B., Su, X.-H., Trees, D., Rice, P. A., Massari, P., & Genco, C. A. (2018). Transcriptome Analysis of *Neisseria gonorrhoeae* during Natural Infection Reveals Differential Expression of Antibiotic Resistance Determinants between Men and Women. *mSphere, 3*(3), e00312-18.

Ochman, H., Lawrence, J. G., & Groisman, E. A. (2000). Lateral gene transfer and the nature of bacterial innovation. *Nature, 405*, 299.

Olsen, L. R., Huang, B., Vetting, M. W., & Roderick, S. L. (2004). Structure of serine acetyltransferase in complexes with CoA and its cysteine feedback inhibitor. *Biochemistry, 43*(20), 6013-6019.

Page, R., & Peti, W. (2016). Toxin-antitoxin systems in bacterial growth arrest and persistence. *Nat Chem Biol, 12*(4), 208-214.

Pandey, D. P., & Gerdes, K. (2005). Toxin-antitoxin loci are highly abundant in free-living but lost from host-associated prokaryotes. *Nucleic acids research, 33*(3), 966-976.

Pedersen, K., Christensen, S. K., & Gerdes, K. (2002). Rapid induction and reversal of a bacteriostatic condition by controlled expression of toxins and antitoxins. *Molecular Microbiology, 45*(2), 501-510.

Pye, V. E., Tingey, A. P., Robson, R. L., & Moody, P. C. (2004). The structure and mechanism of serine acetyltransferase from *Escherichia coli*. *Journal of Biological Chemistry, 279*(39), 40729-40736.

Ramage, H. R., Connolly, L. E., & Cox, J. S. (2009). Comprehensive Functional Analysis of *Mycobacterium tuberculosis* Toxin-Antitoxin Systems: Implications for Pathogenesis, Stress Responses, and Evolution. *PLOS Genetics, 5*(12), e1000767.

Ramsey, K. H., Schneider, H., Cross, A. S., Boslego, J. W., Hoover, D. L., Staley, T. L., Kuschner, R. A., & Deal, C. D. (1995). Inflammatory cytokines produced in response to experimental human gonorrhea. *Journal of Infectious Diseases, 172*(1), 186-191.

Remmele, C. W., Xian, Y., Albrecht, M., Faulstich, M., Fraunholz, M., Heinrichs, E., Dittrich, M. T., Müller, T., Reinhardt, R., & Rudel, T. (2014). Transcriptional landscape and essential genes of *Neisseria gonorrhoeae*. *Nucleic acids research, 42*(16), 10579-10595.

Robson, J., McKenzie, J. L., Cursons, R., Cook, G. M., & Arcus, V. L. (2009). The vapBC Operon from *Mycobacterium smegmatis* Is An Autoregulated Toxin–Antitoxin Module That Controls Growth via Inhibition of Translation. *Journal of Molecular Biology, 390*(3), 353-367.

Sala, A., Bordes, P., & Genevaux, P. (2014). Multiple Toxin-Antitoxin Systems in *Mycobacterium tuberculosis*. *Toxins, 6*(3), 1002-1020.

Shao, Y., Harrison, E. M., Bi, D., Tai, C., He, X., Ou, H.-Y., Rajakumar, K., & Deng, Z. (2011). TADB: a web-based resource for Type 2 toxin-antitoxin loci in bacteria and archaea. *Nucleic acids research, 39*(Database issue), D606-D611.

Sharp, J. D., Cruz, J. W., Raman, S., Inouye, M., Husson, R. N., & Woychik, N. A. (2012). Growth and translation inhibition through sequence-specific RNA binding by *Mycobacterium tuberculosis* VapC toxin. *The Journal of Biological Chemistry, 287*(16), 12835-12847.

Sharrock, A., Ruthe, A., Andrews, E. S. V., Arcus, V. A., & Hicks, J. L. (2018). VapC proteins from *Mycobacterium tuberculosis* share ribonuclease sequence specificity but differ in regulation and toxicity. *PloS one, 13*(8), e0203412-e0203412.

Simms, D., Cizdziel, P. E., & Chomczynski, P. (1993). TRIzol: A new reagent for optimal single-step isolation of RNA. *Focus, 15*(4), 532-535.

Swanson, J., Robbins, K., Barrera, O., Corwin, D., Boslego, J., Ciak, J., Blake, M., & Koomey, J. M. (1987). Gonococcal pilin variants in experimental gonorrhea. *The Journal of Experimental Medicine, 165*(5), 1344.

Thomas, B., & Akoulitchev, A. V. (2006). Mass spectrometry of RNA. *Trends in Biochemical Sciences, 31*(3), 173-181.

Tuomanen, E. (1986). Phenotypic tolerance: the search for β-lactam antibiotics that kill nongrowing bacteria. *Reviews of infectious diseases, 8*(Supplement_3), S279-S291.

Unemo, M. (2015). Current and future antimicrobial treatment of gonorrhoea – the rapidly evolving *Neisseria gonorrhoeae* continues to challenge. *BMC Infectious Diseases, 15*, 364.

Unemo, M., & Shafer, W. M. (2014). Antimicrobial Resistance in *Neisseria gonorrhoeae* in the 21st Century: Past, Evolution, and Future. *Clinical Microbiology Reviews, 27*(3), 587-613.

Wall, D., & Kaiser, D. (1999). Type IV pili and cell motility. *Molecular Microbiology, 32*(1), 01-10.

Wang, J., Gray-Owen, S. D., Knorre, A., Meyer, T. F., & Dehio, C. (1998). Opa binding to cellular CD66 receptors mediates the transcellular traversal of *Neisseria gonorrhoeae* across polarized T84 epithelial cell monolayers. *Molecular Microbiology, 30*(3), 657-671.

Wi, T., Lahra, M. M., Ndowa, F., Bala, M., Dillon, J.-A. R., Ramon-Pardo, P., Eremin, S. R., Bolan, G., & Unemo, M. (2017). Antimicrobial resistance in *Neisseria gonorrhoeae*: Global surveillance and a call for international collaborative action. *PLOS Medicine, 14*(7), e1002344.

Wilbur, J. S., Chivers, P. T., Mattison, K., Potter, L., Brennan, R. G., & So, M. (2005). *Neisseria gonorrhoeae* FitA Interacts with FitB To Bind DNA through Its Ribbon−Helix−Helix Motif. *Biochemistry, 44*(37), 12515-12524.

Winter, A. J., Williams, C., Isupov, M. N., Crocker, H., Gromova, M., Marsh, P., Wilkinson, O. J., Dillingham, M. S., Harmer, N. J., Titball, R. W., & Crump, M. P. (2018). The molecular basis of protein toxin HicA–dependent binding of the protein antitoxin HicB to DNA. *Journal of Biological Chemistry, 293*(50), 19429-19440.

Winther, K., Tree, J. J., Tollervey, D., & Gerdes, K. (2016). VapCs of *Mycobacterium tuberculosis* cleave RNAs essential for translation. *Nucleic acids research, 44*(20), 9860-9871.

Winther, K. S., Brodersen, D. E., Brown, A. K., & Gerdes, K. (2013). VapC20 of *Mycobacterium tuberculosis* cleaves the Sarcin–Ricin loop of 23S rRNA. *Nature Communications, 4*, 2796.

Winther, K. S., & Gerdes, K. (2009). Ectopic production of VapCs from *Enterobacteria* inhibits translation and *trans*-activates YoeB mRNA interferase. *Molecular Microbiology, 72*(4), 918-930.

Winther, K. S., & Gerdes, K. (2011). Enteric virulence associated protein VapC inhibits translation by cleavage of initiator tRNA. *Proceedings of the National Academy of Sciences of the United States of America, 108*(18), 7403-7407.

Winther, K. S., & Gerdes, K. (2012). Regulation of enteric vapBC transcription: induction by VapC toxin dimer-breaking. *Nucleic acids research, 40*(10), 4347-4357.

Workowski, K. A., & Berman, S. M. (2007). Centers for Disease Control and Prevention Sexually Transmitted Diseases Treatment Guidelines. *Clinical Infectious Diseases, 44*(Supplement_3), S73-S76.

Workowski, K. A., Bolan, G. A., Centers for Disease, C., & Prevention. (2015). Sexually transmitted diseases treatment guidelines, 2015. *MMWR. Recommendations and reports : Morbidity and mortality weekly report. Recommendations and reports, 64*(RR-03), 1-137.

World Health Organization. (2011). *Emergence of multi-drug resistant Neisseria gonorrhoeae: Threat of global rise in untreatable sexually transmitted infections.* Geneva: World Health Organization.

Yamaguchi, Y., & Inouye, M. (2011). Regulation of growth and death in *Escherichia coli* by toxin–antitoxin systems. *Nat Rev Micro, 9*(11), 779-790.

Yu, C., McClure, R., Nudel, K., Daou, N., & Genco, C. A. (2016). Characterization of the *Neisseria gonorrhoeae* Iron and Fur Regulatory Network. *Journal of Bacteriology, 198*(16), 2180.

Zhang, Y., Zhang, J., Hoeflich, K. P., Ikura, M., Qing, G., & Inouye, M. (2003). MazF Cleaves Cellular mRNAs Specifically at ACA to Block Protein Synthesis in *Escherichia coli*. *Molecular Cell, 12*(4), 913-923.

Zhu, L., Zhang, Y., Teh, J.-S., Zhang, J., Connell, N., Rubin, H., & Inouye, M. (2006). Characterization of mRNA interferases from *Mycobacterium tuberculosis*. *Journal of Biological Chemistry, 281*(27), 18638-18643.